Macro-stability safety assessment for flood defenses with buried pipes

Tijmen Groot

6/1/15

Colophon

Title:	Macro-stability safety assessment for flood defenses with buried pipes
Description:	Master thesis
Data publication:	01-06-2015

Author:	T. Groot BSc.
Email:	tijmen91@live.nl
Phone:	+316 36 42 72 22
University:	University of Twente
Faculty:	Faculty of Engineering and Technology
Department:	Water Engineering and Management
Supervisors:	
University of Twente:	Prof. Dr. SJMH (Suzanne) Hulscher
University of Twente:	Dr. J.J. (Jord) Warmink
University of Twente:	J.P. (Juan Pablo) Aguilar-Lopez MSc.
Deltares:	ir. Raymond van der Meij

Abstract

A growing demand for multifunctional flood defenses causes the direct need for more knowledge and understanding of the effects of a structure placed inside a flood defense, called transition, to the physical condition of a flood defense (van Loon-Steensma & Vellinga, 2014). Constructors and policy makers do at the moment not have a complete understanding of the direct implications on safety caused by transitions (Morris et al., 2012). This leads to the situation that concepts of multifunctional flood defenses will not be approved (lack of norms) or executed (to high risk). Therefore the goal is to deliver geotechnical information which predicts the safety of a flood defenses under influence of a transition during an extreme loading situation. Focus of this research is mainly on making a model which predicts the effect of a buried pipe on the development of macro-stability failure mechanism since the structure element pipeline is in present-day one of the mostly applied structures within dikes (Finsbury, Steven L. Stockton, & Loudiere, 2013).

The geotechnical conditions, which provide information about the effect of a pipeline on macro-stability are simulated with a 2D, stationary coupled model build in the finite element software COMSOL 4.4. This model applies a coupled combination of a Darcy model for modelling the flow of water in the porous media and a Drucker-Prager linear elastic perfectly plastic model for modelling the soil displacements in the soil skeleton. The model predicts the potential slip circle for the dike of the macro-stability failure mechanism, not the critical slip circle. Analysis of the effect of the pipe to the potential slip circle is based on the calculated effective plastic strains, a dimensionless monotonically increasing scalar value describing the unrecoverable portion of the true strain beyond the yield limit (Melnikova, 2014).

Validation of the model is performed using the data of the Southdike, an IJkdijk real scale experiment. The Southdike has been brought to failure by means of macro-instability and it was coped with a comprehensive sensor system, therefore perfect for this research. The model predictions are validated on three aspects with this data; safety factor, hydraulic head and displacement. The safety of the Southdike is slightly overestimated due to a smaller slip surface. Hydraulic heads and displacements are modeled within an acceptable range.

The model predicts the characteristic of the pipe such as location, size, material and the content of the pipe influence the development of the macro-stability failure mechanism. This can be a negative or positive influence, closely related to the principles of Bishop. The change in safety condition of the macro-stability failure mechanism cannot be addressed solely to a single characteristic of the pipe. A combination of characteristics of the pipe and the conditions of the dike determine the safety situation. The soil conditions and the loading conditions also have a significant influence to the effect of the pipe on the safety condition of the macro-stability failure mechanism.

The general conclusion is that for certain conditions the characteristics of the pipe have a positive influence to the development of the macro-stability failure mechanism. Combinations of characteristics and conditions determine the gain in safety for macro-stability failure mechanism. Therefore the second conclusion is that for every individual situation with different conditions and characteristics of the pipe, a calculation has to be performed to know the safety situation to macro-stability of the flood defense.

Preface

This report is made as completion of my Master's Thesis and with that it marks the end of my study in Civil Engineering and Management at the University of Twente. In the period between December 2014 and June 2015 I have worked on this research with the goal to asses if a pipeline placed inside a dike has an influence on macro-instability and the related safety level of the dike. As part of a PhD research of Juan Pablo Aguilar Lopez, it marks a first step into research which has to purpose to gain more knowledge into the effect of structures placed inside dikes and there effect on the safety.

I want to specially thank Juan Pablo for his time, enthusiasm, help and support during this research. Next I want to thank my main supervisors Suzanne Hulscher and Jord Warmink from the University of Twente for all their really useful feedback on my reports. I was really motivated by their enthusiasm about the research and I appreciate the consistency of feedback during my research. Furthermore I want to thank Raymond van der Meij for his support during this research. His experience into soil mechanics provided to be extremely helpful and I want to specially thank him for his helpful tips.

I would also like to thank Frank van Gool of COMSOL for his technical support during the model building in COMSOL. As well as 'stichting IJkdijk' for providing the data for this study and Deltares for providing me the software of D-Geo stability.

Finishing my Master Thesis marks also the end of my time as a student in Enschede, at the University of Twente. I would like to thank my friends for the great times I had since the moment I came in Enschede in 2009. Finally I want to thank my family for the awesome support during my whole study.

Tijmen Groot

Enschede, June 2015

Contents

List of symbols

Symbol	Unit	Description
z	[-]	Limit state condition
F_{LC}	[-]	Characteristic strength of limit state condition
S_d	[-]	Loading condition on flood defense structure
R_{char}	[-]	Strength flood defense structure
FoS	[-]	Factor of safety
FR	[-]	Resisting force on slice
FD	[-]	Driving force on slice
F_{SR}	[-]	Strength reduction factor
c	[Pa]	Cohesion
c_{margin}	[Pa]	Cohesion at instability (failure)
$\boldsymbol{\phi}$	[degree]	Friction angle
$\boldsymbol{\phi_{margin}}$	[degree]	Friction angle at instability (failure)
$\boldsymbol{\sigma_{eff}}$	[N/m^2]	Effective stress tensor
$\boldsymbol{\sigma_{ij}}$	[N/m^2]	Total stress tensor
p	[Pa]	Hydrostatic water pressure
$\underline{\underline{\mathbf{I}}}$	[-]	Unit tensor
$\boldsymbol{\sigma_x}$	[Pa]	orthogonal normal stress
$\boldsymbol{\tau_{xy}}$	[Pa]	orthogonal shear stress
$\boldsymbol{is_{dry}}$	[-]	Parameter defining wet/dry state soil
$\boldsymbol{g_{const}}$	[m/s^2]	Gravitation constant
$\boldsymbol{H_{ini}}$	[m]	Parameter defining initial hydraulic head complete model
$\boldsymbol{p_{ini}}$	[Pa]	Initial pore pressure variable
$\boldsymbol{\rho_s}$	[kg/m^3]	Soil density
$\boldsymbol{F_B}$	[N/m^3]	Buoyancy force
$\boldsymbol{\nabla}$	[-]	Gradient operator
$\mathbf{E}$	[Pa]	Young's Modulus
$\boldsymbol{\nu}$	[-]	Poisson value
$\boldsymbol{\varepsilon}$	[-]	volume deformation (strain state)
$\underline{\underline{\dot{\boldsymbol{\varepsilon}}}}$	[-]	deformation tensor (strain rate)
$\mathbf{F}$	[Pa]	Plastic yield function
$\boldsymbol{\varepsilon_p}$	[-]	Plastic strain state (intensity)
$\underline{\underline{\dot{\boldsymbol{\varepsilon}}}}_{\mathbf{p}}$	[-]	Plastic strain rate tensor
$\mathbf{q}$	[-]	Plastic multiplier
$\mathbf{P}$	[-]	Plastic potential
$\mathbf{K}$	[Pa]	Bulk modulus
$\mathbf{I_1}$	[Pa]	First effective stress variant
$\vec{\boldsymbol{u}}$	[m/s]	filtration velocity
$\boldsymbol{\kappa}$	[m^2]	permeability coefficient
$\boldsymbol{\mu}$	[Pa*s]	dynamic viscosity of water
$\boldsymbol{K}$	[m/s]	Hydraulic conductivity
$\boldsymbol{\varepsilon_p}$	[-]	Porosity

Q_m	[m^3]	volume intensity of external sources and sinks
τ_f	[Pa]	shear stress at material failure
e	[-]	Void ratio (porosity)
C	[-]	Compaction ratio
H	[Pa]	Stress history
T	[K]	Temperature
α	[-]	Drucker Prager constant
J_2	[Pa]	second deviatoric stress invariant
k	[-]	Drucker Prager constant
I_2	[Pa]	Second effective stress variant
int_j	[-]	Parameter defining data interpolation table j
$Ramp\_stage$	[-]	Parameter defining stage for quasi-ramping
F_{exc}	[N/m^3]	Equivalent load to excavated trench
$solid2.Tax$	[Pa]	Surface traction force x-direction
$solid2.Tay$	[Pa]	Surface traction force y-direction
P_c	[Pa]	Pressure of container
P_{cw}	[Pa]	Pressure of water in container
P_b	[Pa]	Pressure of water in basin
P_t	[Pa]	Pressure of water in trench
K_0	[-]	Variable derived from K0-test
E_{undr}^{50}	[Pa]	Undrained 50 percentile Young's modulus
E_{ODO}	[Pa]	Young modulus derived with Odometer test
G	[Pa]	Stiffness moduli
σ_{max}	[N/m^2]	Biggest principal stress
σ_{min}	[N/m^2]	Smallest principal stress

Chapter 1. Introduction

A flood defense (henceforth: FD) is still one of the most important structures providing safety to people living in areas vulnerable to floods. For a long time a FD had only served to fulfil its primary function, providing safety against floods. However due to global changes as the increase in density of the population, urbanization, global warming and the increase of wellness, society demands FD's to be able to fulfil more than one function. A multifunctional FD (multifunctional dike) can fulfil these needs. This type of FD has the advantage of providing safety against floods and at the same time provide us with the benefits of the present economic and social interest (van Loon-Steensma & Vellinga, 2014). An example is the new multifunctional dune at Katwijk where an underground parking lot is built in the dunes (Gemeente Katwijk, 2013).

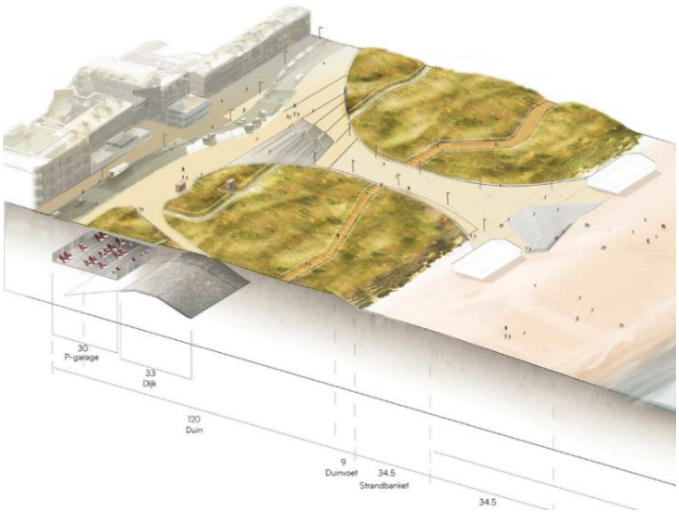

Figure 1; Cross section multifunctional dune Katwijk (Gemeente Katwijk, 2013)

The multifunctional FD is an interesting option to meet the new safety regulations of the new Deltaplan (Rijkswaterstaat, 2014). This plan describes that, due to global warming and new insights in the safety assessment methods for dikes, a lot of dikes have to be heightened and reinforced. With an multifunctional FD concept, local conflict due to for example space problems (Figure 2) can be prevented (van Loon-Steensma & Vellinga, 2014). The multifunctional FD also offers new opportunities to facilitate urban development, transport infrastructure, recreation, agricultural use and nature conservation (Vellinga, 2008; Hartog et al., 2009). It is even believed that these other functions can help in creating and financing the dike (van Loon-Steensma & Vellinga, 2014, p. 414).

Figure 2; House build against dike (Geoscience, 2013)

An essential step, before a multifunctional FD can be widely adopted into society, is to create new design rules for this type of FD. Design rules are crucial to provide contractors certainty their build FD structure can prevail a specified type of flood. FD design rules are based on the safety (factor) of the FD at a specified situation. Therefore FD design rules can only be made if there is a complete understanding of the behavior of the FD at a certain situation. This is not the case for a multifunctional FD because it differs from a traditional FD (van Loon-Steensma & Vellinga, 2014). This makes it really hard to create and adopt new policies for multifunctional FD. In many cases this means regular safety norms are applied to multifunctional FD's which can lead to an additional risk for a dike ring during high- or low water event. This is the main reason why this research into aspects of multifunctional FD's is so important for flood risk management. This is also mentioned by a European research institution for flood risk reduction. They state that due to transitions in the core of multifunctional FD, processes will occur of which not a complete knowledge is

available (Morris et al., 2012). These transitions have already led to multiple FD failures, for instance internal erosion along a pipeline or dike sliding close to a build house on a FD (Morris et al., 2012)(FloodProBE & Oderker, 2013). Research must provide a clear understanding of these processes changing due to transitions, to provide new rules for the multifunctional FD performance assessment (Morris et al., 2012).

This report will carry out such a safety assessment (also known as performance assessment) to get a better understanding of the processes occurring due to transitions in a FD. This research safety assessment investigates one element of an FD called a dike. A dike (also called levee) is a raised, predominantly earth structure that are not reshaped under normal conditions by the action of wave and current whose primary function is to provide protection against fluvial and coastal flood events along coasts, rivers and artificial waterways (Finsbury et al., 2013, p. 18).

In this research one type of transition will be investigated, a pipeline. A pipe in a dike, often called a buried pipe, is described by the International Levee Handbook as 'structures encroaching into dikes', specified as penetrating structures (Finsbury et al., 2013, p. 146). Pipelines are structures that are not required for the proper operation of the dikes (Finsbury et al., 2013, p. 146). These (third-party) pipes penetrating the dike are built because of stakeholder needs (water service, electrical power, petroleum lines) (Finsbury et al., 2013).

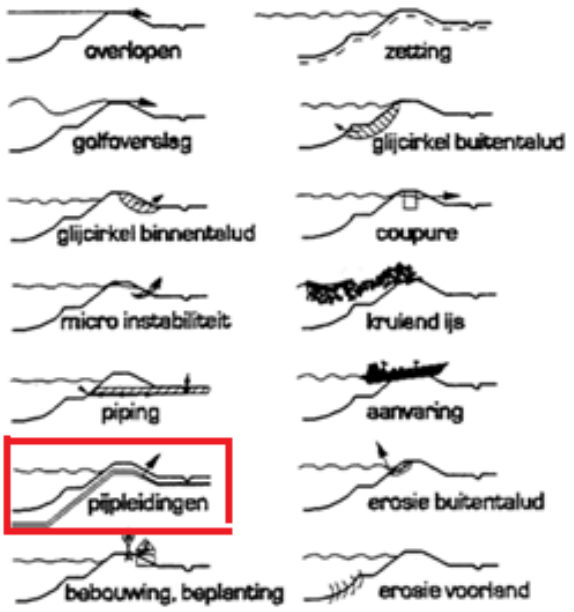

Figure 4; Causes of failure dike (Floodsite, 2014)

These pipes are by the European institutions described as transitions in the dike which can affect different physical mechanisms to behave differently (Morris et al., 2012). Due to changes of the physical behavior the pipe can cause degradation or destruction of one or more components, and so the failure of one or more of the elementary functions of the dike (Finsbury et al., 2013). This will finally lead to complete failure of the dike by breaching or by letting uncontrolled water into the protected area (Finsbury et al., 2013), which happened at the dike breach of Stein in 2004 (van Vollenhoven et al., 2005). In this case water leakage of the pipe in the dike led to macro-instability failure (sliding of the inner slip circle) (Figure 3). This is why a pipeline is defined as one of the 14 possible causes of failure for a dike (Figure 4).

Figure 3; Dike failure at Stein (van Vollenhoven et al., 2005)

The pipe can cause failure of the dike by different failure mechanisms[1]. The safety assessment must be scoped at one specific failure mechanism (Morris et al., 2012). Without specifying on one particular failure mechanism, the conditions defining the safe or unsafe state could not be defined since different failure mechanisms influencing each other (Finsbury et al., 2013). Failure due to a pipeline can be scoped into three types of failure mechanisms; external and internal erosion and macro-instability (Finsbury et al., 2013).

In a safety assessment usually the impact of each failure mechanism on the total state of the dike will be determined (Finsbury et al., 2013). This research will only focus on the relation between a (buried) pipe and macro-stability of the dike. We focus on macro-stability because slope instability failure occurs more often than seepage and internal erosion as breaching failure mechanism (Nagy, 2012). Secondly because there is not a lot of research done on the relation between buried pipes and macro-stability while there is for internal and external erosion in relation to buried pipe (David Pezza & Hal Van Aller, 2005; Wade Anderson et al., 2007).

Figure 5; Pipeline on top of dike (Finsbury et al., 2013)

Macro-instability due to buried pipes

At the moment of failure, macro-instability is defined as an unstable situation in which the ability of the dike to react to a disturbing force by maintaining or re-establishing its position has been compromised (Finsbury et al., 2013). In physical terms, macro-instability occurs when the active strengths of soil particles movement exceed the resistant strengths (Finsbury et al., 2013, p. 170). The pipe effects macro-stability by influencing the physical conditions in the dike (e.g. less soil strength) which can generate soil sliding along a shear surface within the dike (David Pezza & Hal Van Aller, 2005). This report will focus on (deep) rotational sliding as cause of macro-instability, neglecting the effects of settlement and creep (Allsop, Kortenhaus, & Morris, 2007) (see Discussion). Rotational sliding, so named because the failure surface appears as a segment of a horizontal cylinder, may result in slope failures ranging from local sloughing of soil at random areas along the face of an dike to massive circular arc slides extending over the entire dike (U.S. Environmental Protection Agency, 1994).

Figure 6; Installation of buried pipe in embankment (David Pezza & Hal Van Aller, 2005)

[1] A failure mechanism is a performance indicator for the performance assessment of the dike in which the inability to achieve a defined performance threshold is defined (Morris, 2008). The performance of the dike (system) is dependable on the state of the failure mechanism. The failure mechanism can be in safe state and reach an unsafe state at a specific moment (Finsbury et al., 2013).

IJkdijk experiment, Southdike

Data of (deep) rotational sliding, which is essential for quantitative investigation of the pipe on macro-instability, is gained from the Southdike, part of the IJkdijk experiments. The Southdike experiments is a perfect case because it is built to increase the knowledge on one dike failure mechanisms only, deep rotational sliding (A.R. Koelewijn, 2012). This implies very reliable data. Combing this data with the inclusion of a pipeline will provide this research with reliable results for the effect of the pipeline on macro-instability.

Distortion of pipeline

Macro-instability due to (deep) rotational sliding can be caused by changes of the soil particles or due to changes in the state of the pipeline itself. Distortion (or even failure) of a pipeline in an dike can have serious implications for the safety of the dike (AmericanLifelinesAlliance, 2005). Despite the fact that distortion of the pipeline is a key to investigate the effects of a pipeline to the flood risk of a dike (Finsbury et al., 2013), in this research pipeline distortions (corrosion, burst of - and infiltration) will be neglected. This is based on the statement that the required strength and the design life requirements of the pipe should be determined by the methods of the pipe manufacturers (Finsbury et al., 2013).

Important characteristics current pipelines

The investigated characteristics of the pipeline are based on the current norms for pipelines placed in a dike. The legal frame and related policy rules for buried pipes located inside dikes is described in NEN 3650 and NEN3651 (Herder et al., 2012; Hoogheemraadschap De Stichtse Rijnlanden, 2010; Rijkswaterstaat, 2013). These policy rules (norms) give authorization for the placement of a pipeline at a specifically defined location over a dike area. Approval for a specific location is based on the size/type of pipe, the direction in which it is headed and method of installation. In Table 1 a short summary is given at which locations (see Figure 7) authorization will be approved to place a pipeline. The substantiating of these authorizations are based on conditions which could be found in the document 'Beleidsregels – kabels en leidingen in op of langs waterkeringen' (Hoogheemraadschap De Stichtse Rijnlanden, 2010).

		Location							
		Primary flood defense				Regional flood defense			
		Parallel, in the water-work management zone outside of the dike body	Parallel inside the dike body	crossing by means of directional drilling	crossing otherwise than by means of directional drilling	Parallel, in the water-work management zone outside of the dike body	Parallel inside the dike body	crossing by means of directional drilling	crossing otherwise than by means of directional drilling
Type of Proceedings	Cable	Yes	No, unless	N.A.	No, unless	Yes	Yes	N.A.	Yes
	Casing pipes	Yes	No, unless	Yes	NO	Yes	No, unless	Yes	No, unless
	Small pipes (<300mm)	No, unless	No, unless	Yes	NO	Yes	No, unless	Yes	No, unless
	Large pipes	NO	NO	No, unless	NO	No, unless	NO	Yes	No, unless

Table 1 (Hoogheemraadschap De Stichtse Rijnlanden, 2010)

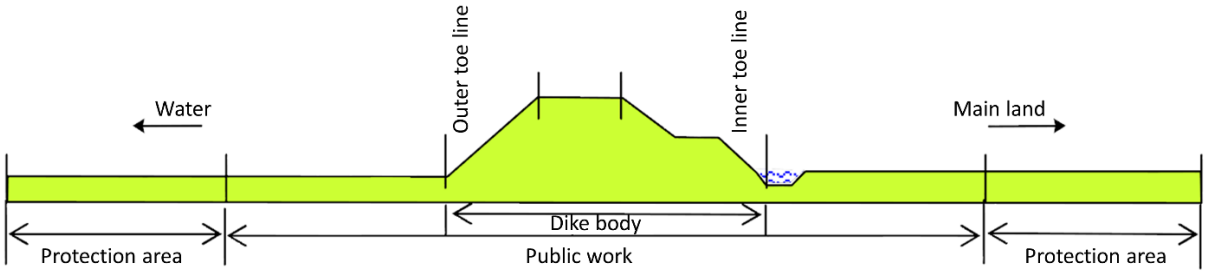

Figure 7; Overview zones around dike body (Dutch) (Hoogheemraadschap De Stichtse Rijnlanden, 2010)

Table 1 shows that all types of pipes are not allowed in the dike body, parallel or cross directional for a primary dike or regional dike. When research institutions state there is not a lot known about the effects of transitions towards safety (Morris et al., 2012, p. 65), this could imply these norms are not particularly based on quantitative data. This makes it very interesting to investigate if these norms are valid or that the negative effects of pipes towards safety are overestimated. Therefore the stated norms will be omitted giving us the possibility to investigate on all the possible locations within the dike, as well as on the different pipeline sizes. The method of implementation, like directional drilling showed in Figure 8, will be neglected (see Discussion).

Figure 8; Deep drilling installation (David Pezza & Hal Van Aller, 2005)

The type of pipe (material content), not particular mentioned in the norms, will be investigated. This is because literature states that the material content of the pipe could have a significant influence on the behavior of the soil (AmericanLifelinesAlliance, 2005; Chi Fai Ng, 1994; Wade Anderson et al., 2007). It is also for practical reasons because a lot of different pipes with their specific diameter are crossing dikes, see Table 2 (van Vollenhoven et al., 2005)

Material	Crossings	Diameter (mm)	Crossings
AC (asbestos)	29	Till 250	104
Crude iron	26	300-600	30
PVC	2	>600	7
PE	5		
Steel	79		

Table 2[2]; Overview pipes in region of Sittard ((WML, 2005)**)**

Summing up, this research will investigate how a (buried) pipe effects macro-stability and the related safety of a dike. It will thereby focus on the geo-mechanical effects, neglecting failure of the pipe itself. This research focuses on three aspects of the pipe; its location in the dike, the size of the pipe, the material of the pipe. For this research the case study of the Southdike (IJkdijk) will be used as validation case.

[2] Table 2 shows the relevance of this research. Because despite of the norms for pipelines still a huge amount of pipes do cross embankments or dikes in a relative small area as Sittard [between 155 and 160 (Source: (WML, 2005))].

1.1. Problem description

A growing demand for multifunctional FD's causes the direct need for more knowledge and understanding of the effects of a transition (structure) to the physical condition of a FD. Constructors do at the moment not have a complete understanding of the direct implications on safety caused by for example placing a house next to the dike, or building a road on top of it. Policy makers want to know if the situation remains safe (and if the transition contributes to extra functionality). This implies at the moment concepts of multifunctional flood defenses will not be approved or form a large risks to execute. If there is a better understanding of the implications of a transition to the physical mechanisms in the dike, better safety regulations could be made, to propose mitigation and/or remedial measures for transition zones in dikes. The problem definition stated for this research is therefore:

"There is not a complete knowledge of the (geotechnical) effects forced by a transition, in this case a (buried) pipe, on the macro-stability of a dike."

1.2. Research objective and questions

The intention of this research is to investigate if a change in function of the dike, in this case providing the functionality of a pipeline, influences the strength and related safety to macro-stability. We investigate if, due to a (buried) pipe, geotechnical processes and the related macro-stability of the dike change in an extreme loading situation. This research must deliver quantitative geotechnical information on which we could state if the safety of a dike is affected by the buried pipe during an extreme loading situation.

Therefore the goal is to develop a model which has the capability to determine the geotechnical conditions for a dike with the inclusion of a pipe at the same time. The safety of this dike has to be determined based on the safety determination methods used for the macro-stability failure mechanism. Based on this goal the following main question is formulated:

Which effect has a buried pipe on the macro-stability failure mechanism of a dike?

To be able to answer the main question, the research is divided into three research questions.

1. How can the geotechnical effects of macro-stability be modeled?
2. To what extent can the model reproduce macro-stability of the Southdike experiment?
3. To what extent and in which way does the buried pipe characteristics contribute to the development of macro-instability?

1.3. Research methodology

In this section the methodology of the research is elaborated. The steps shown in Figure 9 describe the approach how to provide sufficient and relevant information to be able to answer the research questions.

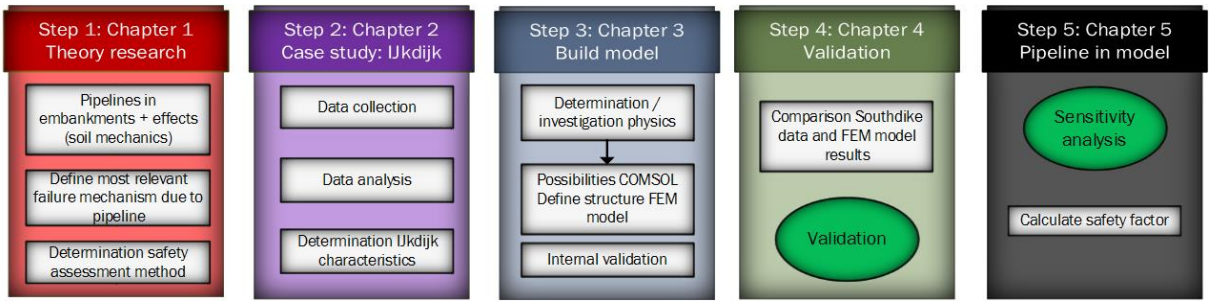

Figure 9; Methodology

Step 1: Literature review:

In the literature review (see introduction) the context (boundaries) of the research are made by stating which aspects will be investigated and which don't, and why this is done. The problem definition, objective and related research questions are formulated based on these aspects.

The conceptual idea of this research is based on the principles of multifunctional dikes (van Loon-Steensma & Vellinga, 2014) and all the investigation done into this subject, provided by (Morris et al., 2012).

Information about the principles of the buried piped is mainly found in documents regarding pipes located in embankments (AmericanLifelinesAlliance, 2005; Wade Anderson et al., 2007). Combing the information about all types of failure mechanisms (Allsop et al., 2007; Nagy, 2012; Vorogushyn, Merz, & Apel, 2009), and information how transitions/pipes affect a dike (David Pezza & Hal Van Aller, 2005; Finsbury et al., 2013; Morris et al., 2012; Wade Anderson et al., 2007) are combined to define that in this research macro-instability will be investigated. Based on this failure mechanism relevant characteristics of the pipe are defined based on failure aspects (Finsbury et al., 2013) and secondly on current practical use and norms of pipelines in dikes (David Pezza & Hal Van Aller, 2005; Hoogheemraadschap De Stichtse Rijnlanden, 2010; Kruse et al., 2013; Rijkswaterstaat, 2013; van Vollenhoven et al., 2005; Wade Anderson et al., 2007).

The performance to macro-stability of the dike will be investigated with an safety assessment method commonly used in flood risk management (Allsop et al., 2007; Balkema, 1998; Morris et al., 2012). For this study the performance (safety) assessment is based on a deterministic approach. With the deterministic method one overall safety factor, for one given configuration of loading and strength is calculated (Finsbury et al., 2013). The deterministic approach in this study does not assess all the possible failure mechanisms and belonging types of loading including corresponding soil strength (scenario's) (Balkema, 1998). It only focuses on one failure mechanism with a certain loading including soil strength characteristics (Finsbury et al., 2013). This approach is better known as a deterministic transient calculation.

In the deterministic transient calculation a limit state condition ('stability' or 'settlement') is determined with respect to the accepted loading of the structure (Allsop et al., 2007). This limit state, defined by the variable *z,* corresponds to a certain strength value or the characteristic strength [F_{LC}]. Exceedance of the limit state condition, variable *z*, means failure and is not accepted (Balkema, 1998; Finsbury et al., 2013);

$$z = F_{LC} - 1 \quad \text{with} \quad F_{LC} = \frac{R_M}{S_M} \tag{1}$$

In which S_M expresses the loading and can for example be a function of the hydraulic loading conditions. R_M represents the strength the flood defense structure and can be a function of e.g. the strength of the soil (Balkema, 1998). In geotechnical calculations this R_M often will be related to shear strength parameters, angle of internal friction and cohesion and/or the deformation properties (Balkema, 1998).

Step 2: Chose and investigate case study: IJkdijk experiments (Southdike)

The used macro-stability experiment in which a dike is brought to failure by (deep) rotational sliding and is measured is called the Southdike, part of the IJkdijk experiments of 2012 (A.R Koelewijn, 2012). First data is collected from the IJkdijk and other related institutions (Deltares). All the data, applicable and relevant data from sensors measurement, laboratory studies, information from the Southdike reports and information from the predictions studies is analyzed. Soil strength parameters are determined by combining the laboratory tests prediction studies values. Knowledge of geotechnical soil determination methods out of laboratory data is therefore essential (NPTEL, 2004). Other data is determined for validation (conditions at defined location) or for defining the conditions and loads active on the Southdike to build the model (A.R. Koelewijn, 2012; A.R Koelewijn, 2012).

Step 3: Build model

In this step, the first research question is answered which makes it possible to build the model: '*How can the geotechnical effects on macro-stability be modeled?'*

For answering this question soil mechanical theories of Mohr Coulomb/Drucker Prager (Jiang & Xie, 2011), Terzaghi , Darcy / Richards, e.g. (Hamdhan & Schweiger, 2011; Liu, n.d.; Verruijt, 2001) are applied combined with the effect of the pipe on the physical state of the soil (Finsbury et al., 2013; Morris et al., 2012; Wade Anderson et al., 2007). The choice for a type of physics is based on the possibilities, advantages and disadvantages of each theory. This is also influenced by, and has influence on, the software used to model macro-instability because the possibilities within the software package creates restrictions to the use of some physical theories (Inc, 2012; Melnikova, 2014). The use software package is called COMSOL which calculates the (soil) physical equations with finite elements (Inc, 2012; Melnikova, Jordand, Krzhizhanovskayaa, & Sloot, 2012; Melnikova, 2014; Potts & Zdravković, 1999; Zienkiewicz, Taylor, & Zhu, 2005) *Therefore final model used to calculate macro-stability of the total Southdike in this report is called the CMS-model (COMSOL Macro-Stability model).*

For the CMS-model some assumptions are applied based on recommendations in literature and knowledge from (COMSOL) experts encountered during the research.

First assumption is that the analysis of the dike will be performed under two dimensional (2D) conditions. Firstly because 2D numerical simulations correspond more closely with the actual behavior of 'long embankments', Southdike is considered as long embankment, than 3D simulations (those are better in simulating short embankments) (Lu, Wang, & Chong, 2005). Secondly because 2D approaches are proven to be satisfactorily and are widely applied by engineers around the world (Bergado & Teerawattanasuk, 2008).

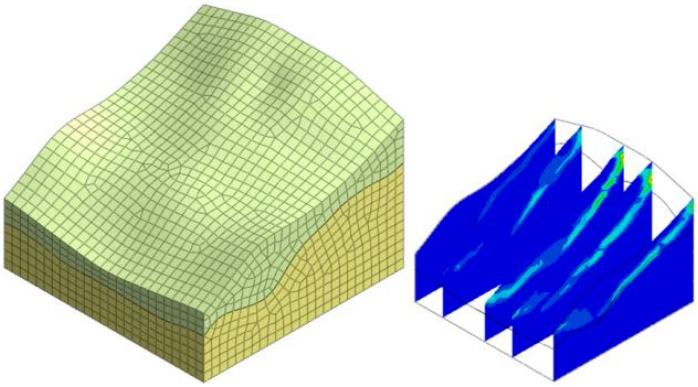

Figure 10; 2D vs 3D calculation (MIDAS, 2015)

The used software for simulating the macro-stability of the Southdike is COMSOL. COMSOL provides the opportunity to create a multi-physics model that solves coupled physics phenomena (doing simultaneously) (Inc, 2012). This is essential to model macro-stability, since the macro-stability is influenced by the pore water pressures (Darcy) and the strength of the soil (Mohr Coulomb) (Finsbury et al., 2013; Melnikova, 2014). The buried pipe will be incorporated with built-in physics interfaces and the support for material properties (Inc, 2013b). The variables or expressions from the buried pipe will be applied to solid and fluid domains and boundaries independently of the computational mesh (Inc, 2012). An advantage is that for the applicability of the model in the future with COMSOL not an in-depth knowledge of mathematics or numerical analysis is required (Inc, 2012). This makes it possible to use our CMS-model also for less experienced people in the future.

For finding approximate solutions to boundary value problems for partial differential equations the CMS-model uses the numerical technique of finite element model, better known as a FEM calculation (Reddy, 2005). The major advantages of FEM for this study is that it uses variational methods (the calculus of variations) to minimize an error function and produce a stable solution (Redaelli, Cividini, & Gioda, 2011).

With the possibilities of FEM we can investigate the different geotechnical properties of the soil layers, or adding a pipe in the model with different properties, add multiple loadings and boundary conditions to the geometry. Due to the well-integrated pre- and post-processing modules of FEM in COMSOL software, using graphic user interface (GUI), we will be able to interpret results more effectively, verify the accuracy and modify the model parameters instantaneously (Inc, 2012). This makes FEM the perfect tool to perform slope stability analysis.

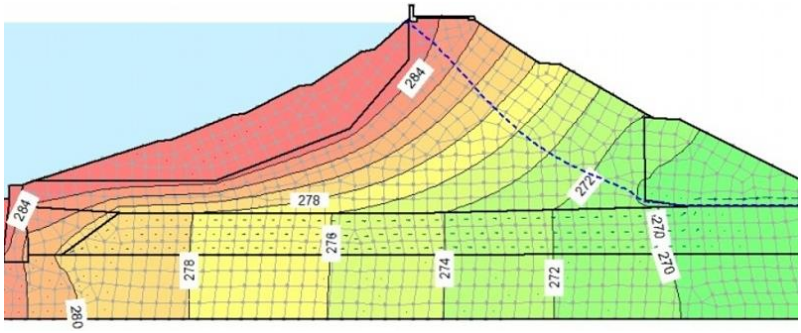

Figure 11; Finite element model (FEM) used for slope stability calculation (MIDAS, 2015)

Step 4: Validation

Valid load and resistance considerations are crucial for the research since proper conclusions could only be based on a valid model. Since the validation of the model will be based on the data of the Southdike the second research question is formulated as followed: '*To what extent can the model reproduce macro-stability of the Southdike experiment?*'

The CMS-model is validated on three aspects. The first aspect is the limited state condition of the dike. The limited state of the deterministic transient approach determining the safety/stability, will be validated with the use of a safety factor. The safety assessment, defining safe (stable) or unsafe (unstable) state of the dike, can be carried out with a limit equilibrium model (henceforth: LEM) or by a finite element model (FEM) (Balkema, 1998; Melnikova, 2014). Both methods are based on the permissible stress design philosophy, stress developed in a structure due to service loads may not exceed the elastic limit (Allsop et al., 2007). In the so called 'model cross validation' the numerical calculated limit state of the CMS-model (FEM) will be compared with the software of D-Geo stability (LEM), provided by Deltares which is allowed despite the different determination methods (see discussion) (Melnikova, 2014; Thompson, 1993; Zheng, Tang, Zhao, Deng, & Lei, 2010).

In the limit equilibrium analysis, dike stability margin is assessed by computing the factor of safety (FOS), describing the capacity of a slope to withstand its own weight together with applied external loadings from surcharge and groundwater (Melnikova, 2014). The factor of safety can be defined as the ratio between the restoring forces F_R (soil shear strength + externally applied restoring forces) to the disturbing forces F_D (soil self-weight + externally applied forces) (Melnikova, 2014) (see Figure 12). This is expressed in the following equation:

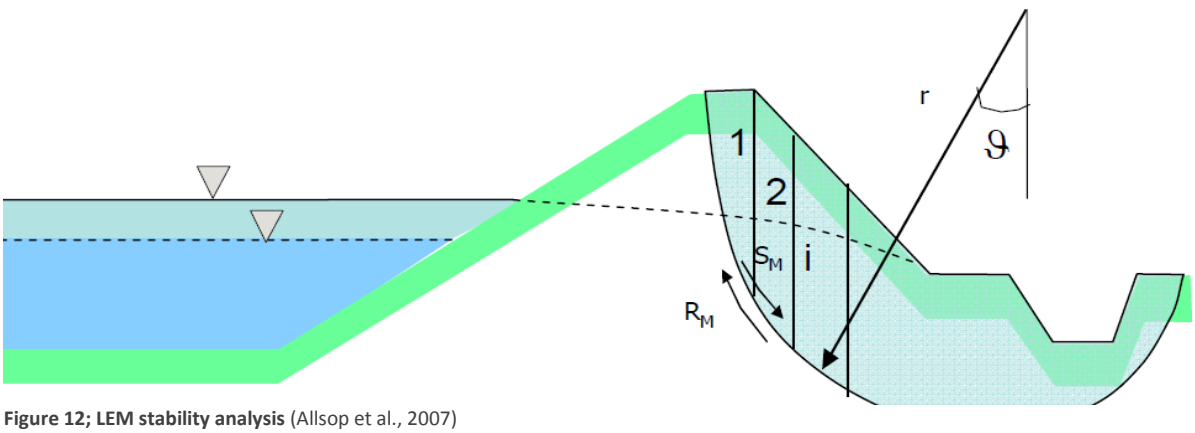

Figure 12; LEM stability analysis (Allsop et al., 2007)

$$FoS = \frac{F_R}{F_D} \quad \textbf{(2)}$$

The safety factor of the CMS-model will be determined applying the strength reduction method, and is therefore called the strength reduction factor (F_{SR}). This is the most practical method for simulating the failure limit state of slopes, determining their sliding surfaces and factor of safety when solving the partial differential equations of soil mechanics in FEM (Melnikova, 2014). The method reduces the parameters of shear strength (cohesion and internal friction angle) of soil slopes progressively until a critical failure limit state is reached (Balkema, 1998). Then, the slip surface of the slope can be automatically obtained from the results, and the factor of safety of strength reserve can be calculated (Zheng et al., 2010). The strength reduction factor is then defined as the ratio of the original and scaled strength parameters.

$$F_{sr} = \frac{c}{c_{margin}} = \frac{\tan(\phi)}{\tan(\phi_{margin})} \quad \textbf{(3)}$$

Where c, ϕ are cohesion and friction angle of soil strata, c_{margin}, ϕ_{margin} are cohesion and friction angle at the margin of instability, under given loadings.

The second validated aspect is the hydraulic head (pore pressures are based on hydraulic heads) in the dike. Data provided by the piezometers of Deltares will be compared with the modeled hydraulic heads. While the CMS-model is a stationary model and calculates the hydraulic heads of an equilibrium situation in time, piezometers provided all the hydraulic heads at any moment in time. The difference is that in the equilibrium situation (stationary model) differences in hydraulic heads (pressures) between soil layers will be blurred, while in the real time-dependent case these pressures will slightly increase dependable on the soil characteristics (Darcy's Law) (Meij, 2015a). This is shown in the figure below;

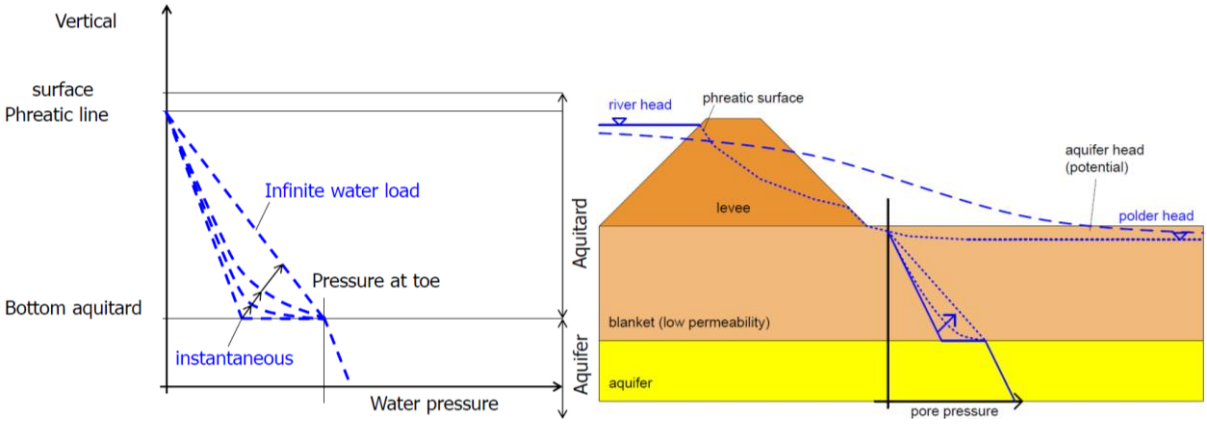

Figure 13; Time dependent vs static water pore pressure distribution (Meij, 2015a)

For a proper validation, time dependent hydraulic head values will be simulated in the CMS-model (stationary model) by averaging the hydraulic heads. An example is shown in Figure 13, where the aquifer potential head is averaged with the potential head of the polder (linear averaging method) (Meij, 2015a). By increasing those averages in multiple stages a quasi-static situation is simulated. This implies that the validation of the hydraulic heads is at the same time a calibration for the CMS-model.

The third validated aspect is the displacements within the Southdike. Therefore data of inclinometers will be compared with the modeled data. The validation is mainly focused on comparing the displacement of the soil located in the slip circle of the Southdike (overall shape is neglected). Validation of the displacements will at the same moment be used as calibration of the CMS-model. The Young's modulus of the soil parameters will be slightly changed.

Step 5: Pipeline in the dike model

Multiple aspects of the pipe can have a different influence on macro-instability of the dike. Therefore the following research question is posed: '*To what extent and in which way does the buried pipe characteristics contribute to the development of macro-instability?*'

For answering this question the characteristics of the pipe are limited to four different aspects (AmericanLifelinesAlliance, 2005; David Pezza & Hal Van Aller, 2005; Wade Anderson et al., 2007) which will be investigated with a sensitivity analysis:

1. The sensitivity analysis starts with changing the location of the pipe. The locations at which the pipe will be placed at locations dependable on the shape of the slip surface. The pipe will be placed at the slip circle so the direct influence on the shape of the slip circle can be investigated. Other locations will be chosen in such a way this research is able make clear conclusions. No criteria further criteria have be set up for the location because case studies show that the locations of the pipelines were mostly random (Rijkswaterstaat, 2014; WML, 2005).
2. The second step of the validation is change the size of the pipe (small, standard, big). Based on the results of step 1 of the sensitivity analysis, locations are determined at which the size of the pipe will be adjusted. The standard diameter size of the pipe used in step 1 is 400mm (thickness 50mm). The small pipe will have a diameter of 250mm (thickness 25mm) and the big pipe a diameter of 600 mm (thickness 50mm). These diameters are based on Dutch standards, confirmed by a case in Sittard (see Table 2 introduction) (Rijkswaterstaat, 2013; WML, 2005).
3. The third aspect is the material content of the pipe. Chosen material types are based on literature (AmericanLifelinesAlliance, 2005; Finsbury et al., 2013; Wade Anderson et al., 2007) and information shown in Table 2 (WML, 2005). Three types of pipe are chosen; steel, concrete and plastic. The two main parameters which defines the material of the pipe is the stiffness and the density (weight).
4. The fourth aspect is the state/condition of the Southdike. It is stated that the effect of the pipe could also be influenced by the state of the soil (Chi Fai Ng, 1994). The positive/negative effect of the pipe could be of a larger/smaller order relative to the situation of the dike. Therefore the material parameter (e.g. cohesion, friction angle) of some parts of the Southdike will be slightly modified.

The results of the sensitivity analysis, shape of the slip circle and safety factor, of all the posed combinations will be compared with the slip circle and safety factor of the standard situation without a pipe. The results of the different characteristics (size and material, parameters) will be also be compared reciprocally. Important to mention is that the CMS-model (FEM) only simulates the potential slip surface due to the possibilities within COMSOL (see discussion). The potential slip surface does not imply full failure of the dike, like the final state, but can still be used for our research (see Appendix F). In this situation the safety factor is around 1, the dike has only physically failed not leading to major displacements

1.4. Thesis overview

The thesis starts with the case description, the experimental dike made for the IJkdijk experiments on which the model will be determined. Chapter 3 gives a detailed explanation of all components and underlining theories, assumptions of the dike model. Also an internal validation is performed. The fourth chapter provides the results of the validation and chapter 5 provides the results of this study, the effect of the buried pipeline on the macro-instability failure mechanism. Finally, in chapter 6 and 7 the limitations/restrictions of this research are discussed and finally conclusions and recommendations are given.

Chapter 2. The Southdike; test side description and soil conditions

This chapter describes the IJkdijk experiment at which the tested dike failed by means of macro-instability. The chapter starts elaborating on the contents of the IJkdijk experiment. What does these experiments imply and why is it such a perfect validation case for this research. Continued with information about the test side, geometry, the experiment, soil build-up and soil parameters. The final paragraph provides information about the data that will be used for validation.

2.1. Southdike experiment and instrumentation

'The IJkdijk' (calibration dike), is a Dutch research program with the two-fold aim to test any kind of sensors for the monitoring of dikes under field conditions and to increase the knowledge on dike failure mechanisms (A.R. Koelewijn, 2012). Several purpose built-dikes have been brought to failure at the IJkdijk test site at Booneschans (Bad Nieuweschans) in the Groningen province, the Netherlands (Vries, Bruin, Peters, Loon, & Koelewijn, 2012). Every IJkdijk was specially designed and brought to failure in accordance to a specific failure mechanism. The dike relevant for this research is the Southdike, part of the IJkdijk tests of August/September 2012, because the Southdike was forced to fail according to macro-instability.

The Southdike was after construction a 4m high dike, 50 meters long at crest level, with a crest of 3m and side slopes of 1:1.5 (Y:X). The core was made of sand, overlain by a 0.5m thick clay layer, see Figure 14 (A.R. Koelewijn, 2012). Detailed drawings of the South dike could be found in Appendix A. The ground level at the test area (Bad Nieuweschans) lies around 1m below the mean sea level, groundwater level around -1.20m (Melnikova, 2014). The dike was founded on very soft layers of clay and peat which in turn lie on a stiff sand layer located about 4 m below the surface level (Melnikova, 2014, p. 67). A small auxiliary dike was built from the adjacent soil along the safe slope of the test dike (at the left side in Figure 14), forming a 1 meter deep basin (Melnikova, 2014, p. 67). Six containers with 3 tons of weight and 28 m^3 volume were installed on the crest of the dike (Melnikova, 2014). During the test, the effective height of the dike was increased by excavation of a 2-meter deep trench along the right slope, the core of the dike was filled with water and the containers were filled with water at certain stages of the experiment (A.R Koelewijn, 2012; Melnikova, 2014).

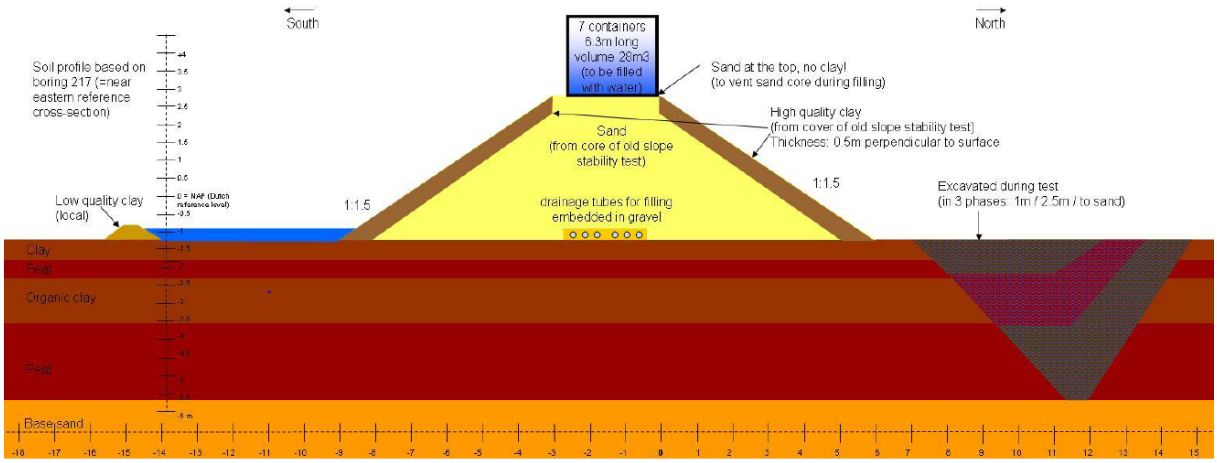

Figure 14; Design Southdike (A.R Koelewijn, 2012)

Goal of the Southdike test, part of the All-in-One Sensor Validation Test of the IJkdijk program, was to increase scientific knowledge about physical mechanisms of dike failures by macro-instability (A.R. Koelewijn, 2012). The Southdike was therefore constructed in such a way it would fail either from rupture

of the clay layer by high pore pressures inside the sand core resulting from saturating this core with water, or by macro-instability involving a deep sliding plane through the original subsoil, with a minimum displacement of at least 20 cm (A.R. Koelewijn, 2012).

The test on the South dike started on Monday September 3rd, 2012, at 12:12 pm (t=0) and failed by slope instability with a deep sliding plane on Saturday, September 8th, at 2:27 pm (t=122.26 hrs) (A.R. Koelewijn, 2012). Because the Southdike failed due to deep rotational sliding it is a perfect case to use for the validation of our 'dike model'. Second reason to use the Southdike as validation case is because it was equipped with a comprehensive sensor system (A.R Koelewijn, 2012; Melnikova, 2014). This comprehensive sensor system included piezometers (Geobeads provided by Alert Solutions), inclinometers (SAAF, StabiAlert, and Geobeads), strain and temperature meters (geo textile from TenCate, fibre optics from Koenders) and settlement gauges, see Figure 15 (Melnikova, 2014).

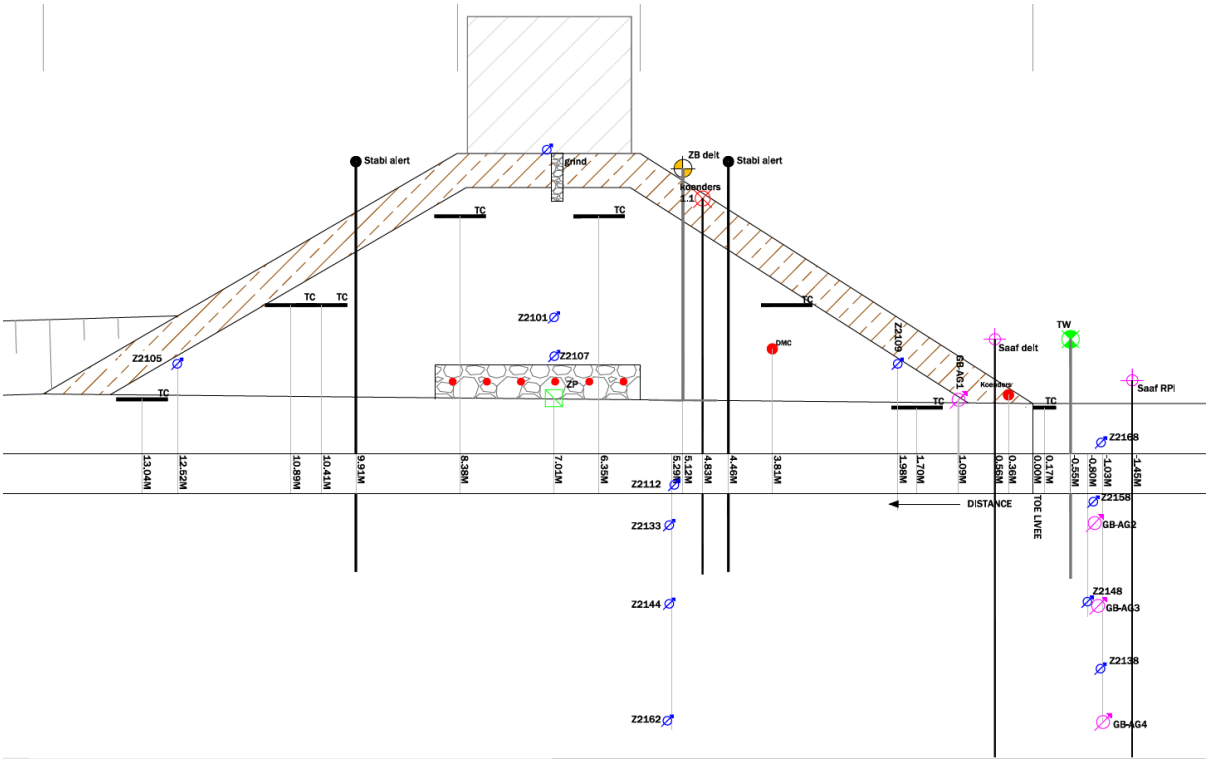

Figure 15 Location of sensors Southdike (east section) (Vries et al., 2012)

All the data of these sensors is provided by the IJkdijk stichting and Deltares. It turned out not all of this (received) data was applicable for research/validation. Some of the sensor data had to be analyzed with the use of additional software of the related companies (Koenders, Geobeds) which was not available. Besides were most of the sensors meeting the other goal of the IJkdijk test, develop efficient dike monitoring system predicting various modes of failures in advance (Melnikova, 2014). Data from those two systems is not compatible with the physics used in COMSOL (only PLAXIS which uses soil hardening models). For the validation of our dike the data from the Deltares piezometers (blue points Figure 15) and the SAAF inclinometers are used (black lines with pink circle top in Figure 15), elaborated in paragraph 2.3.

The experiment

Designers of the Southdike applied some methods during the full experiment to simulate the same conditions of a high water event acting on one side of the Southdike (left-side in Figure 15) to force failure due to macro-instability. Researchers of the Southdike mention that all those stages and loadings steps are important for the final state of the Southdike because the horizontal deformations accelerated at every

increase of the load, just to slow then again later on (A.R. Koelewijn, 2012). This implies that despite the fact that the Southdike is not actually (loaded) equal to a normal dike (slope, containers etc.), it can still be seen as a valid case for this research into dikes. Therefore a detailed overview of the full experiment is given.

Construction of the dike was completed three months prior to the experiment, in June 2012, so the excess pore pressures had enough time to dissipate and the soil consolidated (Melnikova, 2014). Therefore at the start of the experiment on September 3, 2012, maximal settlement of the dike crest had reached 0.9m (east section) up to 1 meter (west section) (A.R. Koelewijn, 2012). With this method the effects of settlement and creep are brought to a minimum.

Because an almost fully consolidated dike is a vital aspect to simulate a real case dike, (makes it more appropriate to use for scientific research) the experiment started with saturating the sand core of the dike by slowly infiltrating water until a phreatic level inside the dike of 0.5m above the level of the toe (-1.15 NAP) (**stage 1**). Due to serious wetting of the area around the toe of the dike this has been aborted at a level of -1.1m NAP (started at -1.4m NAP) (A.R. Koelewijn, 2012).

In **stage 2** the basin at the South side of the dike has been filled. To maintain the level, this basin has been refilled several times after.

In **stage 3** a ditch has been excavated in front of the dike on the North side. This ditch started at 1.5 meters from the toe with a slope of 1:1 at the side of the dike and 1:1.5 at the other side (A.R. Koelewijn, 2012). The excavation has been carried out in three steps, first a depth of 0.5m and a bottom width of 2m, then a depth of 1.0m and a bottom width of again 2m and finally a widening to a bottom width of 4m at a depth of 1.0m (A.R. Koelewijn, 2012).

Stage 4 waiting was cancelled (small deformation rates) and therefore **stage 5** was directly started. The trench was excavated by 0.5m to a total depth of 1.5m, with a bottom width of 4m and side slopes of 1:1 at the dike and 1:2 at the other side (A.R. Koelewijn, 2012). Next, the trench was excavated to a depth of 2m below ground surface (i.e. a ditch bottom at NAP -3.15m) with a bottom width of 4m and the same side slopes as before. Further widening is has not been carried out because of signals of hydraulic fracturing. In these stages (**stage 6**) also water has again been infiltrated into the sand core to a level of 0.25m above the dike toe (A.R. Koelewijn, 2012).

In **stage 7**, the containers of top of the dike were filled with water. On average, every seven hours the water level raised with 0.25m till a level of about 1.75m (except in both outer tanks) (A.R. Koelewijn, 2012).

In **stage 8** the discharge of the controllable drainage tube is increased. In the last half an hour of the test the infiltration even increased to fast, forced pumping into the sand core. Also the water was pumped out of the ditch. This went rather slow, and seepage increase with water level drop, so this went in a non-linear manner (A.R. Koelewijn, 2012).

Between **stage 9 and 10** the failure of the dike occurred (A.R. Koelewijn, 2012). The failure time slightly depends on the location in the dike, on average the dike fails at t=118.5 hrs.

At the last loading **stage 11**, after 30 minutes of forced pumping, at 2:27 pm (t=122.26 hrs), the slope at the trench-side of the dike broke in pieces, after which a slightly more superficial sliding plane occurred and the pore pressure decreased quickly (A.R. Koelewijn, 2012). A few minutes later the failure seemed to have stopped, although the measurements show an increase of the deformations up to half an hour later. The failure is shown in Figure 16.

Figure 16 Failure of South dike (Vries et al., 2012)

Figure 16 shows that the dike did not have the same displacement at every section of the dike. The Southdike physically failed at every section but structural failure, which is clearly shown in Figure 16, occurred at the middle/west section of the dike, at respectively container 4 and 5 (Lang et al., 2012). A detailed drawing of the structural failure is shown in Figure 17. Despite the fact that the structural failure occurred at the middle/west side of the dike, validation is based on data derived from the east section of the dike. This is for practical reasons since the data of the east section was more applicable for the applied validation. This choice does almost have no influence on results because physical failure of the dike due to macro-instability occurred for both sections at almost the same time (A.R. Koelewijn, 2012).

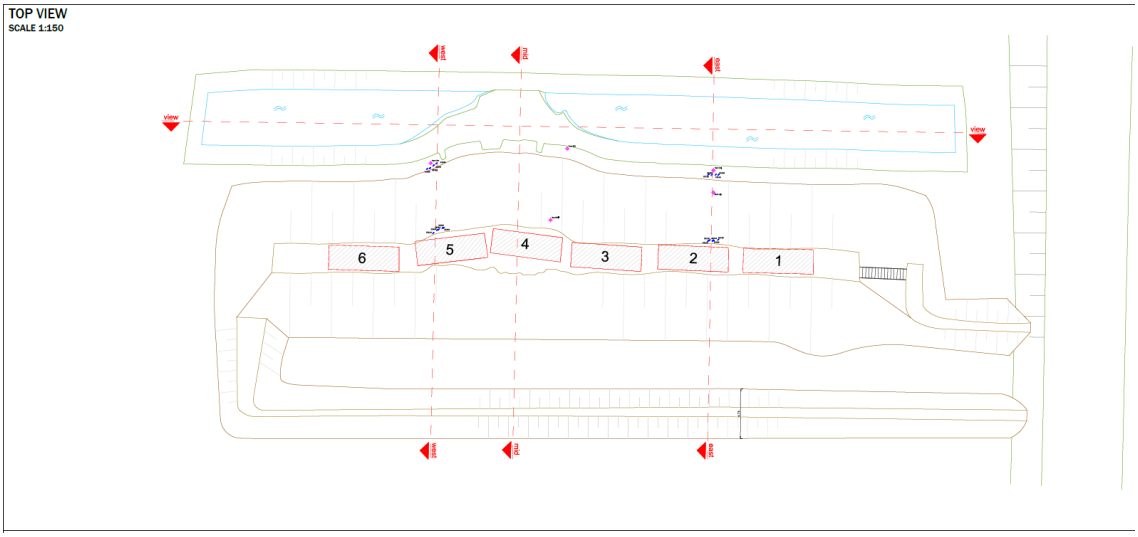

Figure 17; Top view of failure (Vries et al., 2012)

2.2. Soil conditions

The soil conditions of the area of the IJkdijk experiments at Bad Nieuweschans are investigated in 2006, 2008 and 2012. Earlier investigations of the area were done because in 2008 also experiments were carried out on the same location. Therefore especially deep soil investigations are only done in 2006 or 2008. For investigations borings and Cone Penetration Tests were carried out at different locations over the whole test area. The data of the Boring test B05 till B09 which are located on the test location of the Southdike are seen as most relevant for this study. Based on the results of those borings (see Appendix B) the variation in ground conditions across the site could be summarized as shown in Figure 18.

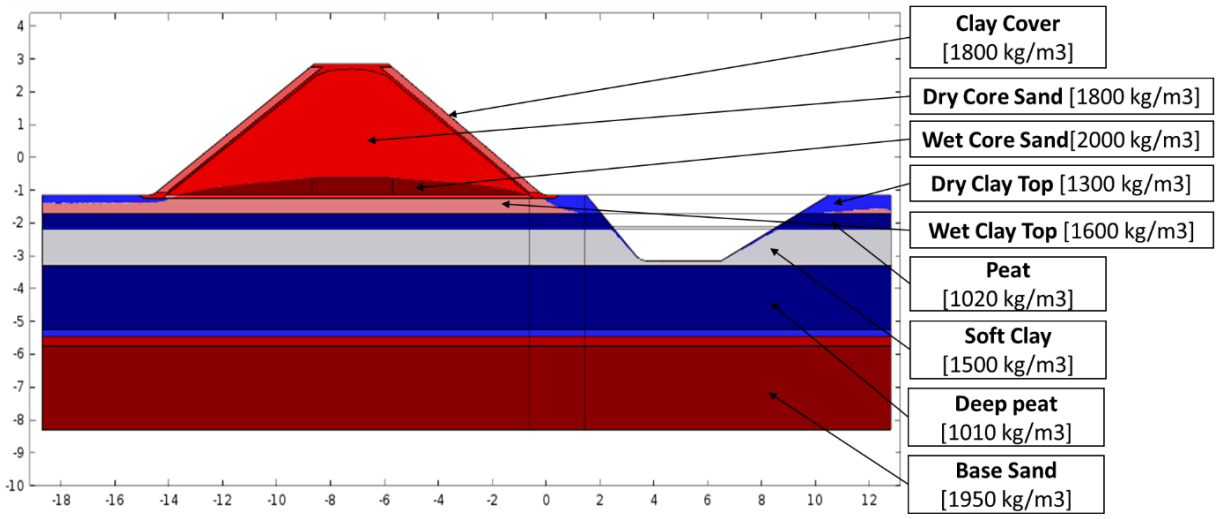

Figure 18; Soil build-up (simulated in COMSOL)

The dike core is made of sand with a very stiff cover layer of clay. Under the dike core there are multiple soft peat and clay layers. First there is a top layer of clay of 60cm continued by a peat layer of 40cm, next a clay layer of 1 till 1.30 meters thick is located under which a thick (deep) peat layer of 2 till 2.40 meters is located. This is all founded on a base sand layer with an undefined depth. In Figure 18 we can see some small layers between the defined soil layers. These are transition layers which have to address the effect of a transition between the different soil layers (see chapter 3).

Other soil strength parameters are based on performed laboratory tests as the Triaxle tests, Odometer test, Direct Shear Sample test and K0-CRS tests, see Appendix B. Missing / comparable soil strength parameters are based on data which is used by competitors of a submissions to predict the time of failure of the Southdike (A.R. Koelewijn, 2012; Lang et al., 2012; Melnikova, 2014). The parameters of the Young Modulus, for especially the soft soils, are slightly modified in a calibration which is based on the results of the validation of the Southdike. All the soil parameters of the main soil layers are presented in the Table 3.

Property	Cover clay	Core Sand	Clay top	Peat	Soft Clay	Deep Peat	Base Sand
Depth below S.L. [m]	-	-	0 – 0.8	0.8-1.2	1.2-2.3	2.3-4.5	>4.50
Young's modulus [MPa]	37.5	26	3.1	1.5	2.3	0.75	150
Poisson value [-]	0.47	0.31	0.48	0.495	0.48	0.495	0.3
Cohesion [kPa]	30	1.8	6.4	7.9	9.7	7.9	0
Internal friction angle [deg]	30.9	28.4	32.9	21.1	23.8	20.8	36.1
Dilatation angle [deg]	20	0	10	0	0	0	5
Saturated density [kN/m^3]	17.5	20	16	10.1	15	10.2	19.5
Unsaturated density [kN/m^3]	16.5	18	13	10	12	10.1	17
Permeability [m/day]	1^-6	0.04	1^-6	1^-5	1^-6	1^-5	0.135
Porosity	0.4	0.33	0.4	0.42	0.48	0.42	0.26

Table 3; determined soil parameters Southdike

2.3. Validation data

The CMS-model is validated on three aspects of the Southdike experiment, safety factor, hydraulic head and displacements. The validation will be based on data derived from sensors located at the east section of the Southdike. The data of these sensors is presented in this paragraph.

Safety factor

The validation of the safety factor is based on a comparison between the FOS (factor of safety) of the LEM software and the SRF (safety reduction factor) of the CMS-model FEM software. The FOS has been determined by 'stichting IJkdijk' presented in the evaluation reports of the Southdike experiment(A.R. Koelewijn, 2012). The FOS calculated is based on all the data they gathered and determined for multiple moments in time of the Southdike experiment. For this analysis the software package 'D-Geo Stability' (version 10.1, build 2.2) has been used, which calculates the safety factor against failure by analytical slope stability models of Bishop [1955] and Van [2001] (A.R. Koelewijn, 2012). The factor of safety for the Simplified Bishops' Method and Uplift Van is determined by the sum of restoring and disturbing forces on all possible circular slip surfaces with arbitrary diameters and center locations (Melnikova, 2014). While for the Simplified Bishop's method slip circles are assumed to be circular, the used Uplift Van method shown in Figure 19 does not assume a circular slip plane and incorporates the horizontal water pressures (A.R Koelewijn, 2012).

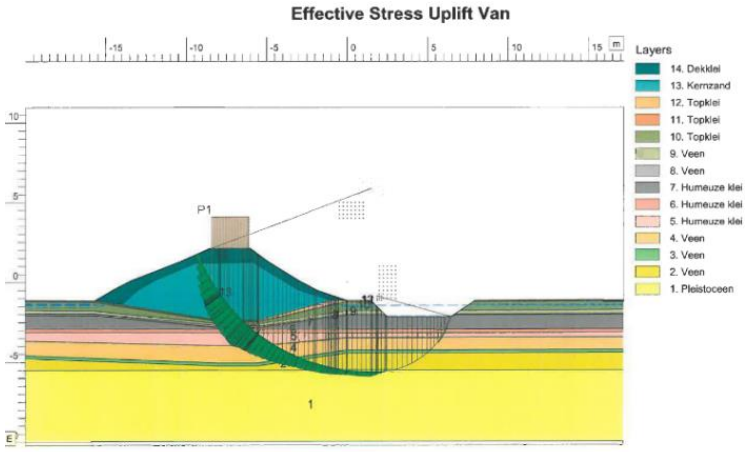

Figure 19; SRF determination using Uplift Van (A.R. Koelewijn, 2012)

The Geo-Stability calculations for the safety factor of the Southdike presented in IJkdijk report uses average values of strength parameters, unit weight and geometry, and measured values for the pore pressure assuming no vertical movement since the start of the test (A.R. Koelewijn, 2012). The results of Bishop and Uplift Van which could be compared with the SRF of the CMS-model are shown in the table below.

Situation	Time (hrs.)	FOS Uplift Van	FOS Bishop
Start of test	0.00	1.74	1.82
After last excavation	52.8	1.05	1.08
Restart of infiltration	67.63	1.08	1.12
Start last infiltration	121.69	1.01	1.05
Maximum pore pressures	122.02	0.92	0.95
Final Failure	122.26	0.94	0.98

Table 4; FOS in time from 'stichting IJkdijk' (A.R. Koelewijn, 2012)

It will turn out that not all the calculated values of Table 4 could be validated because the CMS-model is a stationary model. Comparison of both models is therefore based on a specific moment in time at which the conditions of the final stage of the CMS-model are assumed to be equal to the conditions used in the LEM calculation. This will be at the moment of physical failure of the Southdike. At this moment the driving forces are larger than the resisting forces, but slip, and related huge displacements have not occurred. Based on multiple displacement plots, for instance Figure 20 presented in the IJkdijk report, the moment of

physical failure can be determined. The moment of failure is variable (116.2hrs-120.8hrs) throughout the different sections of the IJkdijk (Vries et al., 2012). The moment to which the CMS-model will be compared is **t=118.5hrs**, which is based on an average of multiple sections.

Based on the moment of failure at t=118.5hrs the used values for the validation of the safety factor (Table 4) are a FOS of 1.03 (Uplift Van) and a FOS 1.07 (Bishop).

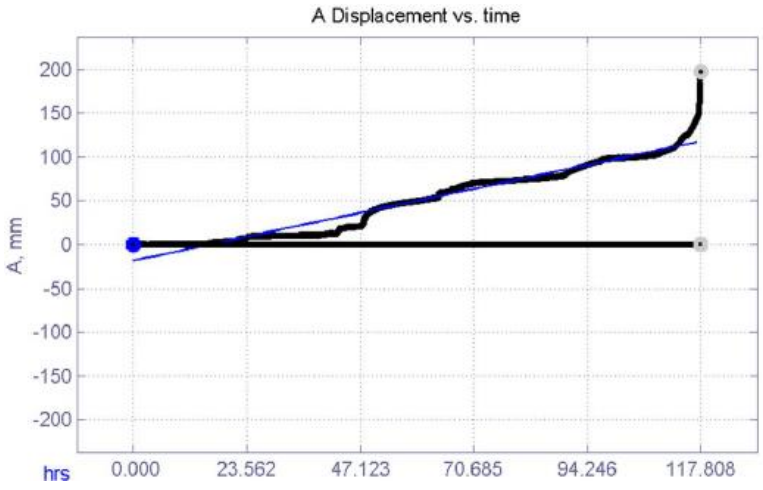

Figure 20; Defined physical moment of failure at specific section Southdike (Vries et al., 2012)

Hydraulic head

Hydraulic head validation data is provided by the piezometers of Deltares. The piezometers were located at the east section of the dike and were numbered with a general tag, Z21xy. All the piezometer locations are boxed in red with their tag, which is shown in Figure 21.

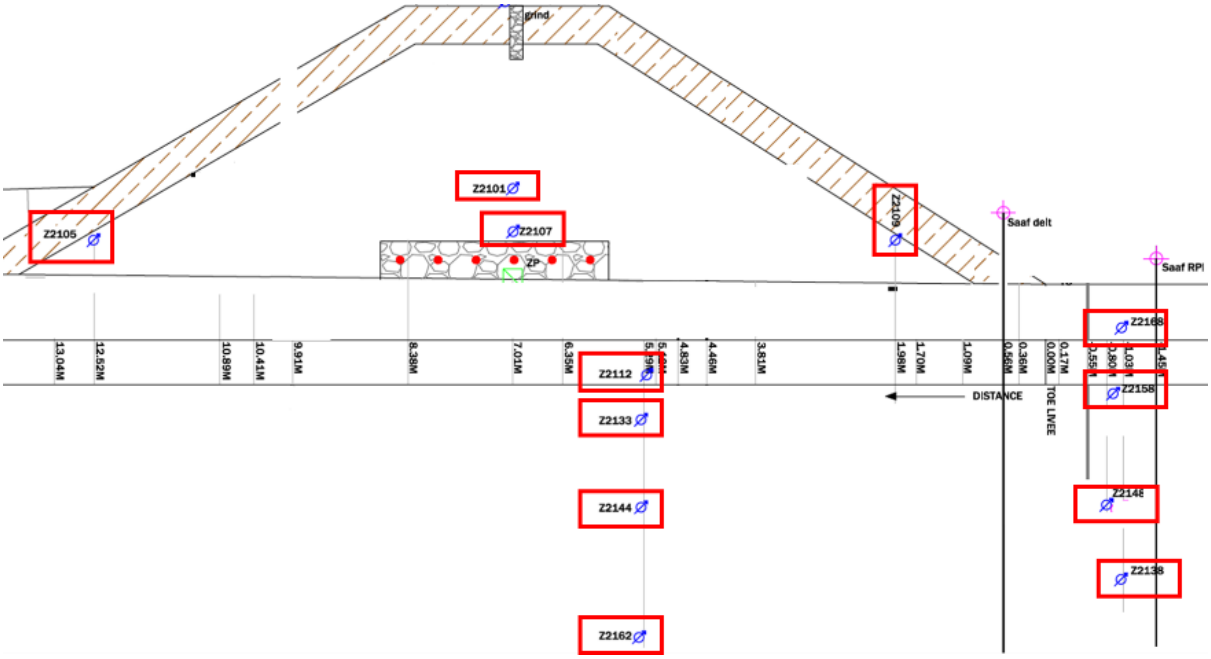

Figure 21; Locations Piezometers east section Southdike (A.R. Koelewijn, 2012)

The piezometers monitored the hydraulic heads inside the core of the Southdike for the complete time of the experiment. The derived results of the piezometers located in the dike core are shown in Figure 22. To use the delivered time dependent data for the stationary conditions of the CMS-model the following steps are undertaken. The initial value and the final value of the simulation are compared with the initial and final condition of the CMS-model (t=118.5hrs). Because the hydraulic head does sometimes have such a variability, the initial hydraulic head is determined based on an average from t=0hrs till t=3hrs. The final hydraulic head is based on an average between the moments t=116hrs and t=119hrs, see Figure 22.

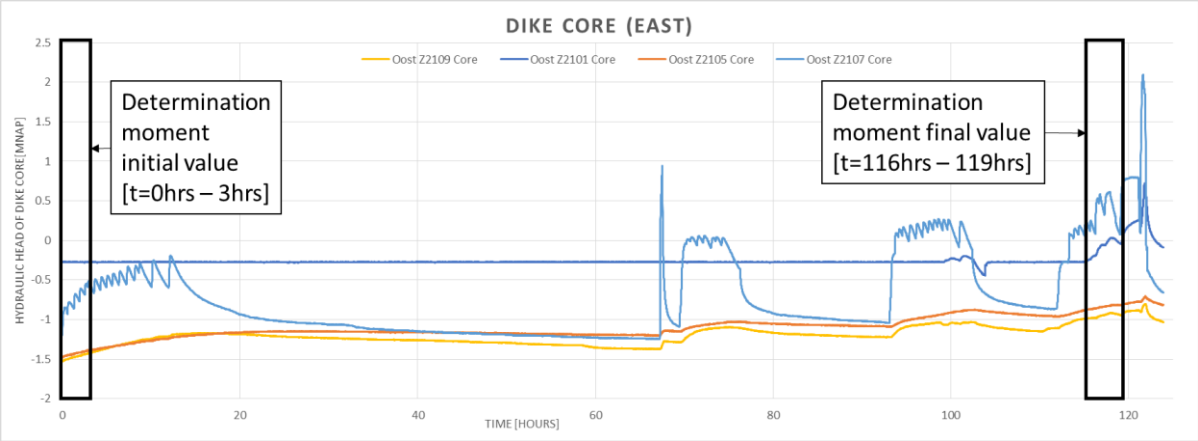

Figure 22; measured hydraulic heads from piezometers dike core

The hydraulic heads for all the piezometer locations, based on this method are shown in Table 5.

Sensor	Location	Depth [m]	Initial Hydraulic Head [m]	Final Hydraulic Head [m]
Z2162	Pleistocene sand	-6	-1.5	-1.8
Z2138	Pleistocene sand	-5.25	-1.4	-1.8
Z2152	Below dike crest	-5.25	-1.25	-1.25
Z2148	Below toe dike	-4.25	-1.4	-1.7
Z2144	Below dike crest	-4.25	-0.65	-0.65
Z2158	Below toe dike	-2.78	-1.2	-1.7
Z2133	Below dike crest	-3.13	-1.5	-0.5
Z2168	Below toe dike	-1.91	-1.5	-1.7
Z2112	Below dike crest	-2.54	-1.5	-0.4
Z2101	Core dike	-0.27	-0.3	0
Z2105	Core dike	-1.75	-1.5	-0.9
Z2107	Core dike	-1.77	-0.85	0.5
Z2109	Core dike	-1.64	-1.5	-0.8

Table 5; Hydraulic head validation data

Displacements

The displacement validation data is derived from two SAAF inclinometers of Deltares placed at the toe of the South dike. One inclinometer named SAAF Deltares was located 0.56m inside the toe on the North side of the dike. The second inclinometer, called SAAF RPI, was located 1.45 m out of the same toe on the North side of the dike, see Figure 23.

The determined moment of physical failure at t=118.5hrs is also used for the validation of the displacements because after this moment the soil of the dike will slip along the slip circle creating extremely large displacements which could not be simulated with the CMS-model (see discussion). The effect of slip on the total displacements (after physical failure of the dike) is shown in Table 6.

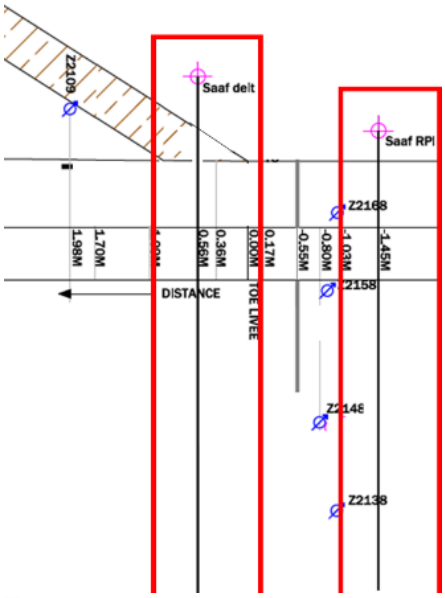

Figure 23; Locations SAAF inclinometers (A.R. Koelewijn, 2012)

Situation	East in toe	Middle under crest	Middle in front of toe	West in front of toe	West in toe
Thursday					
7:50 am	43mm	37mm	49mm	56mm	44mm
Saturday					
1:53 pm	115mm	145mm	160mm	140mm	135mm
2:13 pm	145mm	190mm	200mm	175mm	155mm
2:27 pm	180mm	430mm	470mm	310mm	320mm
2:30 pm	225mm	1450mm	1650mm	900mm	830mm

Table 6; Horizontal displacement measured by inclinometers (A.R. Koelewijn, 2012)

The SAAF inclinometers delivered two types of data, displacement in time and displacement over depth. In Figure 24 is shown how the total displacement at a specific locational depth is determined based on the displacements plotted over time.

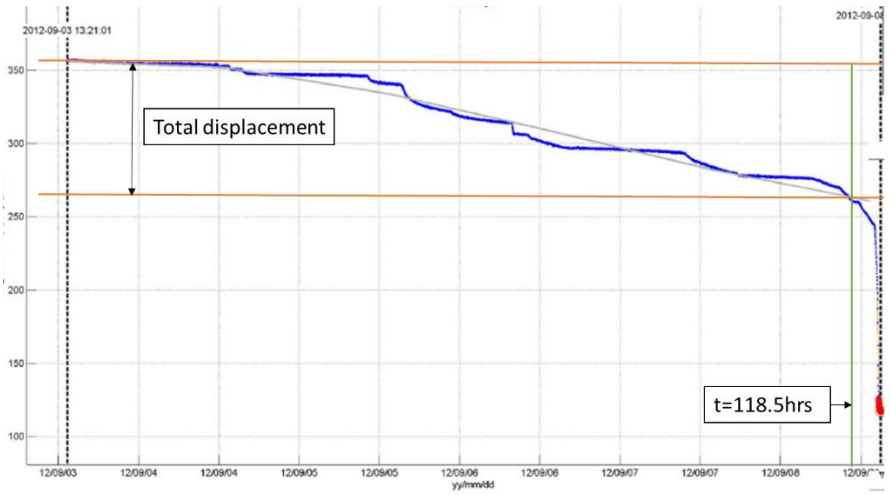

Figure 24; Total displacement in time, Deltares at east section (A.R. Koelewijn, 2012)

The results used for validation are shown in Table 7.

Name sensor	Depth in soil [m]	Total displacement sensor [m]
SAAF Deltares	-2.7	0.0812
SAAF Deltares	-2.1	0.0857
SAAF Deltares	0	0.0926
SAAF RPI	-2.1	0.0941
SAAF RPI	0	0.0864

Table 7; Displacement at depth

In Figure 25 total displacement at the moment of failure (t=118.5hrs) is plotted against the locational depth of the SAAF inclinometer. The color of the graph indicates the scale of the displacements, green is small displacement and red indicates relative huge displacements.

*The shape of this plot for the SAAF Deltares a*nd *SAAF RPI of the east section can be used for validation.*

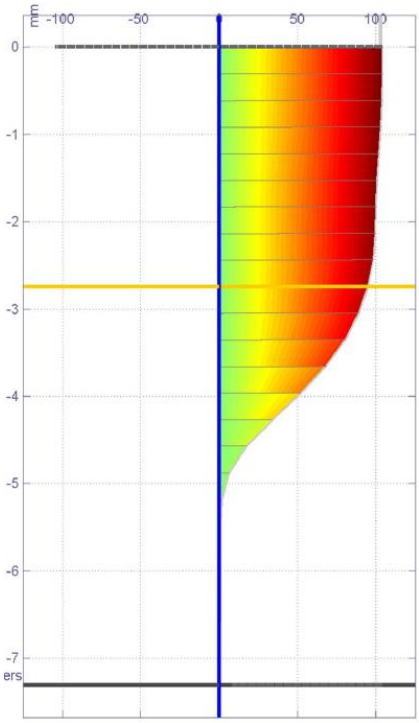

Figure 25; Total displacements at failure along SAAF inclinometer (Vries et al., 2012)

Chapter 3. Development of the macro-stability model

In this chapter the first research question will be answered: '*To what extent can the model reproduce macro-stability of the Southdike experiment*'? This chapter starts with a general description of the final model which in the next sections will be elaborated and supported with some detailed information and assumptions with the applied physics and software used. At the end of the chapter the internal validation is presented to elaborate on the numerical consistency of the model.

3.1. General macro-stability model

To model the geotechnical conditions which have an effect on macro-stability, a 2D coupled model build in COMSOL 4.4, using two mathematical models to describe the behavior of the dike under hydraulic and mechanical loads, has been made. Based on literature reports and other studies, the choice has been made to apply a coupled combination of a Darcy model for modelling the flow of water in the porous media and a Drucker-Prager linear elastic perfectly plastic model for modelling the soil displacements (and effective plastic strains) in the soil skeleton. COMSOL uses a Newton-Raphson iteration scheme to solve the nonlinear algebraic equations at each integration step. During Newton-Raphson iterations, systems of linear algebraic equations are solved by a direct PARADISO solver which is based on LU composition (Inc, 2012). The PARADISO solver is used because it is able to solve quite-ill conditioned problems, it can store the solution out-of-core and tends to be the fastest solver (Inc, 2012).

The defined model used to calculate macro-stability of a dike is in this report called the CMS-model (COMSOL Macro-Stability model). The CMS-model contains all the defined conditions and aspects of the Southdike experiment, which are shown in shown in Figure 26. For better convergence of the CMS-model, since in calculates high non-linear soil mechanical equation, the dike top (green) and subsoil (red) will be in separated stages applied to the model. The subsoil will firstly be induced as foundation of the dike after which the load of the dike top will be gradually applied into the CMS-model. The piezometers (black dots) and SAAF inclinometers (black lines) are as mentioned in chapter 2 used for the validation of the model.

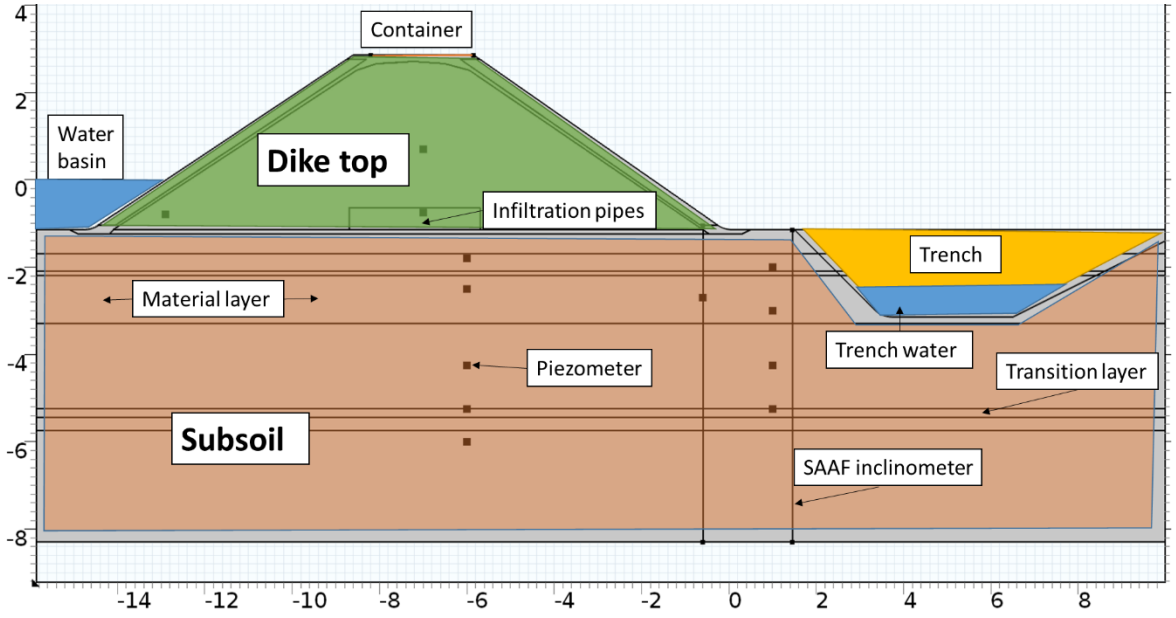

Figure 26; Geometry Southdike in COMSOL

The defined conditions and aspects of the CMS-model are in COMSOL described in the MODEL TREE, see Appendix C. In this Appendix C an overview of this MODEL TREE with all the functionalities and operations

needed for building and solving the CMS-model as well as processing the results is shown. All the components of this MODEL TREE can be viewed as building blocks for the CMS-model. A rough schematization of the MODEL TREE for the CMS-model is shown in Figure 27 to explain how all the components of COMSOL are combined to calculate the physics of the CMS-model. In Figure 27 only the input-output relation between the different components is described, it does not represent the steps in which the CMS-model calculates the final solution.

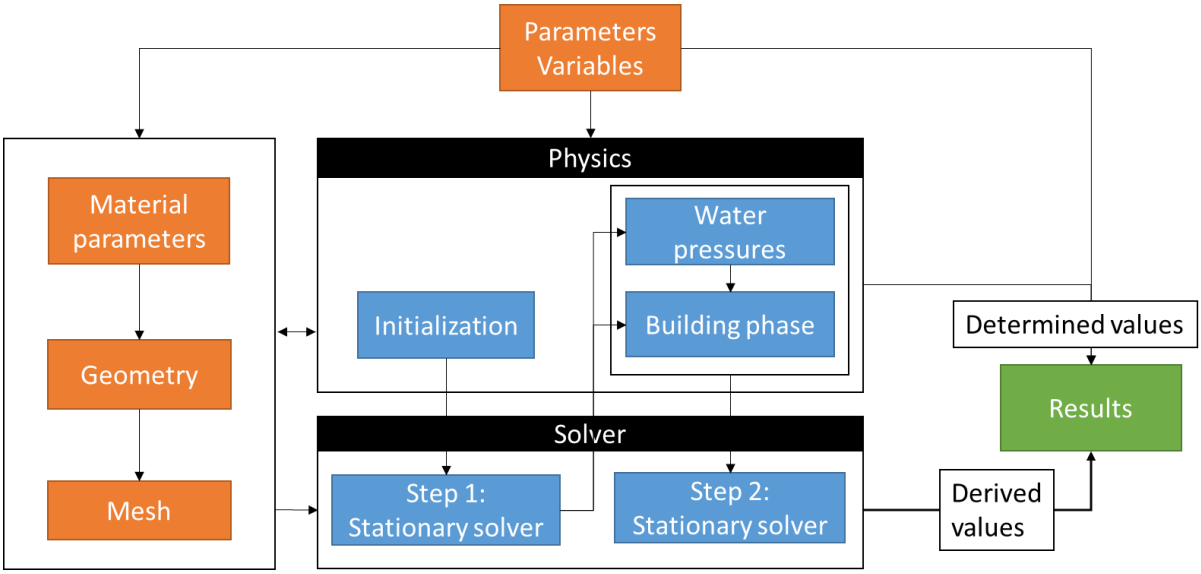

Figure 27; Input-output relation between components within the MODEL TREE of the CMS-model

The main part of the CMS-model is the 'Physics' block. This part represents the physical interfaces which compute the physical equations of the CMS-model. Each single physical-interface calculates its own type of physics, which can be determined with the physical nodes within the specific physical interface. The CMS-model contains three phases, containing physical interfaces; 'Initialization', 'Water pressures' and 'Building phase'. All these phases are separately elaborated in the following paragraphs, zooming in on the founding theories defining the equations and the structure of the related phase.

These physical interfaces will be calculated with two stationary solvers. Solver 1 calculates the 'Initialization', input for the 'Water Pressures' and the 'Building phase' physical interfaces, after which Solver 2 calculates those two physical interfaces simultaneously.

Input for the physical interfaces are the supporting building blocks marked in red (Parameters, Geometry and Mesh). The 'Parameters and Variables' component defines all the parameters and variables which are used as input for all the other components of the CMS-mode. Based on the geometry drawn in the 'Geometry' component physics is addressed to specific parts of the Southdike the same as defining the different soil layers with the 'Material parameter' component. The 'Mesh' component, based on the drawn geometry, is input for the solver to carry out the Newton-Raphson iteration scheme.

3.2. Initialization

The 'Initialization' phase represents the initialization of the CMS-model by calculating the initial stress and strains present in the Southdike. The calculated initial stresses of the 'Initialization' phase are used as initial value for the 'Building' phase. Without these initial conditions the model does not work.

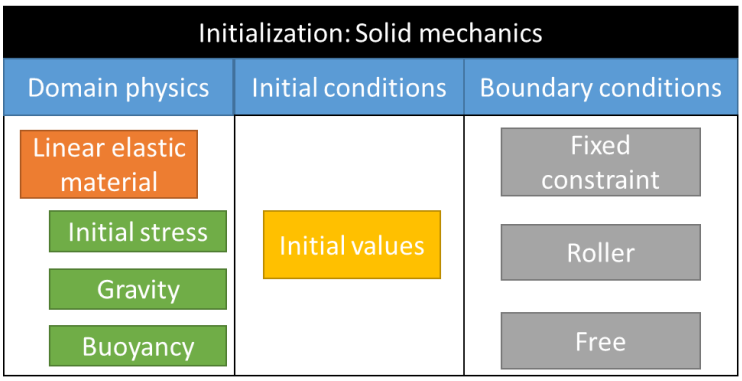

Figure 28; Structure of Initialization physical interface

For the initialization the **Solid Mechanics** (*solid*) physical interface is used. The solid mechanics physical interface is based on solving Navier's equations and computes the stresses and strains and related displacements with the linear elastic material node (Inc, 2012).

To calculate the displacements in the soil, effective stresses have to be determined within the Southdike. Therefore the Solid mechanics physical interface has been modified. In the following section first some theory of soil mechanics is presented to better explain how and why the linear elastic node of the Solid mechanics physical interface is modified.

3.2.1. Theory of soil mechanics

To simulate the behavior of the dike (earth structure), the CMS-model simulates the soil skeleton as a deformable continuum which is subjected to hydraulic and mechanical loads (Melnikova, 2014). For simulating the behavior of the soil various constitutive models have been developed[3], of which the classical isotropic linear elastic perfectly plastic soil model is assumed to be the most suitable one for this study (see Appendix D).

The standard stress-strain relation, see situation on the left in Figure 29, material/soil will first be in the elastic region reaching the elastic limit (yield point) and thereafter in the plastic region in which it plastically deforms and finally fails. The applied elastic perfectly plastic model will however assumes the soil is elastic up to the yield point and perfectly plastic thereafter, see situation on the right in Figure 29. Perfectly plastic implies that it cannot support any further load, so any load that appears beyond this is redistributed to other parts of the dike. When all the stressed material has become plastic by this load redistribution the limit criterion has been reached and failure occurs.

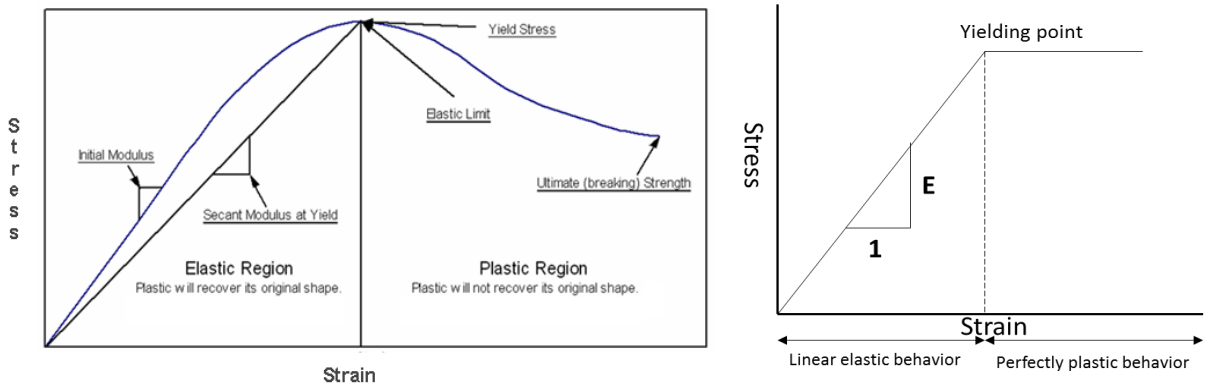

Figure 29; Standard stress strain relation vs. elastic perfectly plastic assumption

[3] Multiple models have been made because simulating soil behavior is difficult because the soil is a multi-phase material which makes the components of soil very complex (Chi Fai Ng, 1994).

The defined elastic perfectly plastic relation between stress and strains is the basis for calculating the soil strength which determines the stability of the dike. The soil strength is mostly dependable of the gravity of the soil through self-weight and stress applied to the soil. Deformation of the particles itself by compression does almost have no contribution to displacements (Ibsen & Jakobsen, 1998).

Effective stress

The structure of the soil is generally formed by quarts particles with voids in-between filled with water and air (Verruijt, 2001). The structure of a soil is of great importance as the particle structure of a soil can carry both normal and shear stress, whereas fluid and air can carry normal stress but not shear stress ((Mitchell and Soga; 2005) as cited in Verruijt, 2001). This important observation is used by Terzaghi for forming the Terzaghi's Law of Effective stress. This law describes that when a (confined) layer of saturated soil is suddenly compressed with an axial load, the load is initially borne entirely by the fluid (Melnikova, 2014). In time, however the load is shifted in part to the structural matrix. Thus the total load is held by the sum of structural stress and the pore pressure (Melnikova, 2014). This can be mathematically expressed (for all stress tensors) by ((Terzaghi, 1943) as cited in Melnikova, 2014);

$$\sigma_{\text{eff}} = \sigma_{\text{ij}} + p\underline{\underline{\text{I}}} \rightarrow \begin{bmatrix} \sigma_x - p & \tau_{xy} & \tau_{xz} \\ \tau_{xy} & \sigma_y - p & \tau_{yz} \\ \tau_{xz} & \tau_{yz} & \sigma_z - p \end{bmatrix} = \begin{bmatrix} \sigma_x & \tau_{xy} & \tau_{xz} \\ \tau_{xy} & \sigma_y & \tau_{yz} \\ \tau_{xz} & \tau_{yz} & \sigma_z \end{bmatrix} + \begin{bmatrix} -p & 0 & 0 \\ 0 & -p & 0 \\ 0 & 0 & -p \end{bmatrix} \quad \textbf{(4)}$$

Where the effective stress tensor $[\sigma_{\text{eff}}]$ describes the stressed state of the soil skeleton. This is the sum of the total stress tensor $[\sigma_{\text{ij}}]$ (obtained from equilibrium equation) and hydrostatic water pressure tensor $[p\text{I}]$. The total stress tensor is describes the total (wet) weight of the soil and, if present, increased with the external load at the surface. The hydrostatic pore water pressure describes the effect of water on the soil skeleton, also called the buoyancy effect. Pore water pressure is a compressive stress and is therefore negative (positive structural stress is a tensile stress on the structural matrix), this means water resists to compressive load (Inc, 2013a).

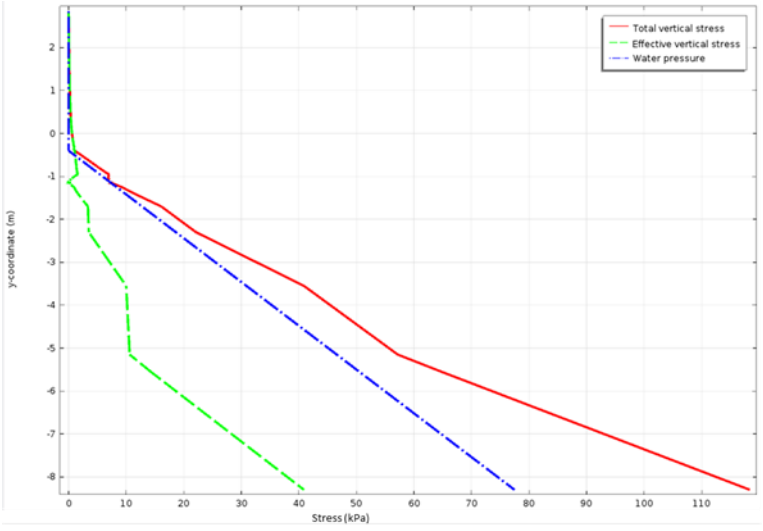

Figure 30; Initial total and effective stress and water pressure in the soil calculated in the 'Initialization' phase

The principles of effective stress asserts that the effective stress controls the stress strain, volume change and strength properties of a soil independent of the pore pressure ((Mitchell and Soga; 2005) as cited in Melnikova, 2014). This is the key difference between standard structural analysis and the one carried out in this report combining a fluid model with a structural model, shown in Figure 30.

3.2.2. Linear elastic material

The Linear Elastic Material node in COMSOL adds the equations for the defined isotropic linear elastic perfectly plastic soil and an interface for defining the related material properties (Poisson value and Young's Modulus). In this material interface the soil will be defined in a wet or dry condition, determining the density

of the soil. The soil is assumed dry if the pore water pressure (Darcy module) is negative, otherwise the soil is assumed to be wet. A dry soil is then defined as: $is_{dry} = p < 0$

This makes it possible to define the density, in this example of sand, for a specific location:

$$\rho_{sand} = \frac{\left(is_{dry} * 18\left[\frac{kN}{m^3}\right] + \left(1 - is_{dry}\right) * 20\left[\frac{kN}{m^3}\right]\right)}{g_{const}} \quad \text{with} \quad g_{const} = 9.81\frac{m}{s^2} \tag{5}$$

For modeling the effective stresses and the related displacements according to Terzaghi, three types of nodes are added to the model:

1. *Initial stress (and strain) node*

The initial stress node defines the stress state in the structure before any constraint or load is applied (Inc, 2013b). To define the initial pore pressures in the soil, an initial hydraulic head is defined as parameter (H_{ini}) which is used to define the initial water pressure (p_{ini}) variable for the 'Initialization' phase:

$$p_{ini} = (H_{ini} - y) * \rho_{water} * g_{const} \tag{6}$$

The value of p_{ini} can be applied as initial stress in the model by:

$$\sigma_{ij} = \begin{bmatrix} -\min(-p_{ini}, 0) & 0 & 0 \\ 0 & -\min(-p_{ini}, 0) & 0 \\ 0 & 0 & -\min(-p_{ini}, 0) \end{bmatrix} \tag{7}$$

2. *Gravity node*

The gravity node will apply gravitational forces at all the physics that has a mass distribution (Inc, 2012). The gravity acts in a fixed spatial direction, in this case negative y-direction. Without other loads or external forces this load will define the total stress in the geometry.

3. *Buoyancy load node*

The effective stress is the difference between the total stress (gravity node) and the pore pressure (p_{ini}). To count for the pore pressure, acting as normal stress, a load is defined in the opposite direction (positive y-direction) of the gravitational force, better known as buoyance force;

$$F_B = (p_{ini} > 0) * g_{const} * \rho_{water} \tag{8}$$

Governing equations

Overall the CMS-model simulates the soil strength by calculating the effective stress influence on the elasto-plastic deformation of the soil skeleton. This is described by the general equations of plastic flow theory in which the linear elastic perfectly plastic strains of the soil skeleton are calculated ((Hill, 1950) as cited in Melnikova, 2014);

$$\begin{gathered} \nabla \cdot \sigma_{ij} + \rho_s g_{const} = 0 \\ \sigma_{ij} = \sigma_{eff} - p \text{ if } p \geq 0 \\ \sigma_{eff} = \frac{E}{1+\nu}\left[\frac{\nu}{(1-2\nu)}\varepsilon \underline{\underline{I}} + \underline{\underline{\dot{\varepsilon}}}\right] \text{ if } F < 0 \\ \underline{\underline{\dot{\varepsilon}}}_{p} = -q\frac{\partial P}{\partial \sigma_{eff}}, \underline{\underline{\dot{\varepsilon}}} = \underline{\underline{\dot{\varepsilon}}}_{p} + \frac{1}{3K} I_1 \cdot \underline{\underline{I}}, \text{if } F = 0 \end{gathered} \tag{9}$$

Where $\nabla = \underline{e}_x\frac{\partial}{\partial x} + \underline{e}_y\frac{\partial}{\partial y} + \underline{e}_z\frac{\partial}{\partial z}$ is the gradient operator; ρ_s is soil density; g_{const} is gravity vector; σ_{ij} and σ_{eff} are the total and effective stress tensors, respectively (compressive stresses are negative); E is Young's modulus; ν is Poisson ratio; $\varepsilon = \varepsilon_{xx} + \varepsilon_{yy} + \varepsilon_{zz}$ is volume deformation (positive for expansion); $\underline{\underline{I}}$ is the

unit tensor; $\dot{\underline{\underline{\varepsilon}}} = (\nabla \underline{U} + (\nabla \underline{U}^{T})/2$ is the deformation tensor; $\underline{U}$ is vector of displacements; $\dot{\underline{\underline{\varepsilon}}}_{p}$ is plastic deformation rate tensor; q is plastic multiplier; F is plastic yield function (F<0 corresponds to elastic behavior, F=0 refers to plastic yield); $K = \frac{E}{3(1-2\nu)}$ is bulk modulus; $I_1 = \sigma_{xx_{eff}} + \sigma_{yy_{eff}} + \sigma_{zz_{eff}}$ is the first effective stress variant.

The flow rule $\dot{\underline{\underline{\varepsilon}}}_{p} = q \frac{\partial P}{\partial \underline{\underline{\sigma}}_{eff}}$ defines the relation between the plastic strain increment in a given direction and the current level of stress in the same direction. If the yield surface, F, and the plastic potential, P, are identical (F=P), then it is called an associated flow rule, otherwise it is called non-associated flow rule (Melnikova, 2014).

The CMS-model is quasi static; inertia effects are not taken into consideration, so inertial mass of an element is irrelevant (no second order time derivatives) (Augustesen, 2006). The mechanical conditions are calculated under plain strain conditions. This is appropriate because the Southdike has a long extend in z-direction compared to the x and y directions in which plane strain conditions prevail (Inc, 2013a). Secondly most researches assume plane strain conditions for numerical simulations of earth structures (Bergado & Teerawattanasuk, 2008).

3.2.3. Initial conditions

The Initial Values node adds initial values for the displacement field and structural velocity field that can serve as an initial condition for a transient simulation or as an initial guess for a nonlinear analysis (Inc, 2012). The CMS-model uses the natural initial condition for a mechanical model assuming zero plastic strain in the domain $\dot{\underline{\underline{\varepsilon}}}_{p} = 0$

3.2.4. Boundary conditions

Within the solid mechanics interface it is possible to use two types of boundary conditions (Melnikova, 2014):

(a) Displacement specified at the boundary; $S1: \underline{U}|_{S1} = \underline{U}_{S1}$
(b) Loading specified at the boundary; $S2: n \cdot \sigma_{ij}|_{S2} = F_{S2}$

For the CMS-model the following specific boundary conditions were applied:

At the bottom of the geometry the **Fixed Constraint** boundary node is implied. This node adds a condition that makes the geometric entity fixed (fully constrained); that is, the displacements are zero in all directions.

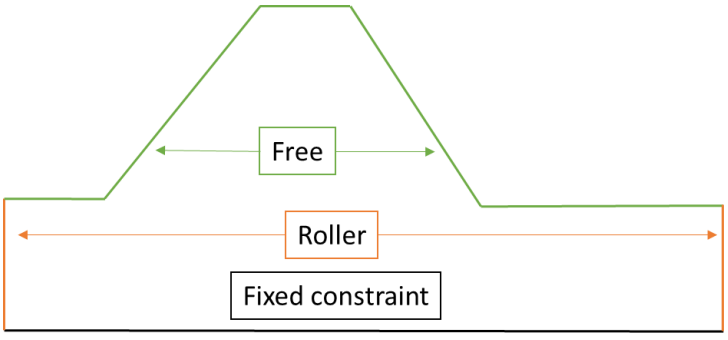

Figure 31; Boundary conditions Initialization

Along the horizontal boundaries the **Roller** boundary node is added. The roller node adds a roller constraint as the boundary condition; that is, the displacement is zero in the direction perpendicular (normal) to the boundary, but the boundary is free to move in the tangential direction (Inc, 2012).

The **Free** node is the default boundary condition (placed automatically at the remaining boundaries) defining no constraints and no loads acting on the boundary.

3.3. Water pressures

In the second phase the hydraulic parameters of the dike under different conditions, using **Darcy's Law** (*dl*) physical interface, will be calculated. Based on the hydraulic parameters the effective stresses can be determined as well as the saturation of the soil.

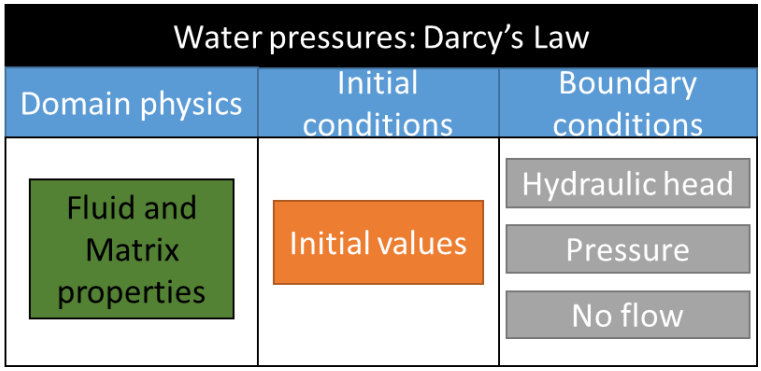

Figure 32; Darcy's Law physical interface overview

The physical interface of Darcy's Law has in COMSOL one main node called Fluid and Matrix properties. Initial values are used as initial condition for the interface. The boundary conditions will be defined as quasi-time steps. This option makes us able to define the conditions of the hydraulic parameters for the whole loading stage of the model, to be able to model the groundwater flow of the Southdike experiment.

3.3.1. Darcy's Law

The main node of Darcy's interface will describe the flow of water using Darcy's Law (1856), in which is stated that the filtration velocity *u* is linear proportional to the pore water pressure (∇p) gradient and to the gravity acceleration(ρg_{conts}) (Melnikova, 2014):

$$\vec{u} = -\frac{\kappa}{\mu}(\nabla \mathrm{p} + \nabla \rho_w g_{const}) \quad \textbf{(10)}$$

Where κ is the permeability coefficient [m^2], μ is dynamic viscosity of water [$Pa \cdot s$], ∇ is the gradient operator, p is relative (absolute minus atmospheric) pore pressure [Pa], ρ_w is the density of water [kg/m^3] and g_{const} is the standard gravity [m/s^2] (Melnikova, 2014).

Darcy's Law physical interface uses the permeability coefficient to calculate the water flow in porous media while in most of the literature the hydraulic conductivity (K) is used. COMSOL uses permeability because it can be defined as a property of the porous media and not of the fluid (Bear, 1979). The hydraulic conductivity can be recalculated into permeability with the following formula:

$$\kappa = K\frac{\mu}{\rho_w g_{const}} \quad \textbf{(11)}$$

Where K is the hydraulic conductivity, [m/s]. In the CMS-model this is done by defining $\frac{\mu}{\rho_w g_{const}}$ as a parameter which makes it easily to recalculate the given hydraulic conductivities into permeability values.

Based on the filtration velocity COMSOL calculates the groundwater flow derived from the Darcy law and mass conservation equation (Inc, 2012).

$$\frac{\partial}{\partial t}(\rho \varepsilon_p) + \nabla \cdot (\rho \vec{u}) = Q_m \quad \textbf{(12)}$$

Under assumption that (a) water is incompressible and (b) the time derivative of filtration velocity is negligibly small $\frac{\partial \vec{u}}{\partial t} = 0$ follows the other main equation used in COMSOL:

$$\nabla \cdot \left[-\frac{\kappa}{\mu}\nabla \mathrm{p}\right] = Q_m \quad \textbf{(13)}$$

Where Q_m is the volume intensity of external sources and sinks.

3.3.2. Initial conditions

The initial conditions for the Darcy's equation are normally not of major importance in the most often used time-dependent study because the initial pore pressures will then fully dissipate in a finite period of time under influence of the external hydraulic loads (Melnikova, 2014). But because the CMS-model uses a stationary solver to calculate the groundwater flow the initial conditions are important for the technical implementation in the software module. The initial condition is based on the pressures calculated with the initial hydraulic head determined for the dike model. The initial hydraulic head was defined as H_{ini}. Therefore the initial pressure state for the Darcy module is defined as:

$$P_{ini} = (H_{ini} - y) * 1000\left[\frac{kg}{m^3}\right] * 9.81\left[\frac{m}{s^2}\right] \quad \textbf{(14)}$$

3.3.3. Boundary conditions

The boundary conditions within Darcy's Law define the progress of the hydraulic parameters in the stationary conditions. Two types of boundaries could be chosen for Darcy's equation. Here the general equations are formulated:

(1) Hydraulic head (pressure) specified at the boundary; $S1$: $p|_{S1} = \rho g(H_0 - y)$ (DIRICHLET condition) If the Hydraulic Head is equal to zero this refers to seepage to atmosphere (Melnikova, 2014)

(2) Specified flow boundaries (NEUMANN conditions), flow velocity across the boundary; $S2$: $V_n|_{S2} = n \cdot [-\kappa\nabla(p + \rho g y)]$, where n is the normal to the boundary surface (Melnikova, 2014).

For the CMS-model only the DIRICHLET boundary conditions is applied shown in Figure 33. Something which is not shown in the figure is that the value of the hydraulic head is not constant along all the boundaries of the CMS-model. The value of the hydraulic head is partially determined out of calibration with the used validation data (2.3).

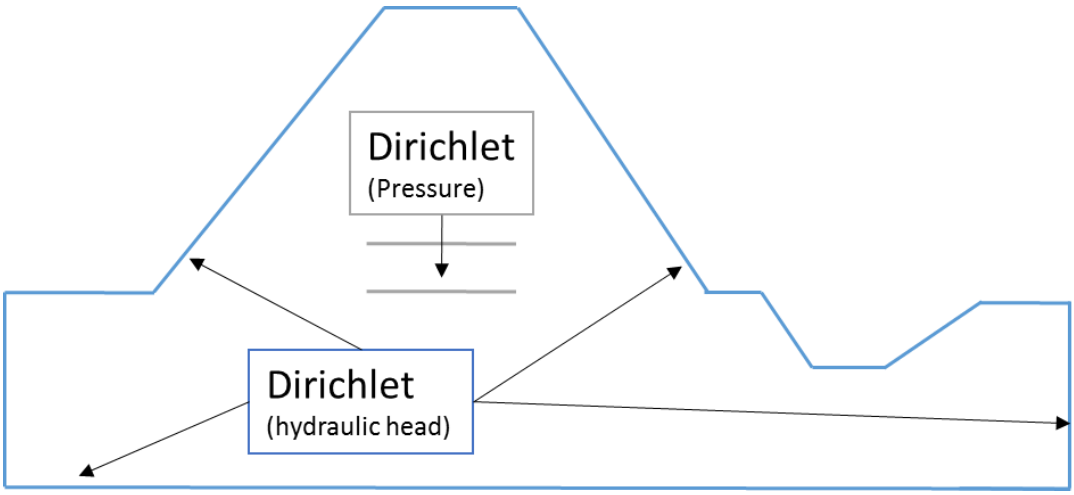

Figure 33; Boundary conditions water pressure stage

3.4. Building phase

The last step of the CMS-model is the building phase. The goal of this phase is to calculate stresses and strains in the geometry occurring due to implied pressures and loads. For the building phase the **Solid Mechanics** (*solid*) physical interface will be used. The structure of the building phase is almost equal to the initializing phase. The key difference is that in this phase the linear elastic material node is extended with the soil plasticity function. With this function the effective plastic strains will be calculated which are vital in show the macro-instability slip circle.

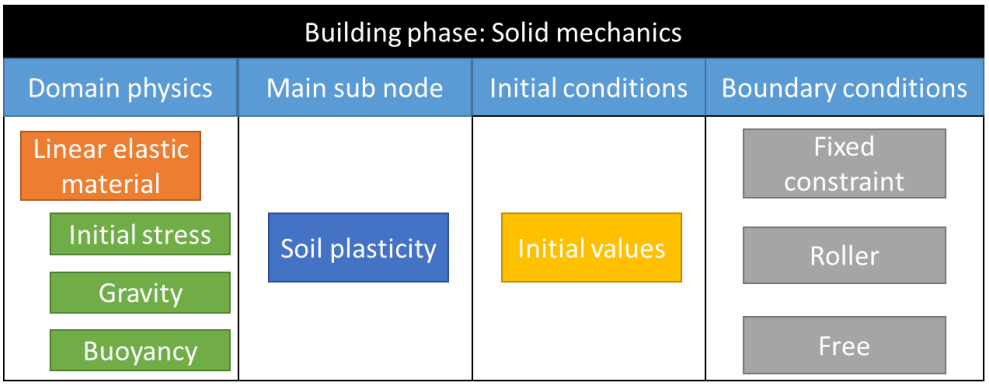

Figure 34; Building phase overview

In the soil plasticity function use a plasticity model to calculate the effective plastic strains. In the following section some theory about these models, and the governing equation of the Drucker Prager soil model used for the CMS-model is elaborated.

3.4.1. Theory plasticity models

The theory of the plasticity models is based on the stress-strain relationship in soils which are mostly mathematical equations based on empirical tests ((Mitchell and Soga; 2005) as cited in Inc, 2013a). The most widely used material relation for soils is the Mohr-Coulomb equation, better known as the Mohr's circle, which states;

$$|\tau_f| = c - \sigma \tan\phi \quad for\ the\ CMS-model \rightarrow |\tau_f| = c - (\sigma - p)\tan\phi \qquad \textbf{(15)}$$

Where τ_f is the shear stress at material failure on the failure (or slip) plane, see Figure 35. The parameter σ is the normal stress on the shear plane. The c, (effective) material cohesion, denotes for the intercept σ=0, and ϕ defines the slope of the shear plane and is called the (effective) internal friction angle.

The Mohr-Coulomb failure plane describes only the influence of some parameters to the shear resistance of soil. However, the strength of the soil in reality depends on a large number of parameters (Inc, 2013a);

$$\tau_f = F(e, c, \sigma, \phi, C, H, T, \varepsilon, \dot{\varepsilon})$$

Where e is the void ratio (porosity), C, the soil compaction, H, the stress history and T the temperature, ε is the strain state and $\dot{\varepsilon}$ the strain rate. With the simulation of the soil behavior in COMSOL the effect of some of these parameters are neglected because the software does not provide the opportunity to take them into account. The rationale behind this is that for many soil tests these parameters are not available because it's too expensive and time consuming to collect them (Jiang & Xie, 2011).

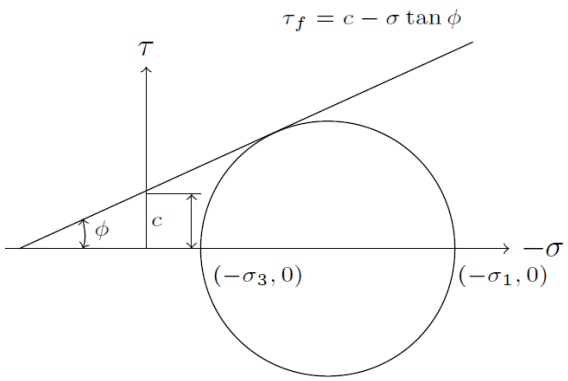

Figure 35; Mohr-Coulomb failure plane (Inc, 2013a)

Plasticity

Since the Mohr-Coulomb stress and strain relation (the linear elastic material node in COMSOL) and related plastic flow and yield conditions are only based on the deviatoric part of the stress tensor a plasticity model (defined in the plasticity node in COMSOL) is needed to take into account the behavior of frictional materials (Bocchi, 2014). Plasticity models with yield functions describe the relationship between stress and strain for a material which exhibits an elastic-plastic response (Bocchi, 2014). Plastic behavior is characterized by an irreversible straining which is independent of time and which can only be sustained once a certain level of stress has been reached (Hill, 1950). There are two classical plasticity models (Mohr-Coulomb and Drucker-Prager) which are commonly used as strength theory in geotechnical engineering. The Drucker-Prager is chosen because it is the most practical option of the two, see Appendix E.

Drucker-Prager

The Drucker Prager (1952) strength criterion, called the Extended Von Mises criterion as well, has been widely used in geotechnical engineering to predict failure strength and be employed for plastic potential in continuum damage mechanic model (Jiang & Xie, 2011). The Drucker Prager model assumes that volume deformations of soil are always elastic, while plastic yielding occurs due to the shear deformations in soil, with sliding between material planes (Melnikova, 2014). The general yield function for the Drucker Prager criterion is expressed by

$$\alpha\sigma_{\mathrm{ij}} + \sqrt{J_2} + -k = 0 \quad \textbf{(16)}$$

In all constitutive models, plasticity yield function $F(\sigma_{\mathrm{ij}})$ is defined as a function of principal stresses or stress tensor invariants. This provides the yield surface, **F**, for the Drucker-Prager criterion is given by:

$$F = \sqrt{J_2} + \alpha I_1 - k = 0 \quad \textbf{(17)}$$

Where I_1 is the first stress invariant and J_2 is the second deviatoric stress invariant. The first effective stress invariant is defined using the trace of Cauchy stress tensor:

$$I_1 = trace(\sigma_{\mathrm{ij}}) \quad \textbf{(18)}$$

The second effective stress invariant is defined by

$$I_2 = \frac{1}{2}\left(I_1^2 - trace({\sigma_{\mathrm{ij}}}^2)\right) \quad \textbf{(19)}$$

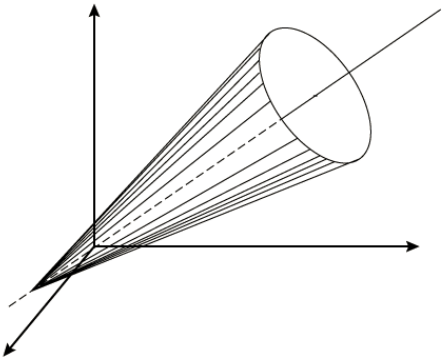

Figure 36; Drucker Prager yield surface (Bocchi, 2014)

The second deviatoric stress invariant can be expressed using the first and the second stress invariants:

$$J_2 = \frac{1}{3}I_1^2 - I_2 \quad \textbf{(20)}$$

The coefficients of the Drucker-Prager model α and k will be matched to the coefficients in the Mohr-Coulomb criterion (cohesion and internal friction angle) because these are available from soil data. This is expressed by;

$$\alpha = \frac{2}{\sqrt{3}} \cdot \frac{sin\phi}{3 \pm sin\phi} \quad and \quad k = \frac{2\sqrt{3}c \cdot cos\phi}{3 \pm sin\phi} \quad \textbf{(21)}$$

3.4.2. Linear elastic material + soil plasticity

In this 'Building' phase the **Solid Mechanics** (*solid*) physical interface contains the linear elastic material node and the soil plasticity node. The following nodes firstly determine the effective stress (Terzaghi):

1. *Initial stress (and strain) node*

For proper functioning of the model a first important step is to add the stresses of the 'Initialization' phase to the model, which can be used as starting point for the calculations. The stress state of the 'Initialization' phase is formulated in COMSOL as; s*olid.s* + a specified coordinate in x-y or z direction. The calculated pore pressures of the Darcy law interface are defined as $+min(-p, 0)$. The effective stress is the sum off the initial stress plus the pore pressures; $solid.sx + \min(-p, 0)$.

But since the initial stress state was already calculated as effective stress based on an initial pore pressure (p_{ini}), these have to be subtracted from the total initial stress state $[-\min(-p_{ini}, 0)]$, otherwise pore pressure are counted double. This leads to the following initial stress node:

$$\sigma_{ij} = \begin{bmatrix} solid.sx + \min(-p,0) - \min(-p_{ini},0) & solid.sxy & solid.sxz \\ solid.sxy & solid.sx + \min(-p,0) - \min(-p_{ini},0) & solid.syz \\ solid.sxz & solid.syz & solid.sx + \min(-p,0) - \min(-p_{ini},0) \end{bmatrix} \quad \textbf{(22)}$$

2. *Gravity and Buoyancy load node*

The stress in the geometry will be implied by the gravity and buoyancy loads. The buoyancy load will be based on the pore pressure determined in the Darcy Law interface. The force on the subsoil is directly implied. For the dike top this is done with incremental steps, in case of the buoyancy force:

$$F_B = (p > 0) * g_{const} * \rho_{water} * int_{buoyancy}(Ramp\_stage) \quad \textbf{(23)}$$

General model

The soil plasticity node contains high non-linear equations and is therefore quite unstable. Multiple solutions have been implemented to create more convergence (stable model):

1. The building phase is modeled with incremental steps to apply all the different loadings, using the function 'auxiliary sweep' of COMSOL: $Implied\ loading = Load * int_j(Ramp\_stage)$.
   The Ramp_stage parameter will increase with the auxiliary sweep simulation, in a stationary model, to partially simulate all the stages of the IJkdijk experiment, 14 steps. All the (loading, boundary) forces are multiplied with a variable (int_J), which is dependent on the parameter 'Ramp_stage'. The variable int_J will be defined by an interpolation function for the specific force.
   The advantage of a slow incremental growth of load is that it ensures a slow variation of the stiffness matrix over the different loading steps. This is provides more stability for the soil plasticity function.
2. A stability factor of 1.5 is multiplied with all the cohesion and internal friction angles of all soil materials, the values which determine the yielding point. By implying a stability factor the model does not have to calculate all the solutions when it is near to failure. When the solutions are far from failure the model runs faster and has a much higher convergence.
3. The solvers of COMSOL could be slightly adapted to deal with the high nonlinearities of the soil plasticity node:
   - Use a constant parametric predictor; In the continuation solver of the parametric steps within COMSOL turn on: 'Use initial damping factor for all parameter steps' and set the predictor on 'Constant'.
   - Turn on the option 'Values of variables not solved for' in the solver of COMSOL. This implies all the values of the 'Initialization' phase are one on one used for the 'Building' phase.

- The method to solve the non-linear equations should be 'Automatic (Newton)' with a low initial damping factor of 0.1.
- The tolerance factor can be reduced from the standard value (1-- 1e-3). The tolerance factor is used for termination of the Newton iterations and is multiplied with the relative tolerance (0.001) which forms the actual tolerance.
- Turn off 'show results while plotting'
- Turn off the geometric nonlinearity option

4. The geometry of the dike can be slightly adapted to create more convergence. Thirst thing is to add transition layers. The transition layer simulates the transition zone also present in inhomogeneous soil (real situation) to reduce differences between the soil strength parameters of the different soil layers. This must provide the model better convergence. For the transition layer, equal depth of both surrounding layers is used and assigned with the calculated average of those surrounding layers. Secondly the geometry is slightly modified. Sharp corners are prevented and replaced by rounding's to prevent extreme values in the corners.

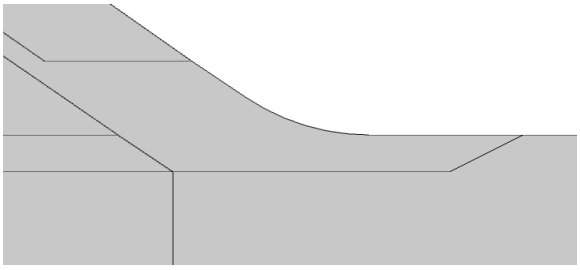

Figure 37; Rounding corners COMSOL (fillet option)

3.4.3. Initial conditions

The CMS-model uses for the building phase the natural initial condition for a mechanical model assuming zero plastic strain in the domain $\dot{\varepsilon}_{=p} = 0$

3.4.4. Boundary conditions

Because the 'Building' phase uses the same Solid Mechanics physical interface the same mechanical boundaries could be applied as presented in paragraph 3.2.4. The boundary conditions, based on the experiment of the Southdike are shown in Figure 38.

At the bottom of the geometry the **Fixed Constraint** boundary node is implied, just like the initial phase. This is also the case for the horizontal boundaries were the **Roller** boundary node is implied.

The **Free** node (default boundary condition) is automatically placed at the remaining boundaries.

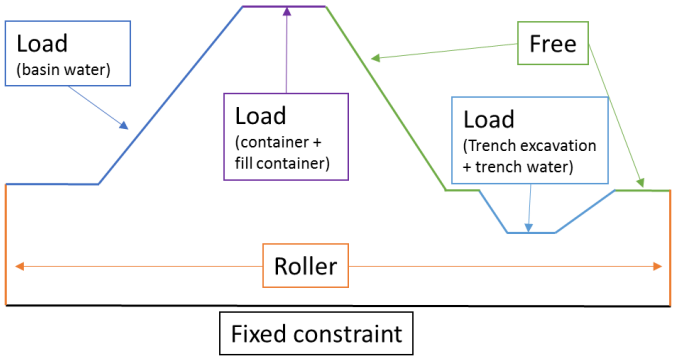

Figure 38; Boundary conditions building phase

During the building phase multiple loadings are added to the model. These will be implied using **Specified Loading** node. The following loadings are implied:

Trench excavation: The boundary of the trench is initialized with a pressure equal to the pressure of the initial situation. This pressure ramped from 1 to 0 in the auxiliary sweep, so the pressure on the soil is gradually removed and with that simulating the excavation of the trench. This is notated as:

$$F_{exc} = \begin{matrix} -(solid2.Tax) * int_{excavation}(Ramp\_stage) \\ -(solid2.Tay) * int_{excavation}(Ramp\_stage) \end{matrix} \quad \textbf{(24)}$$

Weight container: The container is placed on top of the Southdike and had a weight of 3000 tons, a length of 6.7m, an internal width of 2.3m and a height of 1.8m.

$$P_c = 195\left[\frac{kg}{m^2}\right] * g_{const} * int_{container}(Ramp\_stage) \quad \textbf{(25)}$$

Container fill: The volume of the container (28m^3) was filled with water. The container fill load (P_{cw}) is based on the steps taken in the test, which was measured by a Deltares piezometer shown in Figure 39. The figure shows that the water level is raised from zero till 1.75m in six steps. We can also distinguish leakage of water from the containers. This leakage of container #2 at the East side has not been taken into account (A.R. Koelewijn, 2012);

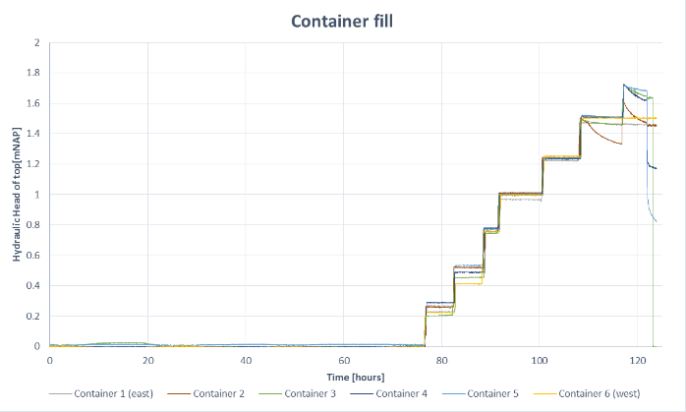

Figure 39; Filling of containers (A.R. Koelewijn, 2012)

$$P_{cw} = 1.75[\mathrm{m}] * \rho_{water} * g_{const} * int_{fill}(Ramp\_stage) \quad \textbf{(26)}$$

Water basin: On the left side of the dike a basin was filled with water. The water level in the basin, relative to N.A.P., measured from the bottom of the basin is shown in Figure 40. The basin load is assumed to be raised till one level (the drop in water level and refills are not taken into account). The maximum water level in the basin is 0.65m. This load in implied as a pressure and as followed defined;

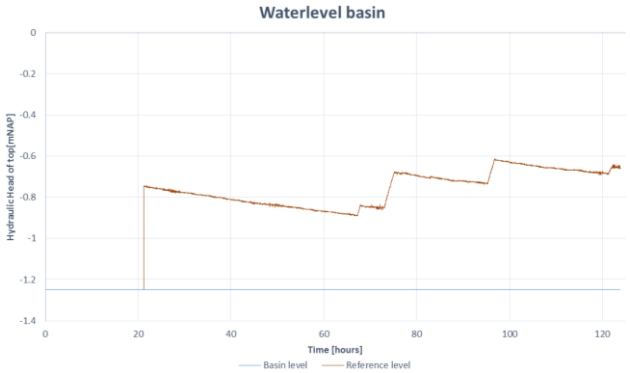

Figure 40; Water level basin (A.R. Koelewijn, 2012)

$$P_b = \left(if\left(y <= -0.6,9810\left[\frac{Pa}{m}\right] * (-0.6 - y), 0\right)\right) * int_{basin}(Ramp\_stage) \quad \textbf{(27)}$$

Trench water: Trench water is measured with the piezometers of Deltares (A.R. Koelewijn, 2012) and gave a maximum water level of 0.75m. At the end of the experiment the water is pumped out of the trench (small drop of water level). This went rather slow based upon the pump discharge, seepage flow into the ditch increased as the level dropped. This went in a non-linear manner and therefore not taken into account (A.R. Koelewijn, 2012). For the loading the water level is used measured relative to the surface level just as presented in Figure 41.

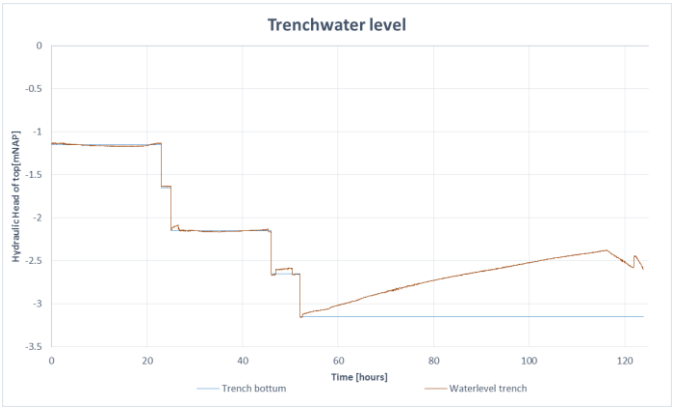

Figure 41; Trenchwater level (A.R. Koelewijn, 2012)

$$P_t = \left(if\left(y <= -2.4,9810\left[\frac{Pa}{m}\right] * (-2.4 - y), 0\right)\right) * int_{trench}(Ramp\_stage) \quad \textbf{(28)}$$

3.5. Internal validation: mesh refinement

The internal validation is performed for the computational mesh of the CMS-model. The mesh in finite element software are the pre-determined quantified grids which limit the calculated solutions. The size and shape of the mesh highly affects the accuracy of the calculated solution, see Figure 42, as well as the computational performance (Pressure Vessel Engineering, 2008). Inaccuracy of the mesh also causes many problems in finite element analysis (Klein, 1999). To deal with this problems, finite element models do not require a uniform precision in the mesh for the simulation, and would be better suited if specific areas which need precision could be refined (Klein, 1999). Therefore a mesh refinement is performed determining the optimal mesh. In a standard mesh refinement the accuracy of the solution within certain sensitive of turbulent regions of simulations is calculated dynamically and during the time the solution (Klein, 1999). Limited time does not allow us to carry out such a study. Luckily COMSOL provides us with already some handy options to refine the mesh iteratively based on computational time, problems during solving and the desired accuracy of our solution.

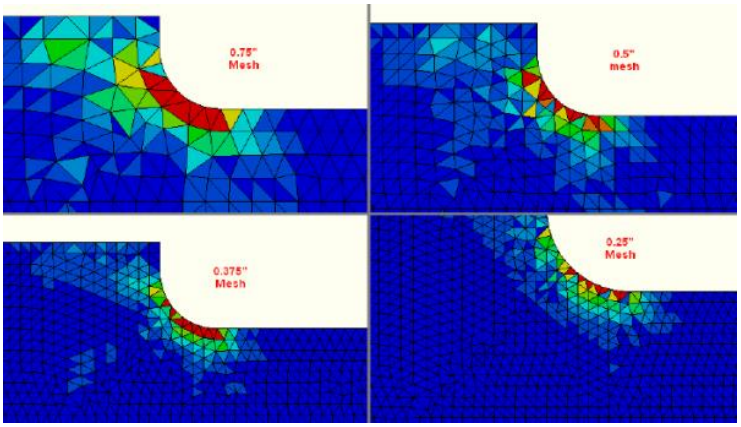

Figure 42; (Pressure Vessel Engineering, 2008)

This is firstly done for the choice of element mesh type. For a 2D environment, the mesh generator in COMSOL can discretize the domains into triangular or quadrilateral mesh elements (Inc, 2012). Both element types are tested resulting shown in Figure 43.

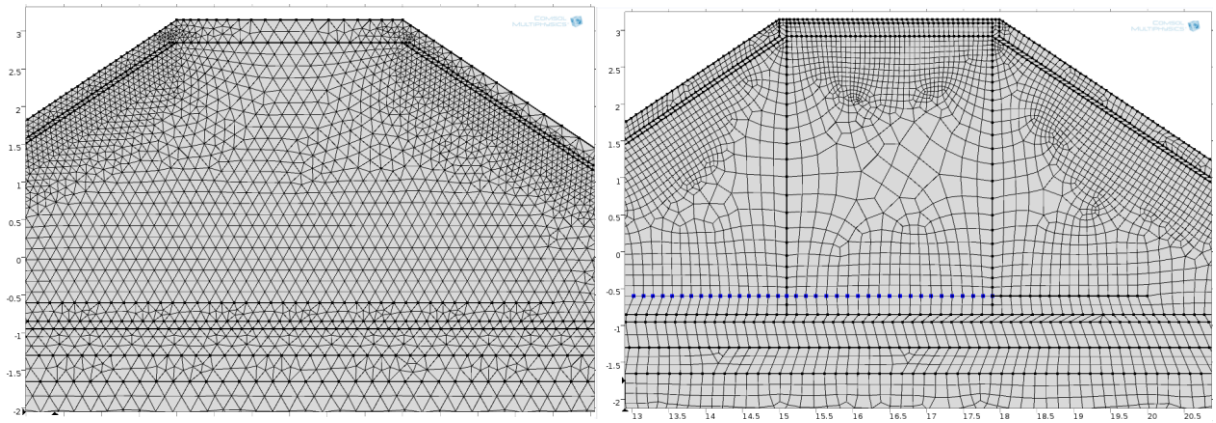

Figure 43; Triangular element mesh vs quadrilateral mesh elements

Results show that triangular elements had more convergence than the quadrilateral elements (in same conditions), see Table 8. This can be caused by the fact that quadrilateral elements perform better in rectangular domains which is not the case for the Southdike.

Mesh type	**quadrilateral elements**	**triangular elements**
Error at stage	1.6 (out of 6)	4.1 (out of 6)

Table 8; Comparison quadrilateral with triangular mesh elements

Based on this result, the optimal size of the triangular elements some is determined (in this run safety reduction stage is not implied). Displacements, hydraulic heads and effective plastic strains are compared for the general situation of the Southdike.

A change in mesh has almost no influence on the calculated values of the pore pressures and displacements (<1%). However, the mesh size has an influence on the effective plastic strains. This is shown in Table 9 where the results of the general mesh sizes are compared to the computational mesh of the CMS-model (value taken from left corner bottom trench).

Size mesh	Elements	Calculation time		Effective plastic strain [-]	
CMS-model	167472 (+831570 internal DOF's)	508 s	(0%)	0.02325	(0%)
Finer	85464 (+421230 internal DOF's)	390s	(-24%)	0.02175	(-7%)
Normal	57636 (+284010 internal DOF's	342s	(-32%)	0.0231	(-1%)
Coarse	49122 (+242010 internal DOF's	277s	(-45%)	0.0218	(-6.7%)

Table 9; Comparison mesh sizes on effective plastic strains

Results show that an increase of the mesh size provides a huge gain in calculation time. The effect of the mesh on the effective plastic strains are relatively low, but should not be underestimated since it are plastic strains defining the potential slip circle. Remarkable is that the normal mesh size simulates better results than the finer mesh. An explanation could be that the normal mesh size better adapts to the many different soil layers of the model.

The effects of the mesh size on the safety factor is shown in Table 10.

Size mesh	Elements	SF	Difference to CMS-model
CMS-model	167472 (+ 831570 internal DOF's)	1.1425	0%
Fine	81482 (+403030 internal DOF's)	1.08	-5.5%
Normal	57378 (+282870 internal DOF's)	1.1025	-3.5%
Coarser	46791 (+230760 internal DOF's)	Error, cannot do complete run	-

Table 10; Comparison mesh sizes on safety factor

A less refined mesh size implies a lower safety factor, so the safety will be underestimated. When the mesh size is too coarse it will lead to a failure of the model (due to high variability of plastic strain between elements).

Based on Table 9 and Table 10, for a practical implementation a normal mesh size would be the most optimal one. For this research this would however have one major drawback, shown in Table 11 and Table 12. Because of the coarser mesh size, the shape and detail of the slip circle will be reduced. This is not practical for the analysis of the differences between the potential slip circles as effect of the pipe.

Mesh refinement 'Normal' (57378 elements)	CMS-model mesh refinement (167472 elements)
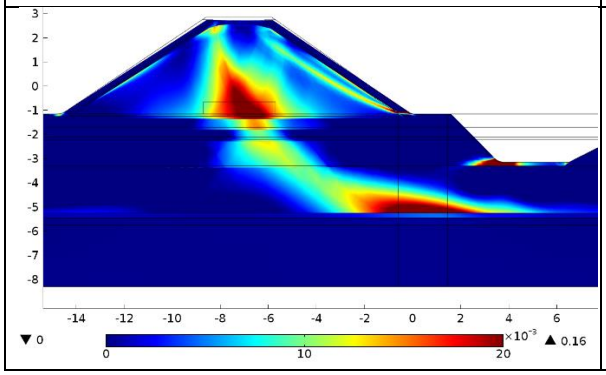	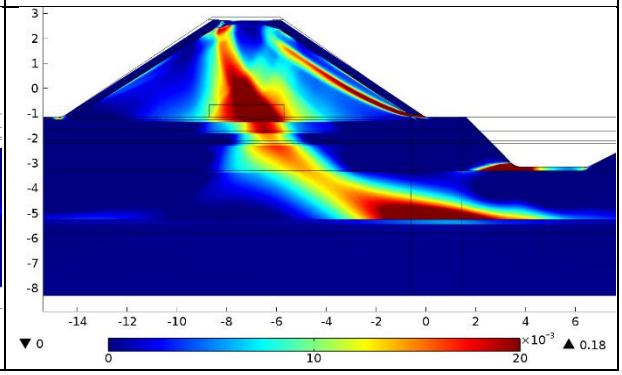

Table 11; Comparison effective plastic strains under influence mesh refinement

Secondly, while the mesh size does not have a big influence on the safety factor in the general situation, it has when a pipe is placed inside the dike (see chapter 5). In a modified case shown in Table 12 (cohesion

increase sand core), the safety factor reduced from 1.37 to 1.2625 (**7.5%**). The plastic strains in the CMS-model are 50% higher and the shape of the slip circle has changed.

Mesh refinement 'Finer' (85464 elements) **SF=1.2625**	CMS-model mesh refinement (167472 elements) **SF=1.37**
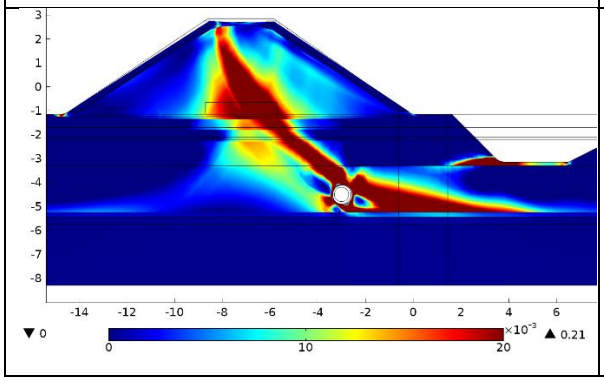	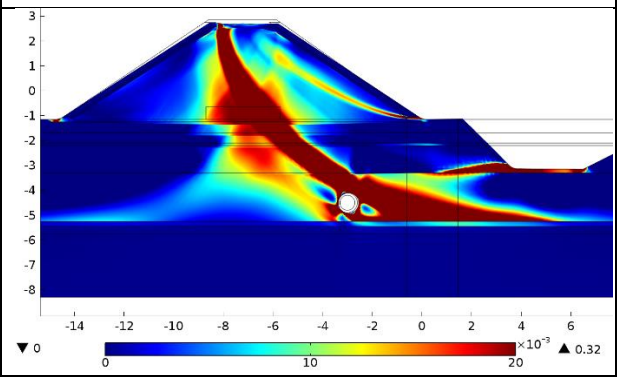

Table 12; Comparison effective plastic strains with pipe under influence mesh refinement

Based on the results of Table 11 and especially Table 12 the CMS-model will solved with an extremely fine mesh of 830.000 degrees of freedom (DOF's). The dike model is solved for 167472 number of degrees (plus 831570 internal DOF's). DOF are the total number of degrees of freedom which is the amount of nodes (#nodes) multiplied with the amount of dependent variables (#dependent variables) (Inc, 2012). The computational mesh is based on triangular mesh elements. Especially the dike core has an extremely fine mesh with a maximum mesh size of 0.015m, see Figure 44.

The dike core needs an extremely fine mesh because the incremental loadings are mainly applied on this dike core which causes high variations in plastic strains (sand core has low cohesion so low yield point). With a smaller mesh the variation in plastic strain is lower between the elements creating more convergence and a more stable model.

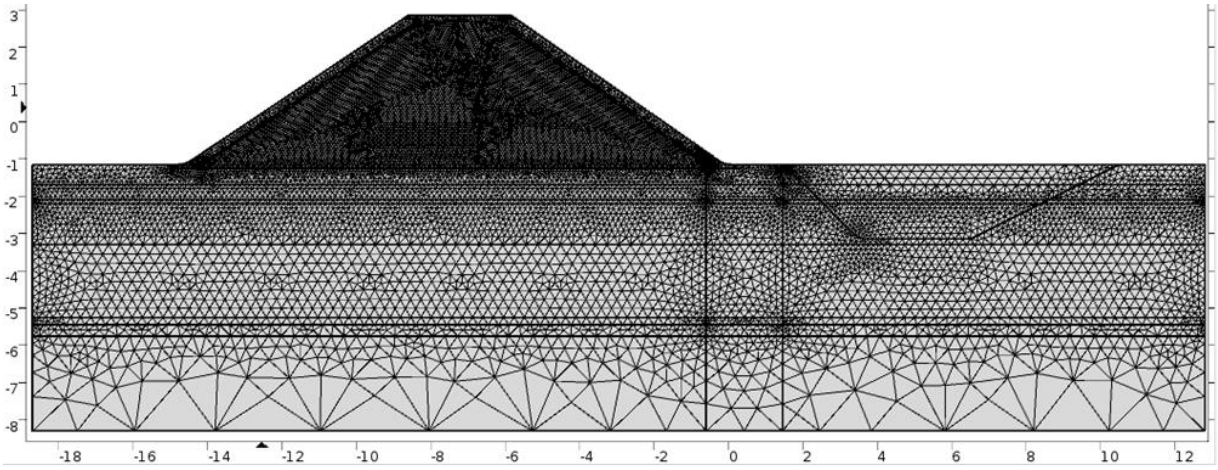

Figure 44; Final mesh dike model

Chapter 4. Validation CMS-model

This chapter presents the results from the performed validation of the CMS-model with the relevant data collected from the comprehensive sensor system of the Southdike, see paragraph 2.3. Based on the comparison between the data and the predictions a statement could be made how far off the model is compared to the real situation. With this information we can answer the second research question: *'to what extent can the model reproduce macro-stability of the Southdike experiment?'*

4.1. Model Cross validation: comparison of safety factors

For the Southdike, two limit equilibrium models (LEM) were designed to calculate the safety factor of the Southdike for different moments in time. At our defined moment in time, t=118.5hrs, the Bishop model produced a safety factor of 1.07 and the Uplift Van method a safety factor of 1.03 (see chapter 2).

The safety factor of the CMS-model (FEM) is determined with reducing the parameters of shear strength, better known as the *c-phi reduction method*. After all the loadings are implied and the cohesion and internal frictional angle are gradually reduced, simulation will no longer converge (soil particles out of yield surface). The stage at which the CMS-model cannot find a solution is equal to the safety factor. Comparison of the safety factors is shown in Table 13.

T=118.5 hrs.	**CMS-model**	**Uplift Van**	**Bishop**
Safety factor	1.1425	1.03	1.07

Table 13; Safety factors comparison

The values of the strength reduction method of the CMS-model agree quite well to the LEM software (D-Geo Stability), respectively 10% (Uplift Van) and 6% (Bishop) taken in mind that FEM and LEM models always significantly differ (Melnikova, 2014). The differences probably occur due to the fact that;

- LEM models always underestimate the strength compared to FEM models (Hammah, Yacoub, Corkum, & Curran, 2005; Rabie, 2014).
- The huge amount of soil layers and the related differences in pore pressures used for the model. For homogenous soil safety factor of FEM and LEM must almost be equal (Mansour, 2015), when this is not the case, differences in safety factor occur much easier.
- The variability (in time), and therefore uncertainty of the determined safety factor of the LEM study from the IJkdijk stichting. Bishop varies from 1.12 to 1.05, and Uplift Van from 1.08 to 1.01 within short amount of time close to t=118.5hrs (A.R. Koelewijn, 2012).

For a better comparison of both models, to support a possible cause of the differences in safety factor, the slip circle of the D-Geo stability software (LEM) is compared with the potential slip circle of the CMS-model at the same stage. The potential slip circle is calculated in COMSOL by using the effective plastic strain distributions. 'Effective Plastic Strain' is the total true strain minus the recoverable strain. So, it is the unrecoverable portion of the true strain beyond the yield limit. Effective plastic strain characterizes intensity of plastic strains, it is a dimensionless monotonically increasing scalar value, and it is calculated from the components of plastic strain rate tensor by formula (Melnikova, 2014):

$$\varepsilon_p = \int_0^t \dot{\varepsilon}_p dt \,, \dot{\varepsilon}_p = \frac{\sqrt{2}}{3}\sqrt{\left(\dot{\varepsilon}_{px} - \dot{\varepsilon}_{py}\right)^2 + \left(\dot{\varepsilon}_{px} - \dot{\varepsilon}_{pz}\right)^2 + \left(\dot{\varepsilon}_{pz} - \dot{\varepsilon}_{py}\right)^2 + 6\dot{\varepsilon}_{pxy}{}^2 + 6\dot{\varepsilon}_{pxz}{}^2 + 6\dot{\varepsilon}_{pyz}{}^2} \quad \textbf{(29)}$$

In Figure 45 the results of the Geo-stability calculation of the slip circle using the Uplift Van method is shown for the situation at which the dike has almost failed (SF=1.05). This slip circle is compared with the potential slip circles of the stability assessment of the dike model (SF=1.14).

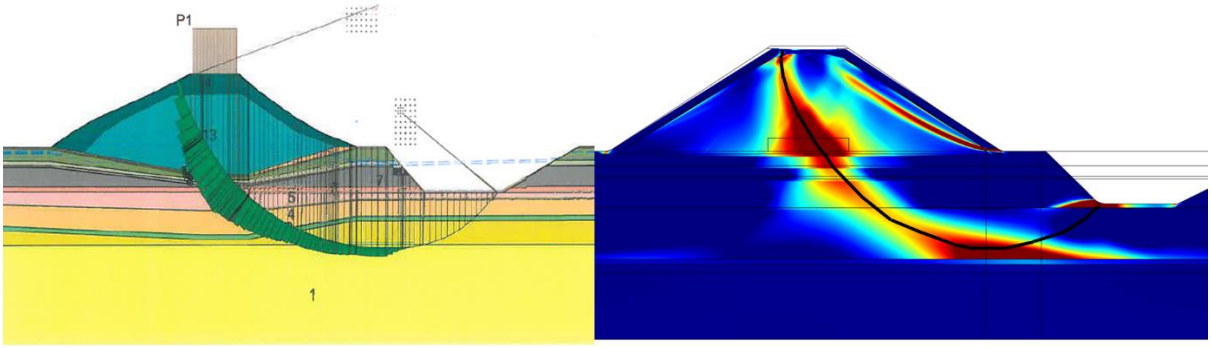

Figure 45; Comparison Southdike slip circles of D-Geo stability and the CMS-model

From Figure 45 we can obtain differences in the shape of the slip circle[4]. The slip surface of D-Geo stability (LEM) is almost a meter deeper therefore advances through the Base Sand layer while in the FEM model this does not occur. Secondly the LEM slip circle progresses until the end of the trench slip circle while the FEM potential slip circle ends at the corner close to the dike. This difference can be addressed to a difference in pore pressures within the soil layers which force the soil to move up earlier. Another explanation could be the difference in modelled composition of the soil compared to the real situation. Both explanations could also have an effect on the safety factor.

In a more quantitative comparison the radius of the slip circles are compared. For the FEM model the radius is determined quite arbitrary but it gives a better idea of the order of difference between the shape of the LEM and FEM slip surface.

T=118.5 hrs.	**CMS-model**	**Uplift Van**
Radius	8-9 meters	10.74 meter

Table 14; Comparison radius FEM vs LEM

The radius of the LEM model is between 20% till 34% larger compared to the radius of the FEM model. This large difference is probably the main reason the safety factor of the Uplift Van method is more than 10% off compared to the FEM calculated safety factor.

Second cross validation

In the second cross validation the CMS-model is compared with a self-made model of the Southdike in D-Geo stability. This gives the advantage of building a model with the same dimensions and soil strength parameters (only transition layers are neglected). The build LEM model is based on the Uplift Van method. This method is used because it takes into account the horizontal water pressures and does not assume a circular slip plane (see Bishop).

The result of the calculation is shown in Figure 46. D-Geo stability calculates a safety factor of 1.06 which is 7% off the safety factor of the CMS-model (1.1425). The radius is 8.25 while the CMS-model had a radius between 8 and 9 meters and the LEM from the IJkdijk stichting had a radius of 10.7 meters.

These results could implicitly confirm that for the LEM calculation of the IJkdijk different soil strength parameters for some soil layers are used. Certainly comparing the slip circle from the LEM of stichting IJkdijk and my self-made LEM slip circle. The self-made LEM does not proceed until the base sand layer, and stresses occur along the whole slip circle while this was not the case with the IJkdijk Uplift Van model calculation.

[4] In the CMS-model multiple slip circles can be distinguished. This is an advantage of FEM software, while in D-Geo stability the shapes of the slip circles are predefined and specific for each modification of the method.

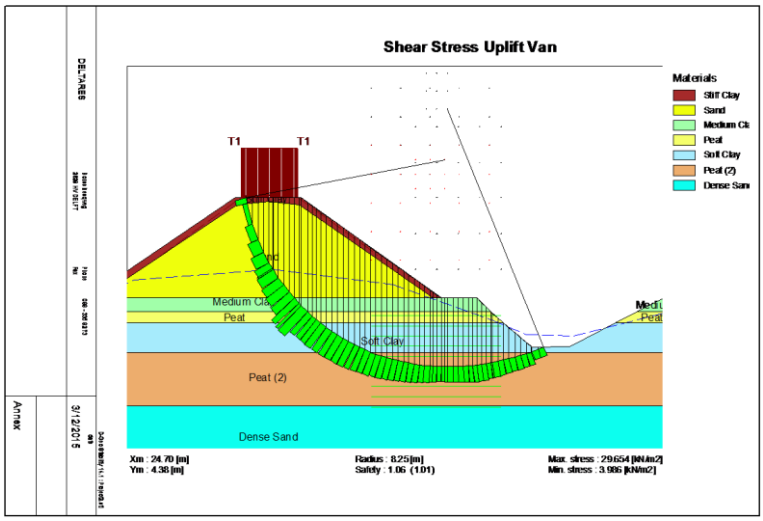

Figure 46; D-Geo stability calculation CMS-model

4.2. Hydraulic head

In this paragraph the validation results of the hydraulic heads are presented. In this validation the initial and final hydraulic heads at the location of the sensors of the time dependent data of the Southdike and the stationary results of the CMS-model are compared, see Table 15.

Sensor	Initial Hydraulic Head [m]			Final Hydraulic Head [m]		
	IJkdijk	CMS-model	Difference	IJkdijk	CMS-model	*Difference*
Z2162	-1.5	-1.4	*0.1*	-1.8	-1.7	*0.1*
Z2138	-1.4	-1.4	*0*	-1.8	-1.7	*0.1*
Z2152	-1.25	-1.4	*0.15*	-1.25	-1.7	*0.45*
Z2148	-1.4	-1.47	*0.07*	-1.7	-1.74	*0.04*
Z2144	-0.65	-1.35	*0.7*	-0.65	-1.6	*0.95*
Z2158	-1.2	-1.55	*0.35*	-1.7	-1.76	*0.06*
Z2133	-1.5	-1	*0.5*	-0.5	-0.55	*0.05*
Z2168	-1.5	-1.65	*0.15*	-1.7	-1.72	*0.02*
Z2112	-1.5	-0.85	*0.65*	-0.4	-0.15	*0.25*
Z2101	-0.3	-0.6	*0.3*	0	0.155	*0.155*
Z2105	-1.5	-1	*0.5*	-0.9	-0.53	*0.37*
Z2107	-0.85	-0.6	*0.15*	0.5	0.7	*0.2*
Z2109	-1.5	-0.9	*0.6*	-0.8	-0.7	*0.1*

Table 15; Initial and final state measured and modeled hydraulic heads

Based on Table 15, the results could be interpreted as quite well. The differences of the initial hydraulic heads are quite large (total 4.47m), what seems logic since the averaging method of Raymond (Meij, 2015a) cannot be yet applied for this situation. The differences of the final hydraulic head are much better (total 2.735m). Sensor 52, 44, which are both located under the dike core, produce a significant lower hydraulic head, respectively -0.45m and -0.95m. This could be another explanation for the higher safety factor of the CMS-model. Inaccuracy of the piezometer is mentioned as 0.1% so cannot be the reason for the differences (Vries et al., 2012).

For a better visualization, the results of Table 15 are expressed in relative rates to show which sensors give relatively the worst results. This is the difference from the sensor compared to the total difference shown in Figure 47.

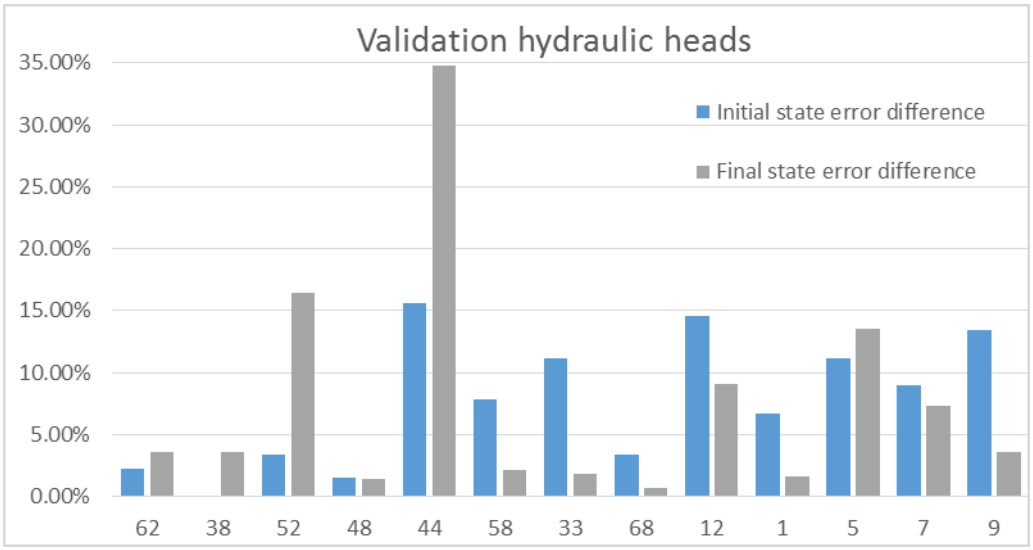

Figure 47; Proportional differences hydraulic head between piezometer sensors and CMS model results

Based on Figure 47 we could definitely state that sensor 44 is not well simulated. Zooming in on this sensor; it is located in a peat layer and has a constant hydraulic head of -0.65m over the entire experiment (so is not influenced by changing conditions). Next, the sensors located above and below sensor 44 show completely different values of hydraulic heads, respectively -1.25m and -1.5m during the experiment. So in real situation, the hydraulic heads remained constant while in the CMS-model the hydraulic heads increased. This error reveals the imperfection of the CMS-model. With the stationary conditions it is almost impossible in case of many soil layers, especially of soil-layers between other soil-layers, to simulate all the pore pressures correctly.

Sensors 52 and 05, which also show relatively high errors, are located close to the dike core were water was infiltrated into the soil during the experiment. The water infiltration implies highly variable hydraulic heads, which are more difficult to simulate in the CMS-model and is therefore the probably reason for the high difference.

Overall the CMS-model simulates the hydraulic head quite well. The described differences of three sensors probably have a small influence on the safety factor (small increase). The results of the hydraulic head validation, in this case the initial stage compared with the final state, is presented in Figure 48.

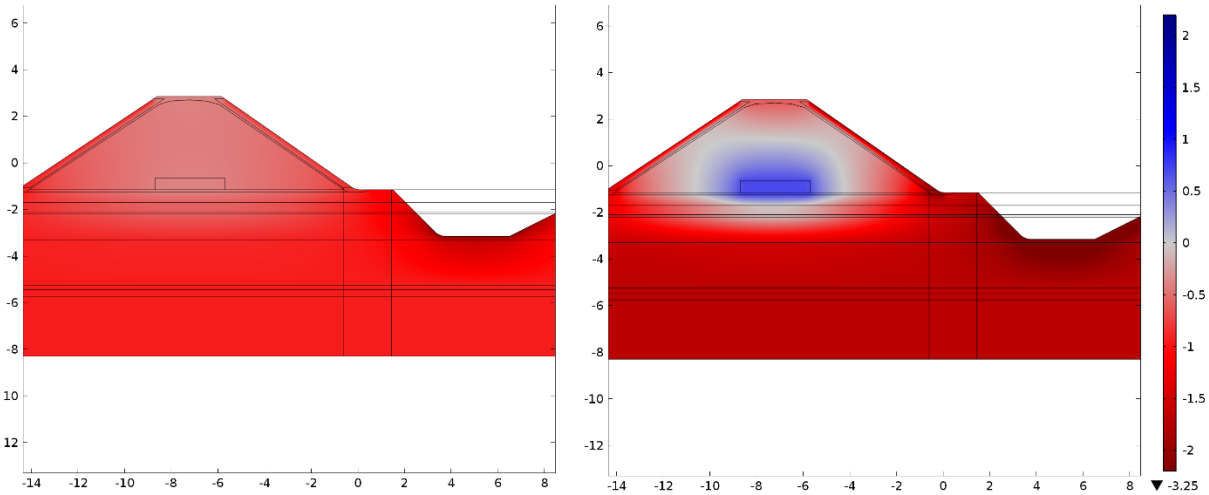

Figure 48; Initial and final state hydraulic head in CMS-model

4.3. Displacements

This paragraph describes the results of the validation between the measured displacements at t=118.5 hours and the predictions of the CMS-model. First the total displacement for 5 specified locations at a certain depth are compared, presented in Table 16. This is done as mentioned in paragraph 2.3 with SAAF inclinometers. These inclinometers have an average maximum inaccuracy of *±1.5mm* (Vries et al., 2012). Therefore the displacements in Table 16 are defined in millimeters. The error mentioned in Table 16 defines the difference in displacement between the sensor and the CMS-model at a specific location, divided by the total displacement measured by the sensor at that specific location.

Name sensor	Depth in soil [m]	Total displacement sensor [m]	Total displacement CMS-model [m]	Difference [m]	Error difference
SAAF Deltares	-2.7	0.081	0.090	0.009	*10%*
SAAF Deltares	-2.1	0.086	0.090	0.004	*5%*
SAAF Deltares	0	0.093	0.092	-0.001	*-1%*
SAAF RPI	-2.1	0.094	0.086	-0.008	*-9%*
SAAF RPI	0	0.086	0.090	0.004	*4%*

Table 16; Validation of the total displacement at a specified location

With a maximum error difference of 10% (≈10mm), the numbers of the CMS-model do agree extremely well to the measured data, this is based on a statement from Raymond van der Meij that displacements can differ up to 200% (Meij, 2015b). The reason for the small differences of Table 16 occur because the model is calibrated for the Young Modulus. This is especially done for the peat and clay layers (and transition layers in between), see Table 17.

Soil layer	Young's' Modulus [MPa]	
	Laboratory value	Calibrated value
Sand/Clay	9.8	11
Clay top	3.2	3.1
Peat	0.95	1.5
Peat/Clay	2.2	1.7
Soft Clay	3.0	2.3
Deep peat	0.8	0.75
Peat/Sand	4.6	5

Table 17; Calibration Young's Modulus

Despite the calibration, some relative high differences occur in the lower layers of the soil. Probable causes;

- Inhomogeneous soil conditions which could never be completely taken into account in CMS-model. This is based on consistency of displacement; CMS-model predictions show a maximum of 4mm difference over the complete depth of the inclinometer while a difference of 11mm is measured.
- The differences in hydraulic head as mentioned in paragraph 4.2
- The determination of the actual moment of failure. Assumed is a failure at t=118.5 while for real soil this differs per location (Vries et al., 2012). For the deeper soil layers failure could have occurred earlier, implying lower displacements than used for this validation.

In a second validation the total displacements (at t=118.5hrs) measured along the depth of the inclinometer is compared to the simulated results of the CMS-model. The data of the CMS-model for SAAF Deltares is derived from a defined line placed at x=0.6m, for SAAF RPI at x=-1.45m. The location and result of the SAAF Deltares inclinometer is shown in Figure 49.

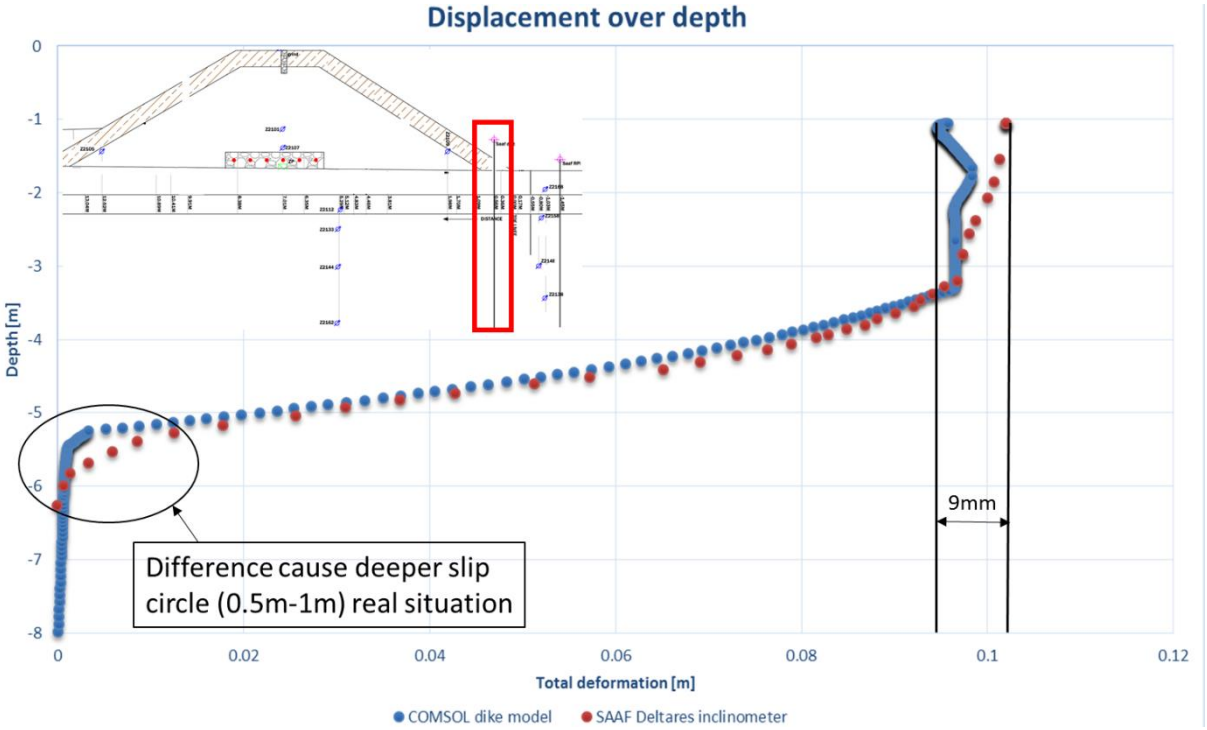

Figure 49; Validation SAAF Deltares inclinometer

Figure 49 shows that the displacements are well modeled in the CMS-model. The maximum inaccuracy is 9mm at the surface which is a really small error (Meij, 2015b). The displacement over the complete depth of the soil, which is important, are extremely well modeled (see blue dots compared to red dots). Inaccuracy occurs at the transitions between layers (transitions cannot be perfectly modeled in FEM). Secondly higher displacements close to the sand layer occur in the real situation compared to the CMS-model. This can be the reason the slip circle, as shown in paragraph 4.1, is located higher compared to the IJkdijk simulations.

Validation of the SAAF RPI inclinometer, located close to the trench, is presented in Figure 50.

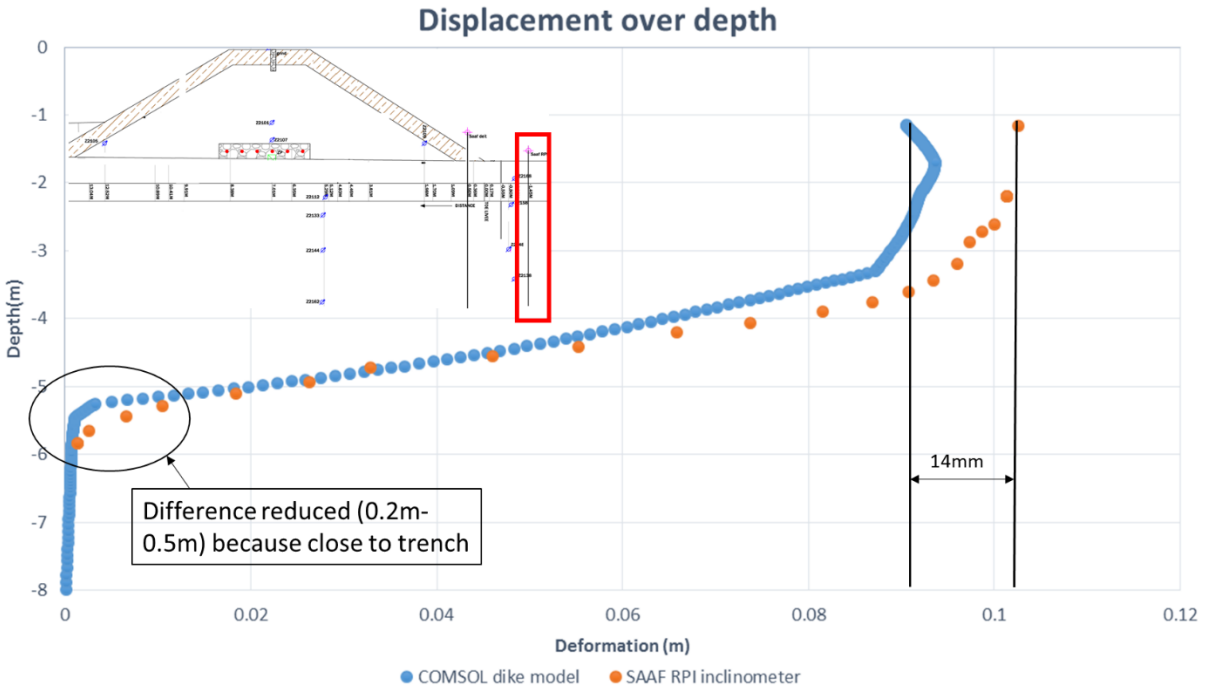

Figure 50; Validation SAAF RPI inclinometer

For the situation close to the trench shown in Figure 50, the displacements are well modeled (Meij, 2015b), partially due to the calibration. The maximum inaccuracy of 14mm is really small (Meij, 2015b). Secondly the total shape of the displacement plot is almost equal. Inaccuracy again occurs at the transition between soil layers and secondly at the displacements close to the base sand layer which implies the slip surface will be less deep compared to the real situation.

This can be caused due to inaccurate values for the soil layers, inhomogeneous conditions of the soil in real situation and the mentioned inaccuracy of the hydraulic heads (paragraph 4.2).

The CMS-model simulates the total displacements (scaled with a factor 10) of the Southdike in the shape as presented in Figure 51 (at failure state, SRF=1). This shape corresponds to deep rotational sliding, a positive result which together with the positive validation results for the safety factor (4.1) and hydraulic head (4.2) provides enough confidence in the CMS-model.

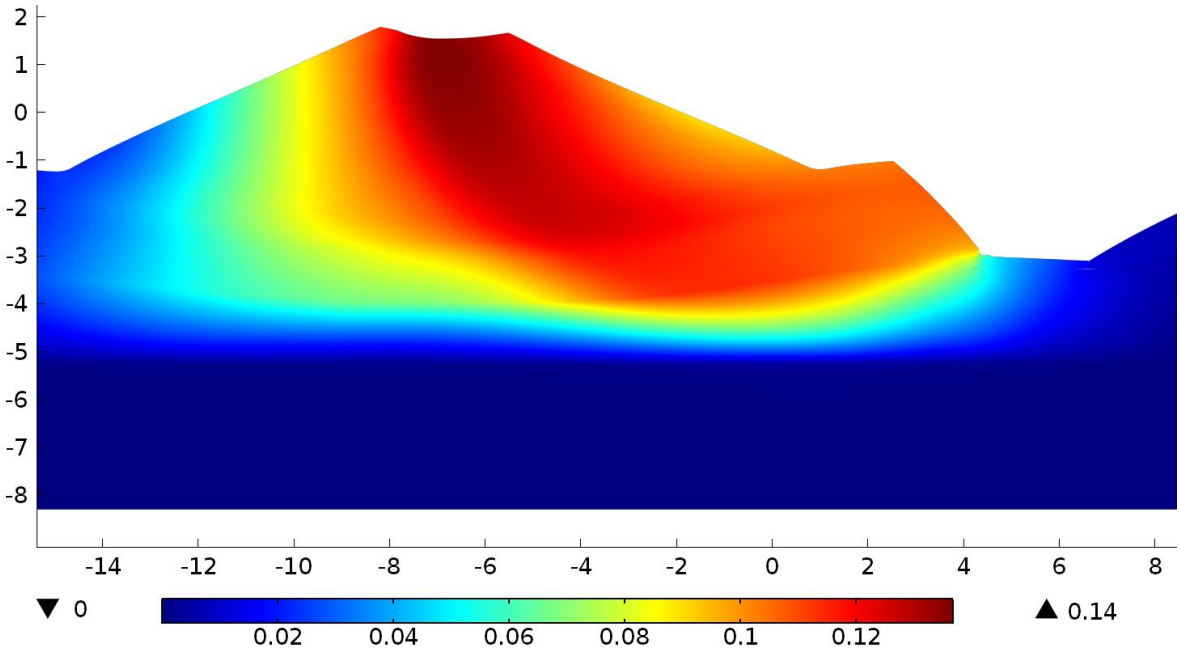

Figure 51; Total displacement (meters) Southdike [shape is scaled with a factor 10]

Chapter 5. Effects of buried pipe on macro-stability

In this chapter the last research question is answered: '*To what extent and in which way does the buried pipe characteristics contribute to the development of macro-instability*'? Section 5.1 investigates the effects of the location of the pipe. Section 5.2 the size of the pipe is investigated, section 5.3 the material of the pipe is investigated and in the last paragraph 5.4, the soil condition of the dike is changed.

The full analysis of the effect of the pipe on macro-instability presented in this chapter is based on defined '*slip circle criteria*' for this report which can be found in Appendix F. All the derived results will be compared with the general situation (*SF=1.1425*) of the Southdike shown in Figure 52. In this case the highest effective plastic strains (0.18) occurred at the corner bottom of the trench (means dike slides into trench). The low effective plastic strains imply only potential, no full dike failure, occurs. So the CMS-model predicts the dike will potentially fail be means of deep rotational sliding.

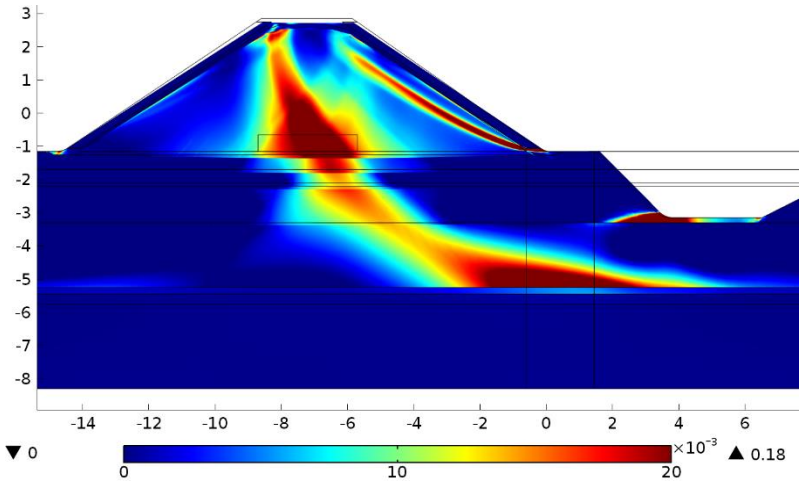

Figure 52; General shape potential slip circle model (effective plastic strain is dimensionless)

5.1. Location of pipe

The effect of the location of the pipe to macro-instability is tested by placing the pipe at 16 different locations, mostly in such a way that they are located at the original slip circle of the general dike (see Figure 52). General characteristics are chosen for the pipe based on the norms (chapter 1). The pipe has a diameter of 400mm, casing of 50mm thick, a density of 2000kg/m^3, Poisson value of 0.33 (same as steel and concrete values) and a Young's Modulus of 3GPa. All the simulations of a pipe placed at 16 different locations (see Figure 53) are presented in Appendix G.

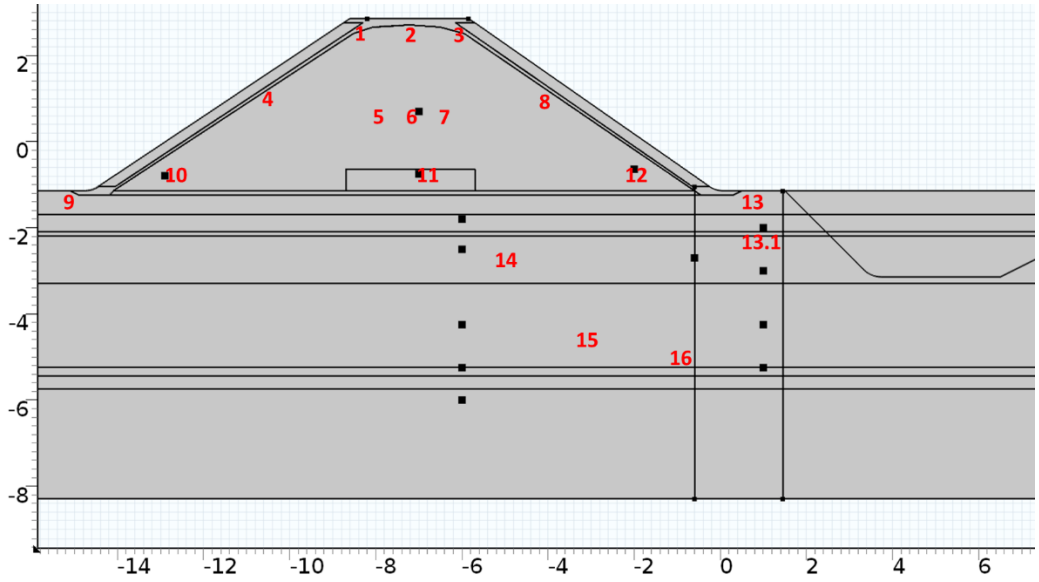

Figure 53; Buried pipe test locations

The effect of the location of the pipe on the safety factor is presented in Table 18.

NR	PIPE LOCATION	SAFETY FACTOR	SF WITHOUT PIPE	PERCENTAGE	RELATIVE
1*	Left top	1.1175	1.1425	97.8%	-2.2%
2	Middle top	1.1825	1.1425	103.5%	3.5%
3	Right top	1.1475	1.1425	100.4%	0.4%
4	Left side	1.1425	1.1425	100.0%	0.0%
5*	Left middle core	1.205	1.1425	105.5%	5.5%
6	Middle core	1.1675	1.1425	102.2%	2.2%
7	Right middle core	1.1825	1.1425	103.5%	3.5%
8*	Right side	1.08	1.1425	94.5%	-5.5% [A]
9	Left next to dike	1.1425	1.1425	100.0%	0.0%
10	Low core left	1.1425	1.1425	100.0%	0.0%
11*	Low core middle	1.2225	1.1425	107.0%	7.0%
12	Low core right	1.165	1.1425	102.0%	2.0%
13*	Right next to dike	1.1425	1.1425	100.0%	0.0% [B]
13.1	*Right next to dike*	*1.165*	*1.1825*	*98.5%*	*-1.5%*
14	Deep middle	1.205	1.1425	105.5%	5.5%
15*	Deep middle-right	1.2275	1.1425	107.4%	7.4%
16*	Deep under toe	1.08	1.1425	94.5%	-5.5%
	[A]; High plastic strains occur and failure due to local slip (explanation in section 5.1.5)				
	[B]; Remarkable results which is not in line with expectations (explanation in section 5.1.6) see therefore location 13.1				
	* Explanation is provided in last part of the paragraph				

Table 18; Safety factors different locations

Table 18 shows that the location of the pipe can have a negative, no or positive influence on the safety factor in case of macro-instability. Based on these results the following general plot could be drawn.

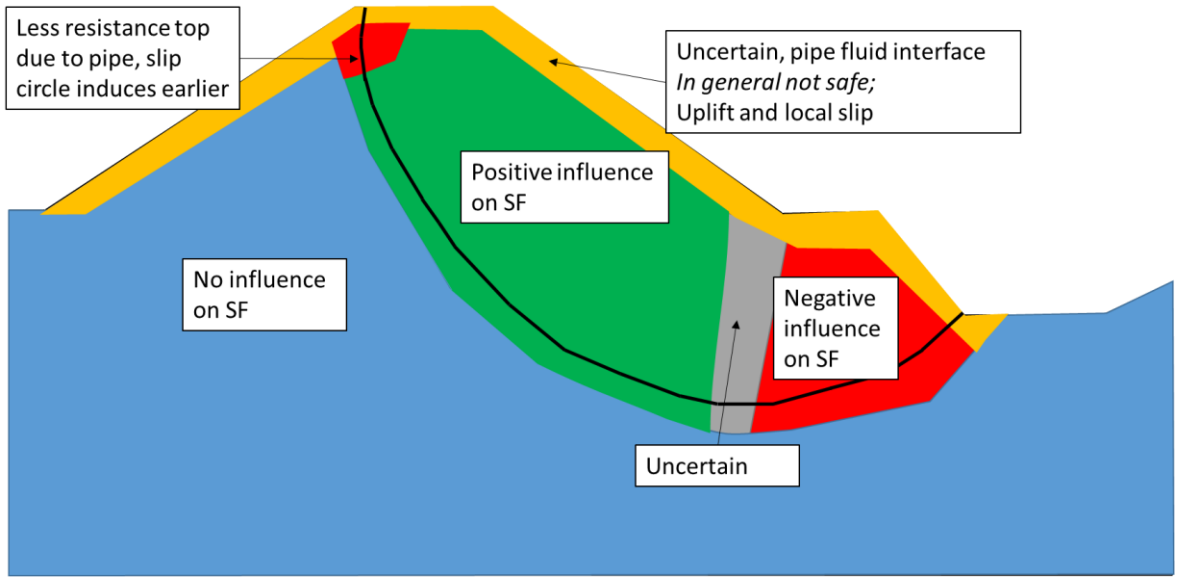

Figure 54; Schematization effects buried pipe on macro-instability safety factor

The results presented in Table 18 and Figure 54 show the influence of a pipe on the safety is closely related to the principle theory of Bishop. For the most remarkable results of Table 18, which have the most influence on the general effects shown in Figure 54, a clear explanation is provided how the pipe has an influence on the potential slip circle and the related safety factor.

5.1.1. Location 1

The CMS-model predicts that Location 1, 'left top', will be slightly more unsafe due to the pipeline (-2.2%).

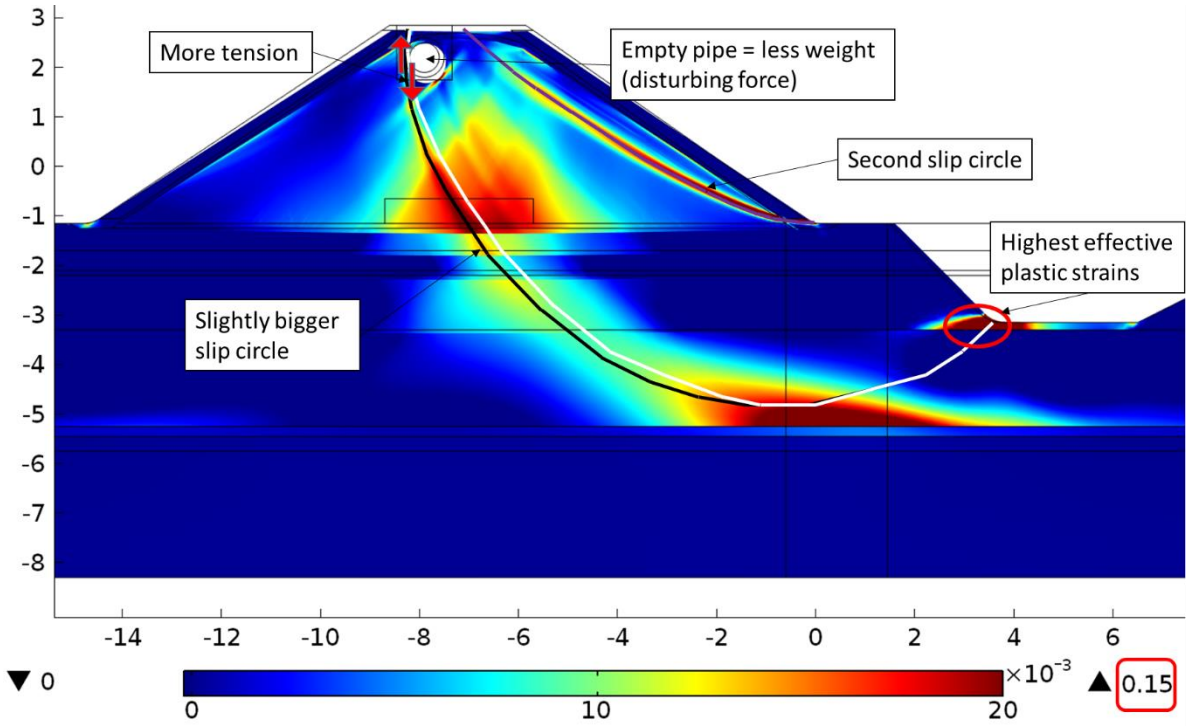

Figure 55; Effective plastic strain, left top [SF=1]

The pipe has a negative influence on the safety factor because it creates a 'cut'. There is no friction between the pipe and the soil inducing higher tension forces along the pipe (with in the same time lower plastic strains, 0.15). Due to the higher tension forces, especially at the beginning of the slip circle (top dike), the potential slip surface can more easily originate. Due to the cut less disturbing forces are needed to create the same potential slip surface. The buried pipe also slightly relocates the potential slip circle in an outward direction. The slightly increase would only have a significant positive effect on the safety factor.

The last aspect is a reduction of disturbing forces due to the pipe. The pipe is simulated as empty, so this implies a difference in weight to the original situation at which this area consisted of sand particles. This means less driving forces (momentum) so an increase of the safety factor (detailed calculation see paragraph 5.2). Overall, the effect of the weight has considerable less influence then the cut, the safety factor decreases.

5.1.2. Location 5 and 11

For location 5 (left middle) as well as 11 (lower core middle) the pipe induces the slip circle to become smaller. Therefore the driving force of the slip surface decreases (momentum) which increases the safety factor, respectively 5% and 7%.

In both situations the pipe is located at the original slip circle, were it resist against the potential slip circle forcing it to redirect in a wider or smaller direction (thereby the pipe moves into the direction of the slip circle/ displacements dike). Because in both situations the slip circle is forced in a smaller direction, this implies the pipe induces compression forces. This means higher effective plastic strains along the pipe are needed to force failure, see Figure 56.

The potential soil-weight difference due to the empty pipe has no influence on the safety factor because the pipe is located in the passive zone of the slip surface.

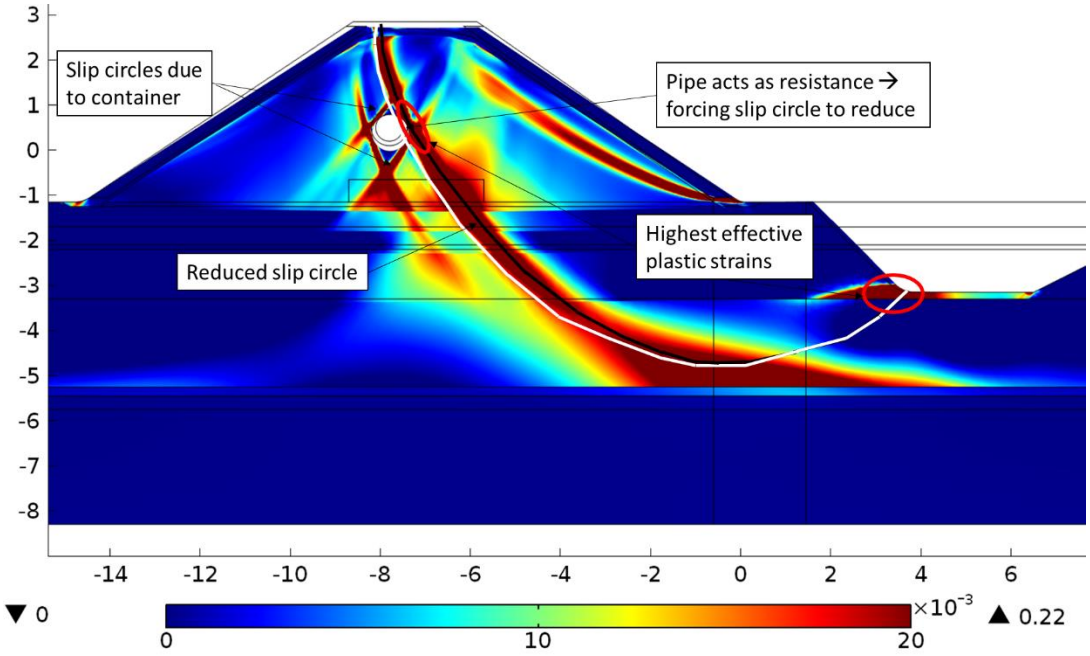

Figure 56; Effective plastic strain, Left middle [SF=1]

Figure 56 also shows potential slip circles propagating in cross direction compared to the general slip circle. These partially occur due to the load of the container on top of the dike. But secondly, as we will see in section 5.4, because of the high displacements of the pipe itself (it is pushed away). This creates high effective plastic strains in front and at the back of the pipe (in direction of displacement). This is also shown in Figure 57.

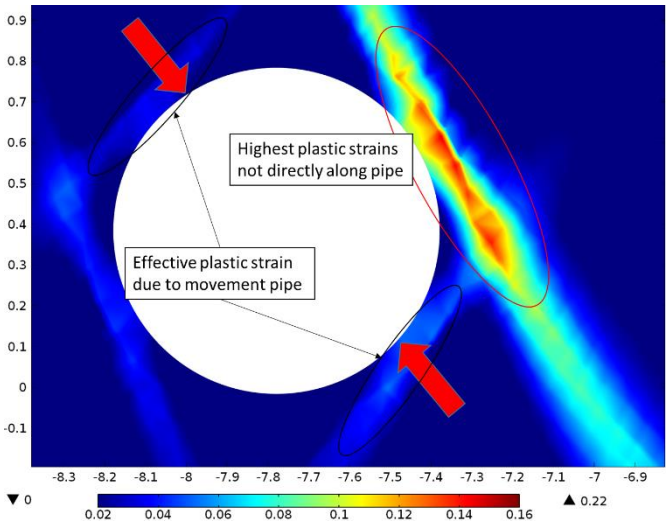

Figure 57; Effective plastic strains next to pipe (different scale)

We observe from Figure 57 that the highest effective plastic strains do not occur directly alongside the pipe. This is probably not completely correct since in real situation a 'cut' with zero resistance will occur next to the pipe inducing high displacements. This has to be solved with a soil-pipe interface which is not done in this report (see discussion).

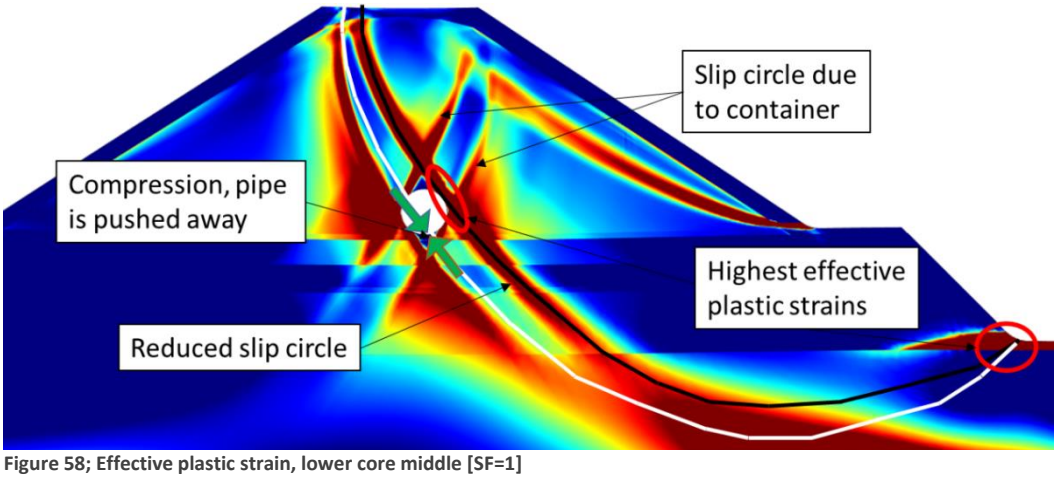

Figure 58; Effective plastic strain, lower core middle [SF=1]

5.1.3. Location 15

Location 15, the most safe location (SF=1.2275, +7.4%), is located in deeper soils below the dike. The explanation could be based on the same mechanism as presented for locations 5 and 11. But since location 15 is located in the deeper parts, the soil induces more resistance against displacement of the pipe, creating higher compression forces and higher effective plastic strains around the pipe. The slip circle cannot go through the pipe so it relocates around the pipe. In this case the slip circle is relocated in upward direction creating a smaller slip surface and a higher safety factor (+7.5%), see Figure 59.

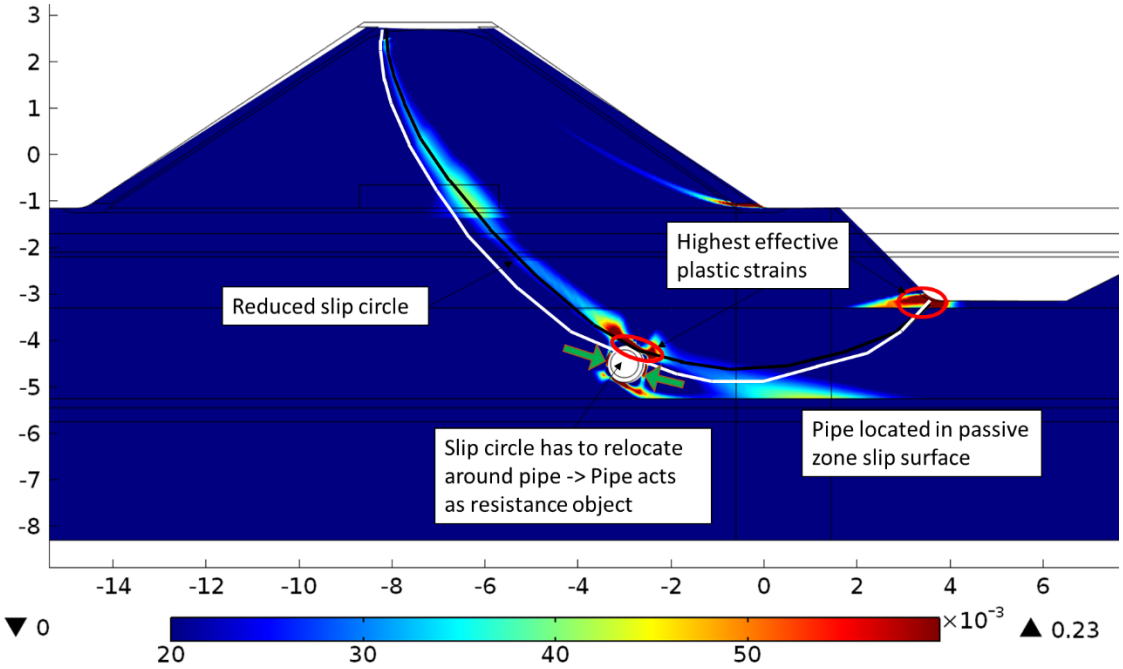

Figure 59; Effective plastic strain, Deep middle-right SF=1 (different scale effective plastic strain)

5.1.4. Location 16

Location 16, is predicted by the CMS-model as the most unsafe location (SF=1.08, -5.5%).

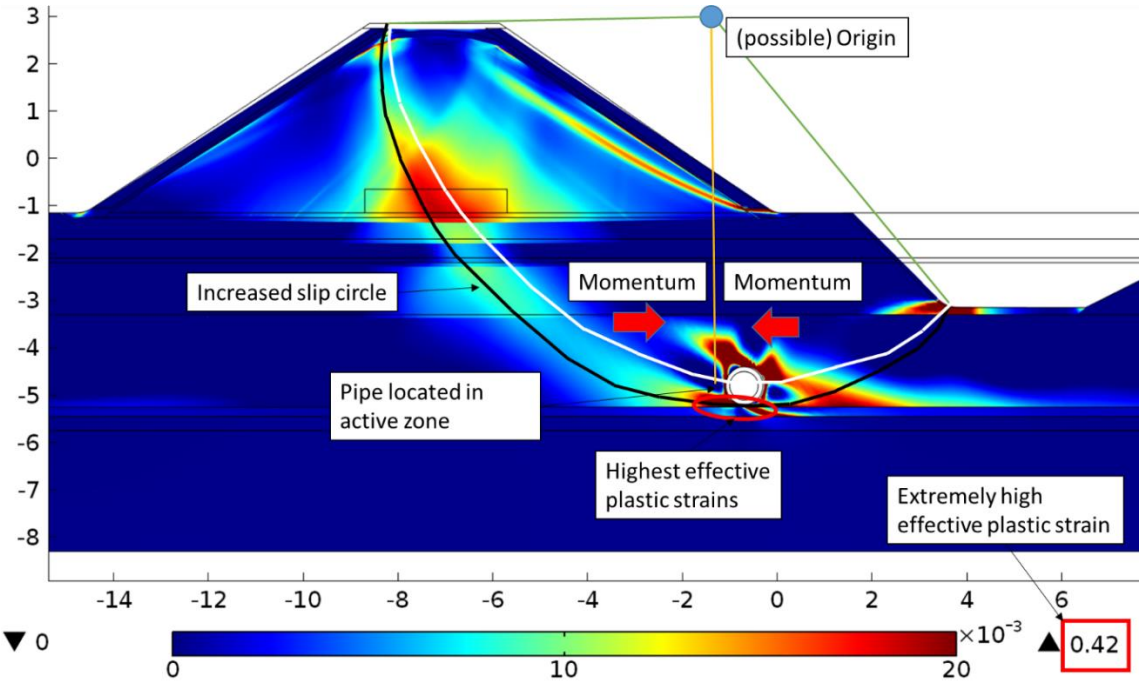

Figure 60; Effective plastic strain, deep under toe, SF=1

Remarkable is that location 16 is located rather close to the safest location 15. The big difference of both locations is that while at location 15 the slip circle relocates upwards creating a smaller slip surface, in case the pipe is placed at location 16 the slip circle is enlarged creating a more unsafe situation. An interest observation is that the highest plastic strains occur below the pipe, a factor 3 higher (0.42) than in the general situation. This occurs at the deepest point of the slip circle, so driving forces are combined with resisting forces inducing high stresses.

The pipe is located in the active part of the slip surface. The pipe has less weight than the original soil, creating less momentum in positive direction, leading to lower safety factor. This explanation is based on the assumption that the origin of the slip surface is located at the location as visualized in Figure 60.

5.1.5. Location 8:

One of the most unsafe locations according to the CMS-model is location 8, a pipe located at the right middle side of the dike. But as we can see in Figure 61, the dike does not fail due to a deep rotational slip circle. In FEM software all the possible slip circles are determined implying also extremely small slip surfaces could be determined. When such a small surface fails, the model will stop, while actually the dike did not fail.

A second reason why pipes cannot be placed so close below the surface is due to uplift. The water pressure forces inside the dike will force the pipe in upward vertical direction because above the pipe is a minimal amount of soil and the pipe itself is empty and cannot provide any resistance against uplift.

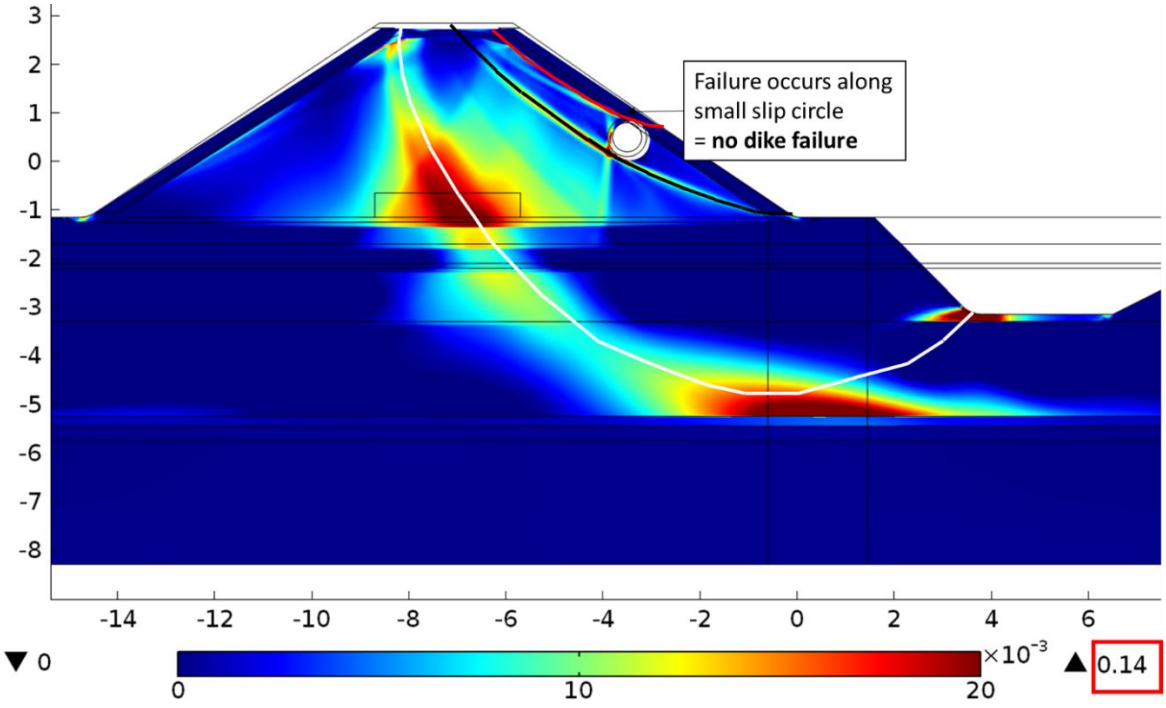

Figure 61; Drawback model; effective plastic strain right middle [SF=1]

5.1.6. Location 13

With the general configurations, the safety factor of location 13 remains constant as was shown in Table 18. However when the configurations of the soil (see 5.4) are changed this location shows as expected (Bishop) negative results as a consequence of the buried pipe. This is done by increasing the properties of the sand core with 0.5kPa (cohesion) and 1 degree (internal friction angle), providing in the situation without a safety factor of 1.1825. In this configuration location 13.1 produced a safety factor of 1.165 (**-1.5%**). This results forms the basis of the general plot seen in Figure 54.

5.2. Size pipe

In this paragraph is investigated if the characteristic size of the pipe has an influence on the development of macro-instability. This has been tested by locating the pipe at two general locations, at the top of the dike and in the middle of the core. These locations are chosen (due to time restrictions) since the pipe had different effects to the safety in both situations. It is expected these effects will be increased or decreased by the size of the pipe. General applicable pipe sizes are used. The big pipe is modeled with a diameter of 600mm and a thickness of 50mm and the small pipe with a diameter of 250mm and a thickness of 15mm.

Big pipe (600mm) → SF= 1.2275	**Small pipe (250mm) → SF=**1.1675
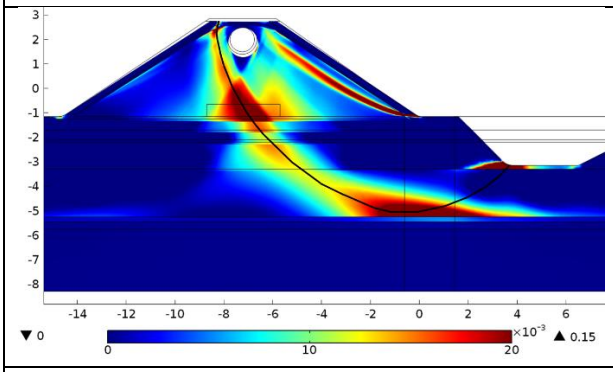	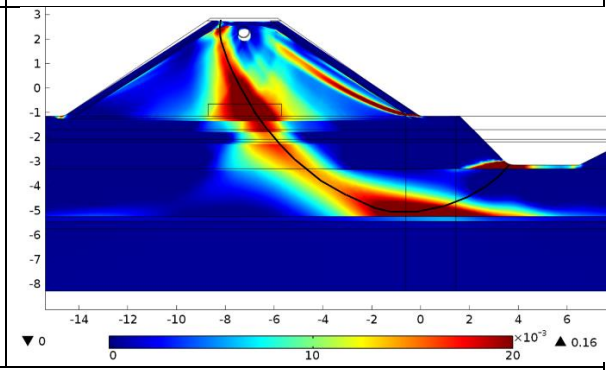

Observations:
- Safety factor big pipe is higher than smaller pipe
- The slip circle is in both situation equal, dike will fail due to deep rotational sliding
- Big pipe induces more soil loss → creates less disturbing forces [density pipe has influence]
- Higher effective plastic strains needed to let dike fail with smaller pipe (compared to big pipe)

Middle top (standard)	Big pipe	Small pipe
SF=1.1825	SF=1.2275 (+3.5%)	SF=1.1675 (-1.2%)

Table 19; Comparison small big pipe middle top location

When comparing both situations with the general situation without a pipe (SF=1.1425), both the small pipe and the big pipe create a safer situation. This can be related to the difference of mass in the slip surface induced by the empty pipe, implying less driving force (momentum) to force failure.

Comparing the different sizes of the pipe, respectively small, standard and big, the effect of mass on the safety factor created by the size of the pipe is key to explain the differences in safety factor.

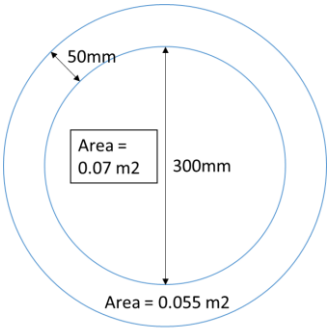

Figure 62; Pipe dimensions

For the standard pipe the dimensions of the pipe are shown in Figure 62. The total surface area of the standard pipe is; $\pi * 0.2^2 * 1 = 0.13m^3$. The surface area inside the pipe is 0.07 m^3, multiplied with the mass of the soil (1800kg/m3) implies a mass loss of 127 kg. The area of the walls is 0.05 m^3, multiplied with the increase of mass due to the walls (2000-1800) implies an increase of mass of 11kg. This leads to a mass deficit of -116kg. The same is done for the big and small pipe shown in Table 20.

Type of pipe	**Total surface pipe [m^3]**	**Area inside pipe [m^3]**	**Area walls pipe [m^3]**	**Mass loss due to core pipe [kg]**	**Extra mass due to pipe [kg]**	**Deficit [kg]**
Standard	0.13	0.07	0.05	127	11	-116
Big	0.28	0.20	0.09	353	17	-336
Small	0.05	0.03	0.02	68	2	-66

Table 20; Calculation weight deficit pipe sizes

The weight deficit presented in Table 20 confirms with the calculated safety factors for the big, standard and small pipe. The ratios between the big pipe and the standard pipe (-220kg, +3.5% SF) and between the small pipe and the standard pipe (+-50kg, -1.2% SF) is almost equal. So at location 5, where the pipe has no influence on the shape of the slip circle, the safety factor is fully determined by the weight of the pipe.

The size of the pipe is also tested for a location where it can have some influence on the shape of the slip circle, location 11 (lower core middle), leading to the following results.

Big pipe (600mm) → SF=1.2275	**Small pipe (250mm) → SF=**1.205
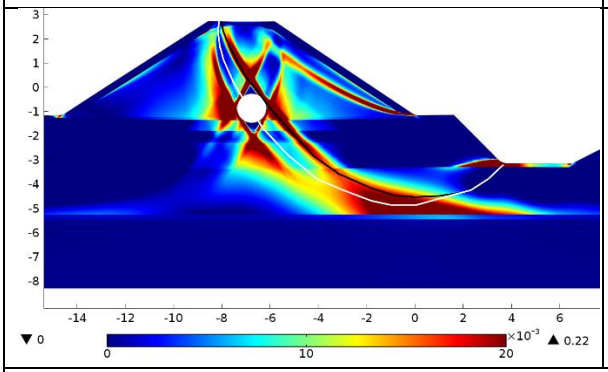	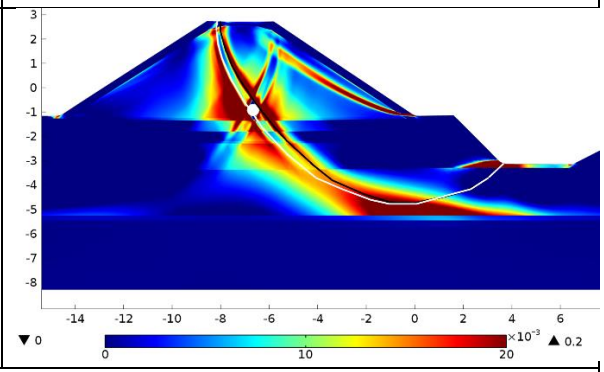
Observations: - Potential slip circle big pipe decreases compared to standard pipe and general situation - Big pipe located in passive zone implying density pipe has no effect - For small pipe, potential slip circle slightly decreased compared to general situation, but increased compared to the standard and big pipe	

Lower core middle (standard)	Big pipe	Small pipe
SF=1.2225	SF=1.2275 (+0.5%)	SF=1.205 (-1.5%)

Table 21; Comparison of size pipe

The small and the big pipe both decrease the potential slip circle leading for both to an increase of the safety factor compared to the general situation (SF=1.1425).

The small pipe has less influence on the potential slip circle compared to the big pipe. Because it has a smaller diameter the potential slip circle is can remain larger compared to the situation of the normal and big pipe. This causes the difference in safety factor.

Remark: There is a turning point at which the pipe will no longer decrease the potential slip circle but will force it to increase. In this situation the pipe is located in the active zone, so implying a weight deficit due to the pipe. The wider slip circle reduces the safety factor while the negative deficit increases the safety factor. Not a location within the slip surface could be pointed out as from where this shift will occur.

This last remark is important because it highlights that the interaction between location and size and the related safety can be highly variable. This implicitly implies proper investigation is needed for every single case a pipe is placed close to the potential slip circle.

5.3. Material of pipe

For three material characteristics of the pipe their influence on macro-stability are tested, respectively steel, concrete and plastic. The properties of those materials are based on general common types of pipes used in the field. The thickness of the pipe is based on standard values.

Type	Density [kg/m^3]	Young's Modulus [GPa]	Size pipe	Thickness pipe [mm]
Standard	2000	3	250mm	15mm
Steel	7850	210	250mm	15mm
Concrete	2650	17	250mm	15mm
Plastic	950	0.9	250mm	15mm

Table 22; Material properties used for different types of pipe

The characteristics are firstly tested when the pipe is placed at the top middle of the dike body. The safety factor of the small pipe (250mm, 15mm) with standard properties (as used for location and size tests) is **1.1675**. In this situation the pipe has a mass deficit of **68kg**. This standard pipe is compared with the steel, concrete and plastic pipe of which the results are presented in Table 23.

Steel pipe → SF= 1.1475	**Plastic pipe → SF=**1.19
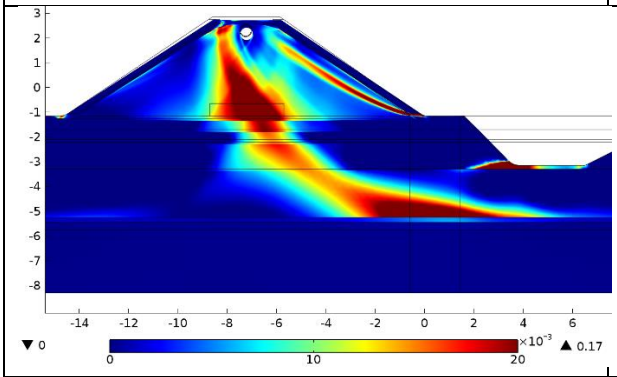	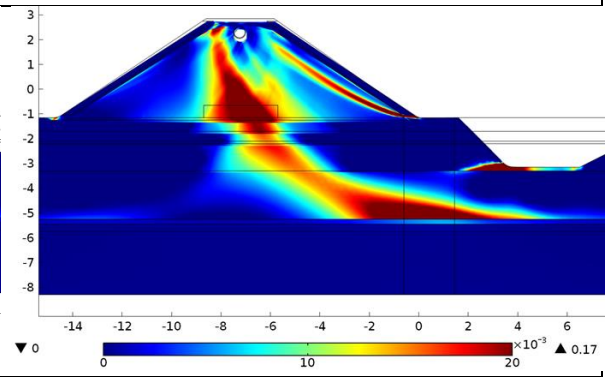

Observations:

- All the situations are more safe compared to the situation without a pipe (SF=1.1425)
- The slip surface does not change, failure in all situations by deep rotational sliding
- The density of the pipe has a major influence towards the safety when the pipe is placed at this location

Middle top (Standard)	Steel	Concrete	Plastic
SF=1.1675	SF=1.1475 (-1.7%)	SF=1.17 (+0.2%)	SF=1.19 (+2%)

Table 23; Comparison material pipe middle top location

The mass deficit of the steel, concrete and plastic pipe, shown in Table 24, could partially explain the higher safety factors of the mentioned pipes. The mass deficit occurs because the pipe are simulated as empty, and because located within the slip surface leads to a loss of driving forces inducing failure to macro-instability.

Type of pipe	Area inside pipe [m^3]	Surface walls pipe [m^3]	Mass loss due to core pipe [kg]	Extra mass due to pipe [kg]	Deficit [kg]
Steel	0.04	0.01	68	66	-2
Concrete	0.04	0.01	68	8	-61
Plastic	0.04	0.01	68	-9	-78

Table 24; Weight deficit material pipe

Results of Table 24 confirm that the mass deficit of all the pipes leads to a safer situation compared to the situation without a pipe (SF=1.1425). A logical relation is also that since the plastic pipe is the lightest pipe, it has the highest safety factor.

An interesting observation is done comparing the steel pipe with the general situation (without pipe). Despite an almost zero mass deficit of the steel pipe (-2kg), the safety factor is still relatively much higher than in the general situation (1.1425 vs 1.1475). A probable explanation is the effect of the high Young Modulus of the steel pipe has a positive effect on the safety factor.

Comparing the standard pipe (-68kg, 0%) relative to the steel pipe (-2kg, -1.7%), concrete pipe (-61kg, +0.2%) and the plastic pipe (-78kg, +2%) no clear effect of the Young Modulus on the safety factor could be distinguished. From the concrete pipe, which is heavier as the normal pipe but still has a better safety factor, you could derive an increase of the stiffness should be positive to the safety factor. However for the plastic pipe, which is just a fraction lighter as the standard pipe (-10kg) but still shows a major increase in safety factor (+2%), it seems that a decrease of stiffness is positive to the safety factor.

To test the effect of the Young Modulus the following test were performed. In a first test (standard pipe, placed at location 11) the CMS-model predicted that due to an increase of the Young Modulus (3GPa to 30GPa) the safety factor decreases (1.2225 to 1.205). In a second test the CMS-model predicted that due to a decrease of the Young Modulus (3GPa to 1GPa) the safety factor also decreases (1.2225 to 1.205). This makes it impossible to make a statement of the effect of the Young Modulus (stiffness) on the safety factor.

Returning to the material characteristics; in a second test the different material types are tested at a location in which the pipe has more influence of the shape of the slip circle (location 11), see Table 25.

Steel pipe → SF=1.1425	**Plastic pipe → Pipe fails**
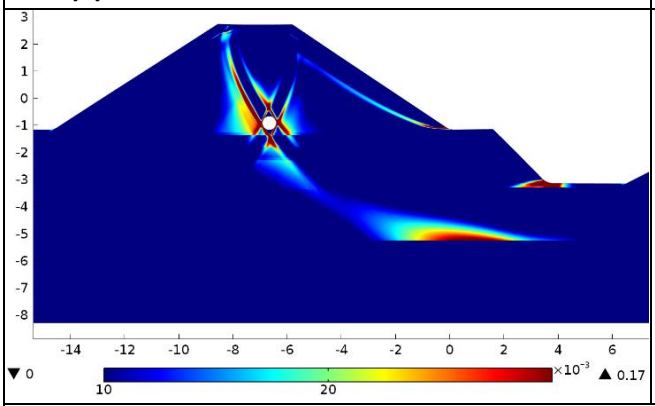	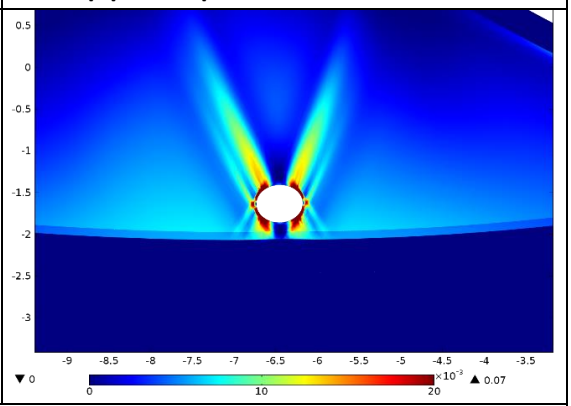
Observations: - The safety of the steel pipe decreased while pipe is located in the passive zone - The plastic pipe failed under influence of all the loads	

Middle top (Standard)	Steel	Plastic
SF=1.1625	SF=1.1425 (-1.7%)	Total failure

Table 25; Comparison material type left middle location

The results show that the small steel pipe relocates the potential slip circle differently compared to the small standard pipe (same diameter), visualized in Figure 63. In Figure 63 the green slip circle represents the potential slip circle of the small steel pipe while the black circle represents the standard small pipe. This test clearly shows that the radius of the slip circle increased as a consequence of more weight of the pipe and probably due the change of stiffness of the pipe. Due to the increase of the slip surface with the steel pipe (green line) the safety factor decreased.

Despite of the slightly small potential slip circle in case of the small steel pipe compared to the situation without a pipe, safety factors are equal. This seems logical since the small steel pipe just has a mass deficit of -2kg and the stiffness of the pipe probably has no influence on the results in this case.

The most important observation from Figure 63 is even when the pipe is placed at the same location and has the same size, still the potential slip circle can differ due to other characteristics. A probable explanation is that the steel pipe responds differently to uplift (pore pressure). Pipes with less mass do have more tendency to move upward.

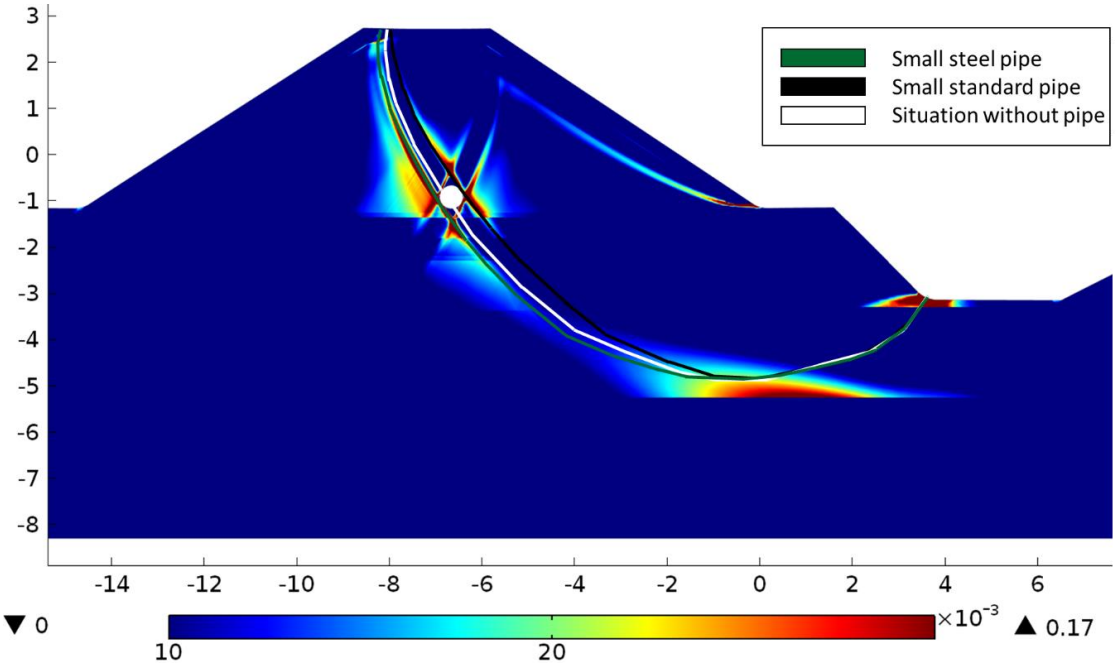

Figure 63; Comparison effective plastic strains small pipes at location 11

A remarkable observation is the plastic pipe fails when it is placed in the core of the dike. The cause can be assigned to the low stiffness of the pipe and the density of the plastic pipe. Since the plastic material of the pipe is lighter as the surrounding soil the pipe will experience buoyancy. But in the same time is experience a high load on top due to the soil of the dike + the weight of the containers. This means the pipe will experience extremely high stress at the inner side as shown in Figure 64, combined with the small pipe walls lead to high deformation of the pipe. The deformation of the pipe leading to high effective plastic strains of the soil, which it cannot cope.

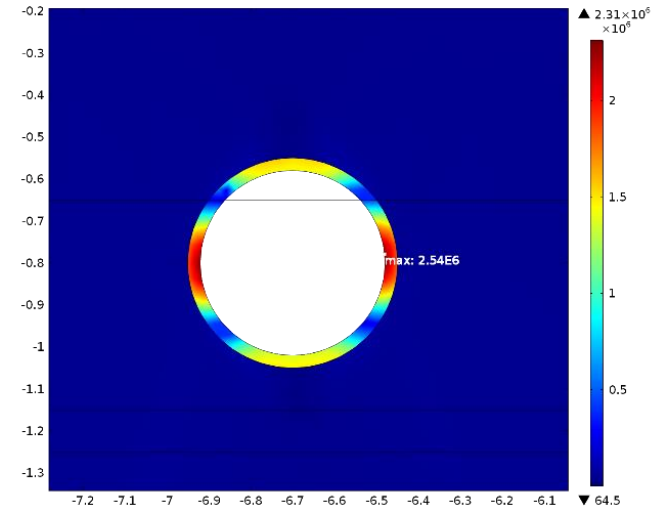

Figure 64; Von Misses stresses small plastic pipe

5.4. Effect pipe in changed soil conditions

In this paragraph the effect of a pipe on macro-instability is investigated in case the soil conditions of the dike are changed. Goal is to state if the effects of the pipe on the safety factor is in the same order of magnitude in case of different soil conditions. Important because otherwise the focus is only on one particular situation of the Southdike while for practical implementation is has to be applied to dikes with all kinds of soil conditions.

To check the ratio between the soil strength increase and the safety factor, the cohesion of the sand core (most influence on slip surface) is increased with **1kPa.** In this situation the safety factor without a pipe is **1.1825**. Multiple locations are tested again of which from which the following statements could be made;

- If there was no influence, changing situation soil has in most cases no impact (*except location 13*)
- Unsafe locations remain unsafe, same order
- Some safe locations become relatively more safe

For the last point mentioned the following example could be provided. When the pipe is placed at the location 15, as shown in Figure 65, the safety factor increases from 1.2225 to 1.37 (+12%) while the situation without pipe increased with 3.5% (1.1425 to 1.1825). This results implies that the positive effects of the pipe could become even more powerful if the dike is more stable.

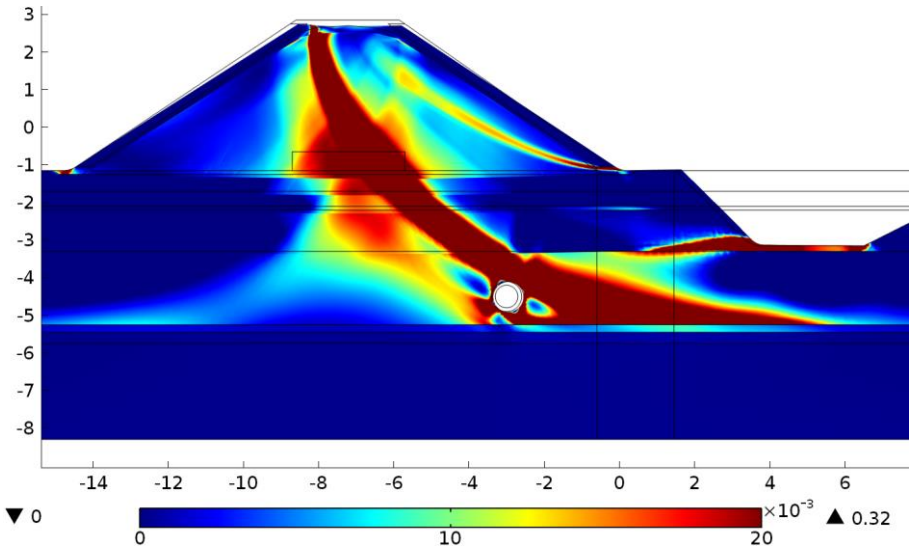

Figure 65; Effective plastic strains at location 15 [SF=1] with +1kPa cohesion increase sand core

In a second test the internal friction angle of the sand core increased and decreased. The effects shown in Table 26 are based when the pipe is placed at location 5.

Internal friction angle	Situation without pipe	Pipe at location 5	Relative difference
< 2 degree	1.1425 to 1.04 *(-9%)*	1.205 to 1.08 *(-10.3%)*	-1.3%
> 2 degree	1.1425 to 1.165 *(+1.9%)*	1.205 to 1.2675 *(+5.2%)*	+3.2%

Table 26; Effect variable internal friction angle on safety factor

As well as with an increase and decrease of the friction angle the influence of the pipe to the safety factor is amplified. In case the safety is reduced the effect is probably smaller because the situation of the dike is already almost at critical situation (failure).

In a last test two soil parameters of the sand core are changed, the cohesion and internal friction angle. The results of location 11 are presented in Table 27. The results from reducing the soil strength parameters

could not be used in this case because the dike failed due to local slip (SF=1.04) and the pipe had no influence. In case the soil strength increased the effect of the pipe remained in the same ratio.

Friction angle, cohesion	Situation without pipe	Pipe at location 5	Relative difference
< 1 degree, < 0.5kPa	1.1425 to 1.04 *(-9%)*	1.2225 to 1.04 (-15%)	-6%
> 1 degree, > 0.5kPa	1.1425 to 1.1825 (+3.5%)	1.2225 to 1.2725 (+3.6%)	+0.1%

Table 27; Effect variable internal friction angle and cohesion on safety factor

5.4.1. Pipe foundation influence

Practical implementation of buried pipes is done by excavating a trench or by directional drilling (location dependent). Both methods do affect the soil conditions around the pipe (more unconfined), which certainly have some influence on the safety factor (see results 5.4).

Situation 1: The soil is less compacted (assumed 10cm around pipe) which implies and increase of the porosity (+0.05), decrease of the angle of friction (0.5 kPa), decrease of the stiffness (10MPa) and decrease of the Poisson value (0.05). The results for location 2 is shown in Table 28.

For situations in which the pipe is located close to the surface this implies locally small slip circles can occur, especially at the sides of the dike. Due to the poor compaction friction between the soil and the pipe is extremely low, so the small soil layer on top of the pipe can slip really easily. In these situations no relevant safety factor can be determined (see drawback paragraph 5.1).

Less compacted pipes placed in the deeper layers of dike leads to a reduction of the safety factor. The 'cut' between the pipe and the soil has more effect, pipe can move easier implying less resistance against the slip circle. For location 5 the safety factor decrease from 1.205 to 1.195 *(-1%)*. No change shape slip circle.

Less compacted, pipe close to surface	Better compacted, pipe in deeper layers
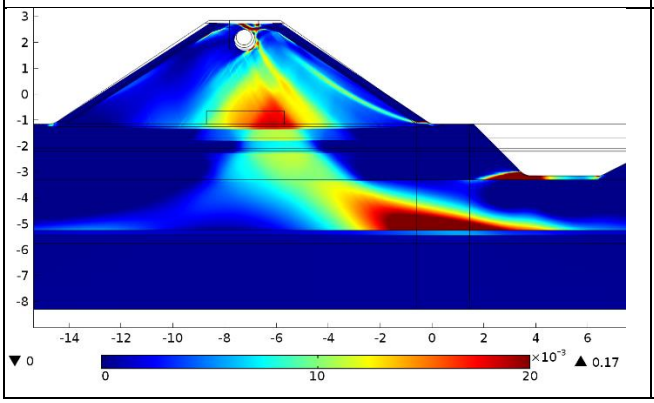	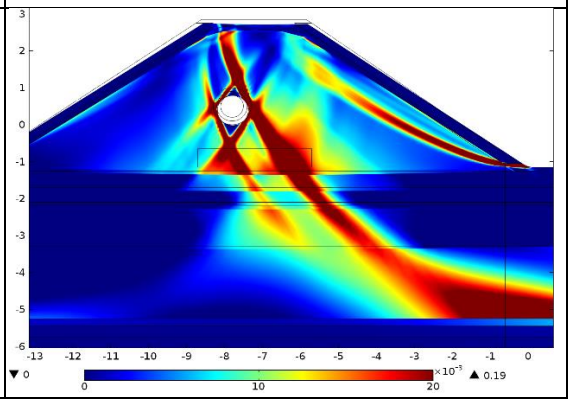

Table 28; Effects less well compacted soil

Situation 2: The soil around the pipe (10cm) is better compacted which implies a decrease of porosity (-0.05), increase of the friction angle (+0.5 kPa), increase the stiffness (+10MPa) and increase of the Poisson value (+0.05). The results for location 5 is shown in Table 28.

Better compaction at the surface implies no local slip, but it has no influence on the deep rotational slip circle. Except when the pipe is placed at the left top (location 1). In this case the slip circle has more problems to initiate due to the better compaction leading to an increase of the safety factor *(SF +1%).*

Better compaction for the deeper soil layers has no significant influence on the safety factor. In case the pipe is placed at location 5 the safety factor remains constant at 1.205 (0%). The length of the slip circle along the pipe is relatively small, so a marginal increase of the strength will not have a large effect on the safety (it is not become more difficult for the slip circle to cut along the pipe).

Chapter 6. Discussion

In this chapter the method, results and added value of this research will be discussed. The model limitations and uncertainties are discussed in paragraph 6.1 and 6.2 respectively. In paragraph 6.3 the processes that have not been modeled and are expected to have an influence on the results are discussed.

6.1. Limitations

Stationary model

The CMS-model does not simulate the state of the dike in a time-dependent situation. In the used stationary conditions groundwater flow (Darcy module) cannot be well simulated (Zheng et al., 2010). In a stationary model run the pore water pressure conditions of the equilibrium situation will be calculated. In the equilibrium situation the water is modeled as it has spread with an infinite amount of time. In stationary conditions the representative value of the pore pressure at a moment in time is therefore not known. This report determines these conditions by recalculating the stationary pore pressures (hydrostatic distribution) (Meij, 2015a; Zheng et al., 2010). These calculated values will always differ compared to the measured values of the Southdike which affects the validation of the hydraulic heads. Therefore the validation could only be performed for the first and final state of the Southdike experiment.

With the stationary model the unconfined conditions of the model could be less well simulated. The soil porosity has less influence on the predictions again because the CMS-model cannot simulate the groundwater flow well and determines the hydraulic equilibrium situation. In a time dependent situation, in for example a very porous soil the groundwater can rapidly distribute itself, while this is not the case in dense soil. In the calculated equilibrium situation calculated these effects are blurred out. This limitation is a drawback for determining the effect of compaction, occurring due to implementation of the pipe. The porosity and the related pore pressures could change differently on both sides of the pipe in short amount of time implying for example higher buoyancy forces. These effect will be under estimated in the CMS-model.

The stationary conditions cannot model the situational pore pressure increases shown in Figure 66. These local pore pressure increases can induce local horizontal displacements. Literature states that, if the dike is consolidated, over a long term these displacement can be maximum 10% higher compared to the situation modeled with the CMS-model (Viggiani, 2012).

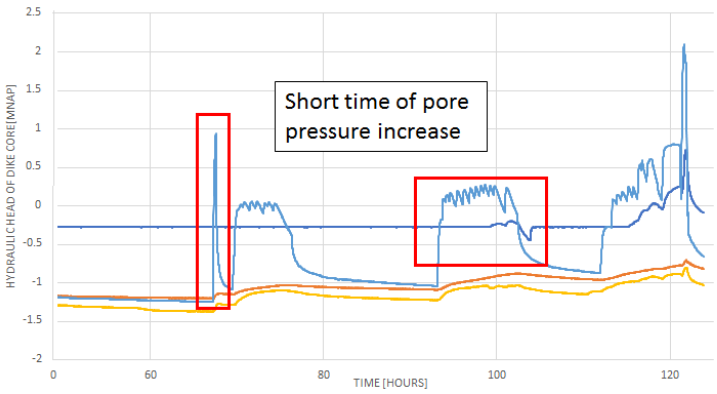

Figure 66; Situational pore pressure increase of the Southdike

Limitations COMSOL

Despite the fact that COMSOL is a perfect program to calculate all types of (non-linear) physics, it is at the moment still not a perfect in use for soil mechanical calculations. The used soil plasticity interface is a

relatively new physical interface within the COMSOL multi-physics software, so has not been tested and updated compared to other geotechnical software. Therefore it behaves quite unstable in many situations. This is why the solvers within the CMS-model had to be adapted to gain more stability. In the solver the relative tolerance had to be lowered, the predictor of the of the parametric steps had to be set constant as well as the initial damping factor had to be used for all parameter steps. These adaptations apply that while normally values of a next step are derived from linear interpolation of all the previous results, this method only uses the constant derived value. This could have a small influence on the derived results, less higher peaks in derived stresses.

A major limitation of COMSOL is that it's not able to model complete failure to determine the final critical slip circle. It calculates the potential slip circle, a situation which is different compared to the situation at complete failure.

Effect initial conditions

Using the potential slip circle situation for explaining the effect of the pipe on the development of macro-instability has the drawback that the used initial conditions could be still important for the determined safety factor. When the dike is at the critical situation (failure), the initial conditions do not influence the results.

The CMS-model uses two types of initial conditions, the initial hydraulic head and the initial displacements. This limitation is tested with the initial hydraulic head, this is expected to be of more importance for the model. The results of this test are shown in the table below:

Initial hydraulic head	Safety factor	Result	Increase due to pipe
-1.4m	1.1825	1.205	+1.89%
-1.8m	1.205	1.2275	+1.87%

Table 29; Effect initial condition (hydraulic head) on derived safety factor

The table shows that the initial condition certainly has some effect on the derived safety factor. It also shows that the effect of the pipe on the safety factor is in both situations almost equal. This means the conclusions derived in this report are not influenced by the chosen initial conditions.

2D model environment

The CMS-model calculates the effect of the pipe in 2D conditions. 2D FEM modeling implies some geometrical simplifications, simplifications to model boundaries and material behavior compared to the real situation in 3D. This implies that the so-called 'length-effect' is neglected in a 2D model environment. This effect could be important to model if we want to know the effect of a pipe over the whole length of a dike (parallel direction) induced by multiple soil conditions and loadings. Due to the irregularities along the length of the dike the safety factor could be different for multiple sections of the dike which could be of influence to the effect of a pipe on macro-instability.

Another limitation of a 2D analysis is that it tends to be conservative (Bergado & Teerawattanasuk, 2008)2. The use of 3D slope stability analysis would be important to model real world problems, to make the designs more economic, and to provide a guide for 2D designs (Bergado & Teerawattanasuk, 2008).

Another limitation of a 2D model environment is that no conclusions could be drawn from the research into the effects of a cross directional placed pipe within the dike, shown in Appendix I.

Southdike situation

The whole research is completely fixed on the situation of the Southdike. In the Southdike experiment the researchers forced by means of a filled container on top and the pumping of water into the dike core a deep rotational sliding circle. These mechanisms could have an effect on the results of the pipe, since the Southdike has failed by slightly other mechanisms than in a real flood situation. To investigate this effect boundary conditions of the CMS-model were changed as presented in Appendix J. Some small testing showed that the effect of the pipe is dependable on the loading implied on the dike.

6.2. Uncertainty

Soil parameters

There will be some uncertainty in the chosen soil parameters since the soil is always characterized by its inhomogeneous conditions. The location at which soil sample are taken are of influence. The soil conditions of the CMS-model are derived from laboratory and predictions tests. The soil samples and laboratory test for some parts of the IJkdijk experimental site are already performed in 2006 or 2008 while the experiment was performed in 2012.

The uncertainty of the soil conditions will have some influence on the performed validation, especially on the derived safety factor for the general situation without a pipe. Uncertainty of the soil parameters would not have an influence on the effect of a pipe on the development of macro-instability. It would only have an influence on the extent in which the safety factor is influenced by the characteristics of the pipe.

Moment of failure

The validation of the CMS-model with the Southdike is entirely based on the moment of failure mentioned in the Geotechnical report from stichting IJkdijk (Vries et al., 2012). This used moment of failure is quite variable throughout the different sections, layers within sections, even the location within a soil layer. This implies that at the defined failure moment in time, parts of the dike did already failed, or did not. In case it already did data is overestimated, when it didn't data is underestimated. This significantly change the result of the calibration and validation. For the effect of the pipe this would again only have an influence on the extent in which the safety factor is influenced by the characteristics of the pipe.

Determination slip circle

The defined slip circle for explanation of the effects of the buried pipe to the development of macro-instability according to Bishop is based on critical slip criteria as presented in Appendix F. The exact location of the critical slip circle is however dependable of many different factors like the actual pore pressures, mobilized strength, time effects and so on. The exact shape of this critical slip circle in the final failure state cannot be precisely known, that is subjected to a margin of uncertainty. The effect of the pipe has therefore to be interpreted as an effect on the potential slip circle. So due the pipe the slip circle will potentially fail with a different shape which influence the current safety condition of the dike.

Model cross validation

It is allowed to perform a model cross validation comparing the FoS (LEM) with the F_{SR} (FEM) (Melnikova, 2014; Thompson, 1993; Zheng et al., 2010). The methods will however refer to different dike models and are not completely identical (Melnikova, 2014). In physical non-linear structures, like elasto-plastic soils, response of structure to the external load does not depend linearly on the strength parameters of soil (Melnikova, 2014). Thus, we cannot expect that scaling of soil properties with constant load in the strength reduction method would give absolutely the same results as computing ration of disturbing and restoring

forces in the original dike in the limit equilibrium analysis (Melnikova, 2014). Modeling the exact same conditions in both models should maximum lead to a difference of 3-5% in the results (Meij, 2015b).

Creep and Settlement

While this research addresses all simulated effects to (deep) rotational sliding, the contribution of creep and settlement will also lead to displacements (strains) (Finsbury et al., 2013).

- Creep is described as the tendency of a solid material to move slowly or deform permanently under the influence of mechanical stresses ((Frost & Ashby, 1982) as cited in Finsbury et al., 2013). Due to creep the dike embankment soil may move away laterally from the crown.
- Settlement is the consolidation of the foundation layers made of soft clays and silts. Settlement affects the actual dike by deforming the embankment. Deformation of the dike can lead to creaking and the development of seepage paths in the different components of the dike leading to instability.

The Southdike is designed in a way to reduce these effects as much as possible (dike is build 3 months prior to experiment). Therefore the effect of those two mechanisms on the validation results will be negligible.

6.3. Unaccounted physical processes

Interface for the condition between pipe and soil

The model does not include an interface which describes the condition between the soil and the pipe. In the CMS-model the pipe is modeled as part of the soil with only different properties. This leads to the situation, as shown by the results of this research, that the slip circle does not always progresses directly along the pipe. Based on literature (David Pezza & Hal Van Aller, 2005) and the opinion of geotechnical expert (Meij, 2015b) this result seems unlikely to happen. They state that a 'cut' has to occur directly alongside the pipe. With an interface the resistance between the material and the pipe, in the form of friction can be defined. This makes it possible to model this 'cut' along the pipe. Expected is that not taking into account this interface just has a marginal error on the slip surface and safety factor (Meij, 2015b).

Implementation of the pipe

The influence of the foundation, situation in which the pipe is placed, is just marginally taken into account in this research, see 5.4.1. This covers the effect of directional drilling because this method will be of marginal effect to macro-instability (Finsbury et al., 2013).

The effect of a pipe placed in a trench can however have some influence on macro-instability. In this situation the pipe will be supported by a foundation of for example placed stones and gravel next to the pipe. These different materials can have an effect on the development of macro-instability. The potential slip circle can be forced to relocate around the foundation or it induces easier through the foundation. This has some implication for the derived safety factor.

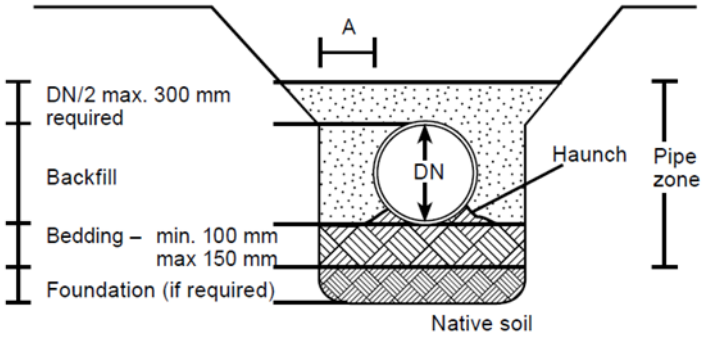

Figure 67; Standard pipe foundation (AMIANTIT, 2006)

Secondly, strong (well compacted) foundations will reduce the effect of buoyancy on the pipe from which is shown it has some influence on the development of macro-instability.

Aspects of the pipe

Some of the aspects which are related to a pipe are not taken into account in the CMS-model. The first aspect is that the pipe cannot fail. This limitation is based on the statement that the required strength and the design life requirements of the pipe should be determined by the methods of the pipe manufacturers (Finsbury et al., 2013). For certain conditions high von Misses stresses occur in the pipe of which could be questioned the question is if in real scenario pipe can cope with these forces.

The second aspect which is not taken into account are some elements of the pipe like a casing, pipe joints, the shape of the pipe and the structure at the outside of the pipe.

Figure 68; Pipe/cable located next to dike (Hoogheemraadschap De Stichtse Rijnlanden, 2010)

The third aspect is the content of the pipe (like gas, water or oil), which has an influence on the safety condition of the macro-stability failure mechanism of the dike as shown in Appendix H. An aspect of this content is that it will dynamically change, high or low volumes in time. These dynamical changing conditions of the content in the pipe together with the changing conditions in the dike could also have an effect on macro-instability. This could however not be tested due to the stationary model.

Undrained conditions

The CMS-model does not include the phreatic surface in the simulation domain which can have a significant effect on the slip surface (Zheng et al., 2010). A phreatic surface is defined in literature as a surface in a porous medium where relative pore pressure is zero. Due to moving water tables pressure on the soil changes creating zones with positive and negative pore pressures, respectively described as saturated and unsaturated soils. The effect of the decreasing and increasing pore pressures on the failure slip circle is shown in Figure 69. The resistance of porous media to the flow is modelled in the CMS-model by Darcy's law suitable for low velocities. Improvement of the model would be to model the unconfined porous flow dynamics by solving the Richards' equation with non-linear rheological properties of the media depending on the effective water content (Melnikova, 2014). These non-linear properties have to be modelled by the Van Genuchten model (Van Genuchten, 1980).

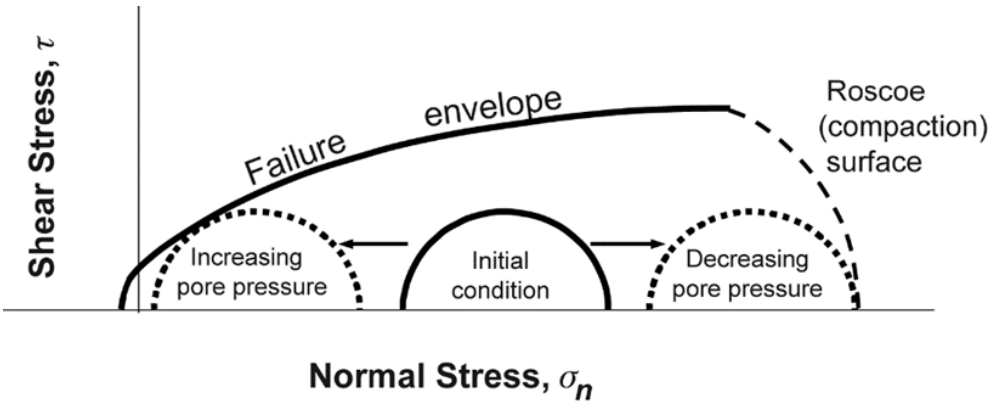

Figure 69; Effect pore pressures on failure envelope

Chapter 7. Conclusions and Recommendations

The main objective of this research was to develop a model which able to simulate the geotechnical effects of macro-stability to investigate how much the characteristics of the buried pipe contribute to the development of macro-stability. This objective led the following formulated main research question; ***which effect has a buried pipe on the macro-stability failure mechanism of a dike?*** The answer and main conclusion of this research is that in certain conditions, the buried pipe has a positive effect on macro-stability failure mechanism. This is based on the provided answers of the research questions of this chapter. This chapter will finish with recommendations for further research.

7.1. Conclusions

1. *How can the geotechnical effects of macro-stability be modeled?*

To model the geotechnical conditions which have an effect on macro-stability, a 2D coupled model build in COMSOL 4.4, using two mathematical models in stationary conditions to describe the behavior of the dike under hydraulic and mechanical loads, has been created (henceforth CMS-model). The CMS-model applies a coupled combination of a Darcy model for modelling the flow of water in the porous media and a Drucker-Prager linear elastic perfectly plastic model for modelling the soil displacements in the soil skeleton. The CMS-model uses a Newton-Raphson iteration scheme, solved by a direct PARADISO, to solve the nonlinear algebraic equations at each integration step. The CMS-model is quasi-static, by applying multiple loading steps to simulate the time dependency of a dike under certain loadings.

The CMS-model uses three phases to calculate the geotechnical conditions of the dike. The first phase is used for initialization of the model, calculating the initial stresses. In the second phase the water pressure in the soil are calculated. The third phase the displacements in the soil skeleton are determined and the related effective plastic strains of the soil (plastic state) to determine the (deep) rotational slip surface.

2. *To what extent can the model reproduce macro-stability of the Southdike experiment?*

The CMS-model is validated on three aspects of the Southdike experiment, safety factor, hydraulic head and displacements. First note is that the CMS-model only predicts the potential slip circle which about equal to the situation at t=118.5hrs of the Southdike experiment (failure at t=122.25hrs).

For the safety of the Southdike a conservative safer situation has been modeled (+10%) compared to the LEM study (Bishop and Uplift Van) which can mainly be addressed to calculating a smaller, still almost identical, slip circle. The simulated hydraulic head matches the measured data quite well (<0.3m), except from situation located close under the dike core. In these situation the hydraulic head is underestimated (for specific soil layers) implying the pore pressure in the actual dike was higher. The displacements of the deep rotational slip circle over the complete depth of the foundation layer are after calibration all simulated within a small range of the measured inclinometer values (maximum 15% off).

3. *To what extent and in which way does the buried pipe characteristics contribute to the development of macro-instability?*

The characteristic of the pipe such as location, size, material and the content of the pipe influence the development of the macro-stability failure mechanism. In general a negative or positive influence is closely related to the principles of Bishop. For certain conditions the characteristics of the pipe have a positive influence to the development of the macro-stability failure mechanism.

The change in safety condition of the macro-stability failure mechanism cannot be addressed solely to a single characteristic of the pipe. Combinations of characteristics and conditions determine the gain in safety

for macro-stability failure mechanism. Therefore for every individual situation with different conditions and characteristics of the pipe a calculation has to be performed to know the safety situation to macro-stability of the flood defense.

The buried pipe changes the shape of the slip circle when located close to or on the potential slip circle. The pipe can relocated the potential slip circle inwards creating a smaller slip circle implying a higher safety factor or the pipe forces the potential slip circle to relocated outwards creating a larger slip circle implying a lower safety factor.

For the particular situation of the Southdike general locations could be addressed at which the pipe has a positive or negative effect to the development of macro-stability.

The weight of the pipe (density) has a substantial influence on the development of macro-instability when located within the slip surface of the dike. This could be directly related the principles of Bishop.

No clear statement can be made for the effect of the size and stiffness of the pipe on the development of macro-instability. This is again dependable on the situation under which the pipe is subjected.

The soil conditions and the loading conditions also have a significant influence to the effect of the pipe on the safety condition of the macro-stability failure mechanism. The contribution of the pipe to the development of macro-instability is non-linear dependable on the soil conditions of the dike. More unstable soil conditions lead to proportional larger decrease of the positive effects of the pipe. More stable soil conditions lead to proportional higher positive effects of the pipe to macro-instability.

7.2. Recommendations

The conclusions of this study primarily serve a scientific purpose, which is to increase the understanding of the effects of pipes on macro-stability. However, the findings are also of practical importance since they point out what the possibilities regarding structures in dike to make feature norms for practical implementation. To make this possible additional studies are needed to further improve the CMS-model to provide more support or extend some of the drawn conclusions.

Conditions dike

The soil conditions of the dike showed to have a significant influence on the effect of a pipe to the development of macro-instability. Therefore a lot more testing has to be done to examine the effects of the pipe in different configurations (different potential slip circles). Important is changing the soil conditions in the dike; soil strength parameters, pore pressures and the loading conditions.

In addition, those tests have to be performed for a complete different dike. This can be a dike with a different geometry or for example a dike-dune. A strong recommendation is to perform this testing with less different soil layers to reduce the uncertainty of each layer.

The dike should also be subjected to different types of transitions/structures than a pipe. This can be for example a foundation of a house, parking lot or a flood wall.

Model

The conditions of the CMS-model should also be investigated in a 3D environment for practical reasons. A 3D environment makes it possible to investigate the situation in which the pipe is placed in cross-directional direction. And if inhomogeneity over the length of the dike has an influence on contribution of the parallel placed pipe to macro-instability.

For academic purpose the CMS-model should be made time dependent. The Darcy module functions more efficient in time dependent conditions, leading to a better simulation of the groundwater flow and a better distribution of the pore pressure over the different soil layers. With a time dependent Darcy module proper research could be performed of the effects of the unconfined conditions around the pipe. A time dependent CMS-model also provides the opportunity to model non-stationary boundary loads. These are important to for example investigate the influence of the standard wave on dike with a buried pipe (effects changes high and low water level).

Pipe conditions

The CMS-model should be include with the interface in COMSOL named 'Contact Pair'. This interface can define the interaction between the soil and the pipe. Therefore the soil and the pipe have to be modeled as to complete different objects. In a box, shown in Figure 70, the friction, sliding resistance and traction between the pipe and soil can be defined. Until now, efforts to apply this interface have not succeeded, mostly due to time restrictions. In these efforts the pipe remains underdetermined compared to the soil. Therefore errors occur in the initial stage of the model.

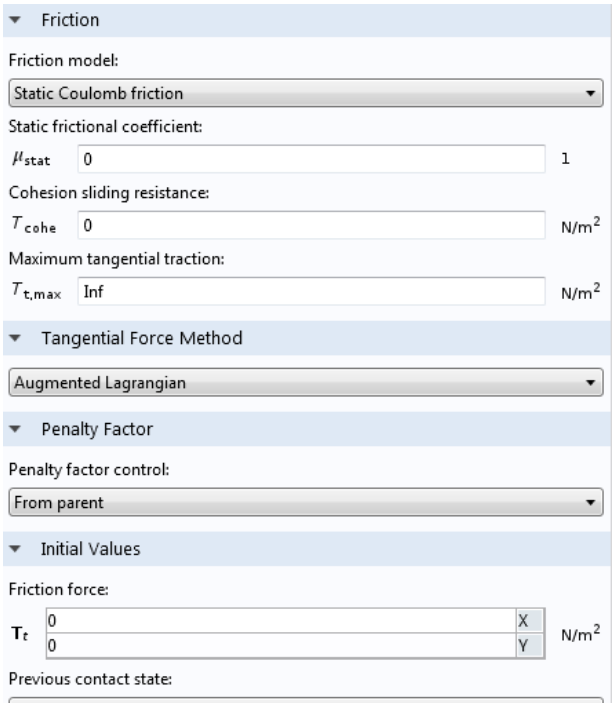

Figure 70; Contact Pair option in COMSOL

For practical reasons the effect on macro-instability due to method of implementation of the pipe should be extended. Especially focusing on the effect of a standard used foundation. For instance simulating gravel or stones alongside the pipe.

More investigation should be performed on the situation when the pipe is filled with a specific substance, not only assuming oil. In addition the dynamically changing condition of the content of the pipe (for example; a first empty sewer pipe gets filled and afterwards becomes empty again) has to be investigated with a time dependent CMS model. Such changes could significantly affect the horizontal displacements.

Chapter 8. References

Allsop, W., Kortenhaus, A., & Morris, M. (2007). *Failure Mechanisms for Flood Defence Structures*. *FLOODsite publications*.

AmericanLifelinesAlliance. (2005). *Guidelines for the Design of Buried Steel Pipe* (Vol. 2001).

Augustesen, A. H. (2006). *The Effects of Time on Soil Behaviour and Pile Capacity*. *Aalborg University*. Aalborg University.

Balkema. (1998). *Dikes and Revetments: Design, Maintenance and Safety Assessment* (1st ed.). Kristian Pilarczyk.

Bear, J. (1979). *Hydraulics of Groundwater* (1st ed.). New York: McGraw-Hill.

Bergado, D. T., & Teerawattanasuk, C. (2008). 2D and 3D numerical simulations of reinforced embankments on soft ground. *Geotextiles and Geomembranes*, *26*, 39–55. doi:10.1016/j.geotexmem.2007.03.003

Bocchi, F. (2014). Yield Surfaces and Plastic Flow Rules in Geomechanics. Retrieved February 3, 2015, from http://www.comsol.com/blogs/yield-surfaces-plastic-flow-rules-geomechanics/

Chi Fai Ng, P. (1994). *BEHAVIOUR OF BURIED PIPELINES SUBJECTED TO EXTERNAL LOADING*. University of Sheffield.

David Pezza, P. E., & Hal Van Aller, P. E. (2005). *Technical manual: conduits through embankment dams*. Denver.

Finsbury, R. H. L. S. of, Steven L. Stockton, P. E., & Loudiere, D. (2013). *The International Levee Handbook*. (U. A. C. of Engineers, Ed.). London: CIRIA.

FloodProBE, & Oderker, M. (2013). *Design concepts of multifunctional flood defence structures*. Delft.

Floodsite. (2014). Toetsen waterkeringen. Retrieved November 4, 2014, from http://www.floodsite.net/juniorfloodsite/html/nl/student/thingstoknow/geography/waterkeringtoets.html

Gemeente Katwijk. (2013). www.kustwerkkatwijk.nl - Welkom. Retrieved September 30, 2014, from http://www.kustwerkkatwijk.nl/public/index.php?id=1

Geoscience, F. of. (2013). Rhine-Meuse delta studies. Retrieved October 6, 2014, from http://www.geo.uu.nl/fg/palaeogeography/results/flooding

Hamdhan, I. N., & Schweiger, H. F. (2011). Slope Stability Analysis of Unsaturated Soil with Fully Coupled Flow-Deformation Analysis. *Iamg 2011*, 1–18. doi:10.5242/iamg.2011.0063

Hammah, R. E., Yacoub, T. E., Corkum, B., & Curran, J. H. (2005). A comparison of finite element slope stability analysis with conventional limit-equilibrium investigation. *Proceedings of the 58th Canadian Geotechnical and 6th Joint IAH-CNC and CGS Groundwater Specialty Conferences–GeoSask*.

Herder, A. J. den, Achterhuis, E. J., Baars, P., Beijer, A. J. W. de, Bokhorst, J. R. van, Bruggen, E. van, … Dijkstra, H. A. M. (2012). *NEN 3651* (Vol. 3651). Delft. doi:ICS 23.040.10; 93.010

Hill, R. (1950). *The Mathematical Theory of Plasticity*. Oxford: Oxford University Press. 1950.

Hoogheemraadschap De Stichtse Rijnlanden. (2010). *Beleidsregels op grond van de Keur van het Hoogheemraadschap De Stichtse Rijnlanden 2009* (Vol. 2010).

Ibsen, L. B., & Jakobsen, K. P. (1998). *Limit State Equations for Stability and Deformation*. Aalborg Universitet.

Inc, C. (2012). *COMSOL Multiphysics User guide* (4th ed.). Los Angeles: COMSOL.

Inc, C. (2013a). *Geomechanics Module*. Los Angeles.

Inc, C. (2013b). *Introduction to Comsol Multiphysics* (COMSOL 4.4.). Los Angeles: COMSOL.

Jiang, H., & Xie, Y. (2011). A note on the Mohr-Coulomb and Drucker-Prager strength criteria. *Mechanics Research Communications*, *38*(4), 309–314. doi:10.1016/j.mechrescom.2011.04.001

Klein, R. I. (1999). Star formation with 3-D adaptive mesh refinement: the collapse and fragmentation of molecular clouds. *Journal of Computational and Applied Mathematics*, *109*(1-2), 123–152. doi:10.1016/S0377-0427(99)00156-9

Koelewijn, A. . (2012). *Design of IJkdijk All-in-One / Sensor Validation Test*.

Koelewijn, A. R. (2012). *IJkdijk All-in-one Sensor Validation Test - Geotechnical Analysis*. Delft.

Kruse, dr. H. M. G., Meijers, dr. ir. P., Ferrer, C. D. C., Lange, drs. G. de, MSc, T. V., Havinga, ir. H. R., … Heinsbroek, dr. ir. A. G. T. J. (2013). *Effecten geïnduceerde aardbevingen op het Gasunie- netwerk in Groningen*. Delft.

Lang, B., Kraut, H., Klöckner, F., Speckens, C., Joubert, R., & Mokhov, I. D. (2012). *All-In-One Sensor Validatietest - Eindrapport*. Den Haag.

Liu, M. D. (n.d.). Soil Plasticity and the Structured Soil Plasticity and the Structured Cam Clay Model, (6), 95.

Lu, Y., Wang, Z., & Chong, K. (2005). A comparative study of buried structure in soil subjected to blast load using 2D and 3D numerical simulations. *Soil Dynamics and Earthquake Engineering*, *25*, 275–288. doi:10.1016/j.soildyn.2005.02.007

Mansour, Z. S. (2015). Traditional Methods vs . Finite Difference Method for Computing Safety Factors of Slope Stability, *5*(4), 1119–1130.

Meij, R. Van Der. (2015a). Macro stability of flood protection embankments. Enschede: Deltares.

Meij, R. van der. (2015b). *Meeting with Raymond van der Meij*. Enschede.

Melnikova, N. B. (2014). *Finite Element Analysis of Levee Stability for Flood Early Warning Systems Natalia Melnikova*. University of Amsterdam.

Melnikova, N. B., Jordand, D., Krzhizhanovskayaa, V. V., & Sloot, P. M. A. (2012). Slope Instability of the Earthen Levee in Boston , UK : Numerical Simulation and Sensor Data Analysis. In *Elsevier Editorial System(tm) for Computers and Geotechnics* (p. 16). Amsterdam: Elsevier.

MIDAS. (2015). 3D Slope stability. Retrieved March 18, 2015, from http://en.midasuser.com/training/tutorial_list.asp?nCat2=132

Morris, M., Benahmed, N., Phillippe, P., Royet, P., Tourment, R., Ham, G. van den, & Beek, V. van. (2012). *WP 3 : Reliability of Urban Flood Defences*. Brussel.

Nagy, L. (2012). STATISTICAL EVALUATION OF HISTORICAL DIKE FAILURE MECHANISM. *Riscuri Si Catastrofe*, *11*(2), 7–20.

NPTEL. (2004). GEOTECHNICAL PROPERTIES OF SOIL AND OF REINFORCED SOIL. *Advanced Foundation Engineering*, *Module 1*(Lecture 4), 20.

Potts, D. M., & Zdravković, L. (1999). *Finite Element Analysis in Geotechnical Engineering: Theory*.

Pressure Vessel Engineering, L. (2008). Mesh Refinement. Retrieved February 3, 2015, from http://www.pveng.com/FEA/FEANotes/RefineAtDiscon/RefineAtDiscon.php

Rabie, M. (2014). Comparison study between traditional and finite element methods for slopes under heavy rainfall. *HBRC Journal*, *10*(2), 160–168. doi:10.1016/j.hbrcj.2013.10.002

Redaelli, M., Cividini, A., & Gioda, G. (2011). Influence of Boundary Conditions in a Finite-Element Analysis of River Levees. *International Journal of Geomechanics*, *11*(5), 399–405. doi:10.1061/(ASCE)GM.1943-5622.0000100

Reddy, J. N. (2005). *An Introduction to the Finite Element Method*. McGraw-Hill.

Rijkswaterstaat. (2013). *Beleidsregel kabels en leidingen in, op of langs waterkeringen*. Den Haag.

Rijkswaterstaat. (2014). Deltaprogramma 2015: Nederland veilig en leefbaar in de 21e eeuw | Nieuwsbericht |. Retrieved October 21, 2014, from http://www.rijksoverheid.nl/nieuws/2014/09/16/deltaprogramma-2015-nederland-veilig-en-leefbaar-in-de-21e-eeuw.html

Tan, D. (2006). *SEISMIC SLOPE SAFETY - DETERMINATION OF CRITICAL SLIP SURFACE USING ACCEPTABILITY CRITERIA*. University of London.

Thompson, J. (1993). The location of critical slip surfaces in slope-stability. *Journal of the South African Institute of Mining and Metallurgy*, (4), 85–95.

U.S. Environmental Protection Agency. (1994). *Technical Report Design and Evaluation of Tailings Dams*. Washington. doi:EPA 530-R-94-038

Van Loon-Steensma, J. M., & Vellinga, P. (2014). Robust, multifunctional flood defenses in the Dutch rural riverine area. *Natural Hazards and Earth System Science*, *14*(5), 1085–1098. doi:10.5194/nhess-14-10-2014

Van Vollenhoven, P., Hulsenbek, mr. J. A., Mertens, dr. ing. F. J. H., Visser, dr. ir. J. P., Spiekhout, ir. J., Suurenbroek, ir. Y. E., … Klumper, H. J. (2005). *Leidingbreuk veroorzaakt dijkverzakking op 27 januari 2004 te Stijn*. Den Haag.

Vermeer, P., & Neher, H. (1999). A soft soil model that accounts for creep. *Proceedings of the International …*, 1–13.

Verruijt, A. (2001). *Grondmechanica*. Delft: Technische Universiteit Delft.

Viggiani, G. (2012). *Geotechnical Aspects of Underground Construction in Soft Ground*. Rome: CRC Press.

Vorogushyn, S., Merz, B., & Apel, H. (2009). Development of dike fragility curves for piping and micro-instability breach mechanisms. *Natural Hazards and Earth System Science*, *9*(4), 1383–1401. doi:10.5194/nhess-9-1383-2009

Vries, ing. G. de, Bruin, ing. H. T. J. De, Peters, D. J., Loon, J. Van, & Koelewijn, dr. ir. A. R. (2012). *All in One-Sensor Validatie Test*. Delft.

Wade Anderson, P. E., Chuck Cooper, P. E., John Frdland, P. E., Michele Lemieux, P. E., Mark Pabst, P. E., David Pezza, P. E., & Hal Van Aller, P. E. (2007). *Technical Manual : Plastic Pipe Used in Embankment Dams*. Denver.

WML. (2005). Gegevens pijpleidingen Limburg. Retrieved November 4, 2014, from http://www.wml.nl/

Zheng, Y., Tang, X., Zhao, S., Deng, C., & Lei, W. (2010). Strength reduction and step-loading finite element approaches in geotechnical engineering. *Joumal of Rock Mechanics and Geotechnical Engineering*, *2010*(1), 21–30. doi:10.3724/SP.J.1235.2009.00021

Zienkiewicz, O. C., Taylor, R. L., & Zhu, J. Z. (2005). *The Finite Element Method: Its Basis and Fundamentals*. Butterworth-Heinemann.

Chapter 9. Appendices

A. Geometry IJkdijk detail drawings

In the reports of the 'stichting IJkdijk' detailed drawings of the Southdike are presented providing an impression how the Southdike is situated. The geometry of the CMS-model is based on these drawing and the locations of the sensors could be visualized with the help of these drawings.

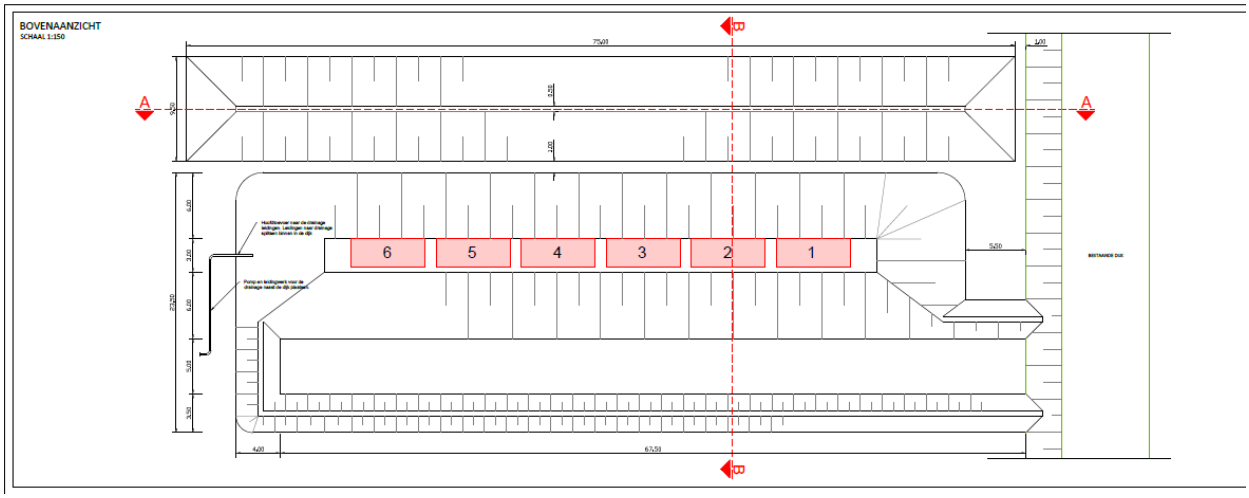

Figure 71; Top view Southdike (Vries et al., 2012)

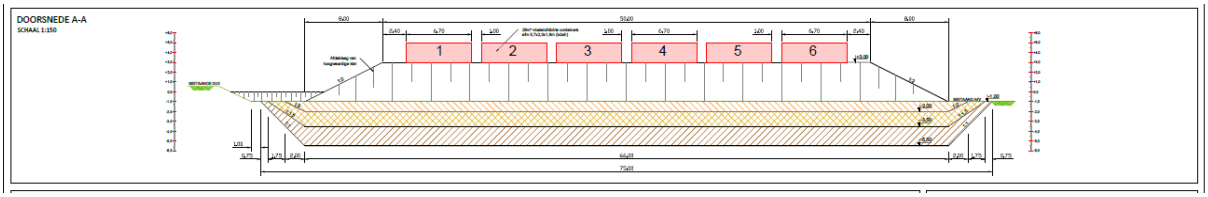

Figure 72; Section A-A Southdike (Vries et al., 2012)

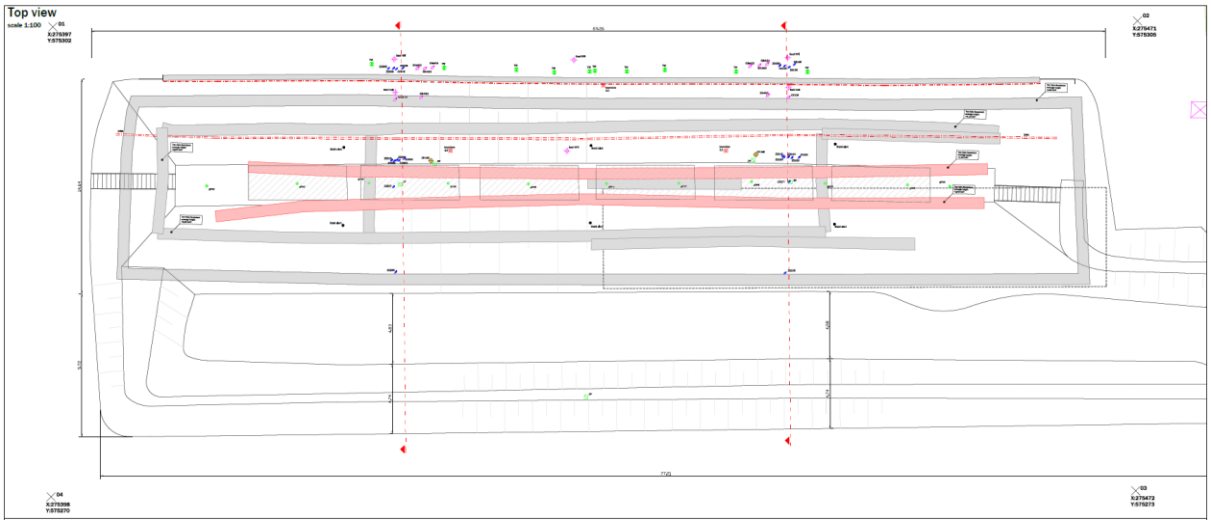

Figure 73; Locations all sensors Southdike (Vries et al., 2012)

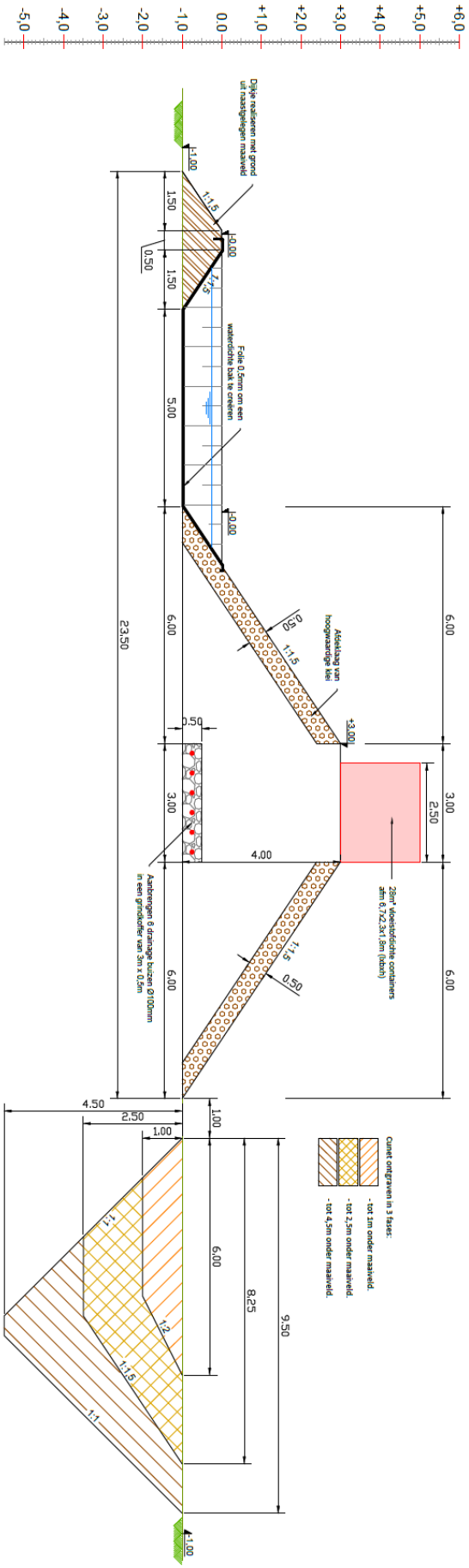

Figure 74; East section Southdike experimental location (Vries et al., 2012)

B. Determination soil strength parameters IJkdijk

In this Appendix all the data is presented which is used for the determination of the soil strength parameters used in COMSOL. The determination of the soil parameters is important as they are the main input for the CMS-model. In the Southdike experiment the failure was induced over a fairly short period of time don't allowing pore pressure water sufficient time to dissipate (Melnikova, 2014). Therefore the soil investigation on side, carried out by Deltares, had taken this so called undrained situation into consideration (Vries et al., 2012). Those tests were specially determined for a stability calculation carried out with Plaxis software package (Lang et al., 2012). PLAXIS applies a soft soil - or a hardening soil-model sometimes using different parameter values to calculate the displacement. COMSOL does not applies these models so those determined values have to be recalculated to values used by the COMSOL software.

Prediction competition soil data

The first representative soil strength parameters of the soil layers are based on a prediction competition. Competitors of this competition had to determine with their own made models at which stage the South IJkdijk will fail. The most useful in this case is the submission of the UVA, which used a model made in COMSOL presenting the following initial soil strength parameters (Lang et al., 2012; Melnikova, 2014):

Property	**2D Drucker-Prager soil model**			
	Core sand	Base sand	Clay – modeled via effective stress analysis	Peat- modeled via effective stress analysis
Density, kN/m3	18 (dry) / 20 (wet)	19	14	10
Young's modulus, drained, MPa	30	150	11.6	1.6
Poisson's ratio, drained	0.3	0.3	0.49 (undrained)	0.49 (undrained)
Cohesion, KPa	0	0	Case 1: 6300 Case 2: 9700	Case 1: 0 Case 2: 4600
Friction angle, grad	30	31.1	29.4	27.5

Table 30; Soil strength parameters UVA (Melnikova, 2014)

The values of the other competitors, using different finite element software, are presented for comparison. Siemens used the PLAXIS software. In their report (unfortunately) not all parameters, determined by HR Wallingford, of the Southdike test were mentioned.

Soil type	**Cohesion [kPa]**	**Friction angle [deg]**	**E50 [MPa]**	**Density [kN/m^3]**	**Horizontal permeability [m/day]**	**Vertical permeability [m/day]**
Soft clay	4.6	29.4		15	10^{-6}	10^{-7}
Peat	9.7	27.4		10	10^{-5}	10^{-6}
Fill Sand	1.95	26.4	10	19	0.1	0.09
Base Sand			50	20	0.0864	0.07
Cover clay				18	10^{-6}	10^{-7}

Table 31; Soil strength parameters Siemens (Lang et al., 2012)

The permeability for our COMSOL model, since it has the capability for a permeability value in x and y direction, can be determined by using the square root of the horizontal permeability square and vertical permeability square.

The last competitor for the South IJkdijk was Arcadis which used GeoStab and GeoSettle software to determine the safety. This software uses less parameters compared to the COMSOL software so the uncertainty of those values are higher.

Soil type	Friction angle	Cohesion
Soft organic	22.46	9.7
Clay toplayer	33.42	3.82
Peat	25.29	5.83
Sand fill	30.47	0.58
Base sand	36.1	0

Table 32; Soil strength parameters Arcadis (Arcadis, 2012)

Soil investigation data

With the data of the soil investigations, carried out by Deltares, the values of the prediction completion could be checked. The data must provide confirmation which of the competitors of the prediction completion presented the best soil strength parameter values.

Determination of the location of soil investigation test data is important because of the non-homogenous conditions of the soil. In a letter of Deltares is stated that the stability test will be carried out around close to S05 and B5, see Figure 75. Therefore all the used laboratory data presented in this Appendix is based on boring B05 till B09.

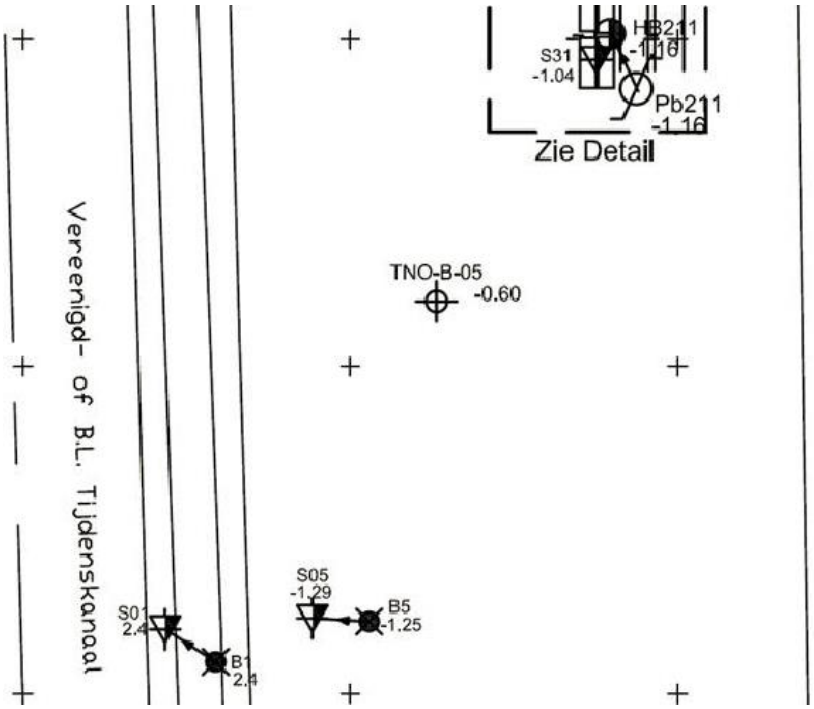

Figure 75; Soil investigation locations (Deltares, 2012)

The first step of defining the geometry of the Southdike is determine the depths/sizes of the soil layers. Due to the non-homogenous characteristics of the soil the size of a soil layer should be based on the borings B05 till B09 shown in Figure 76 and Figure 77.

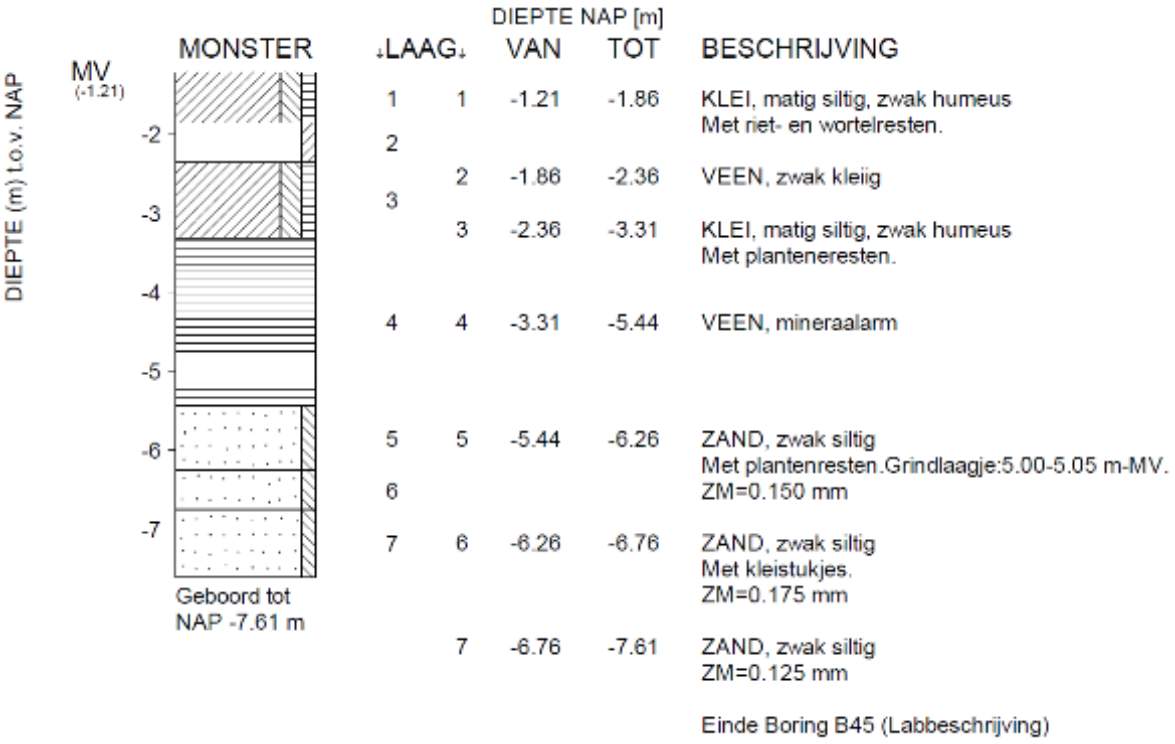

Figure 76; Soil investigation boring 7 Southdike (Deltares, 2012)

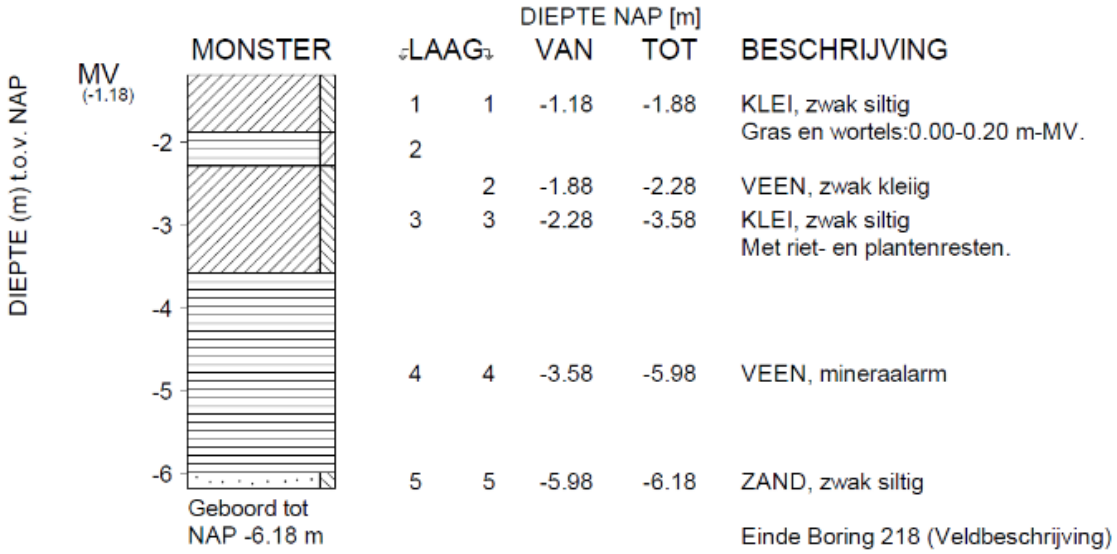

Figure 77; Soil investigation boring 9 Southdike (Deltares, 2012)

Both soil investigations show a top layer of clay of 60cm continued by a peat layer of 40cm, next a clay layer of 1 till 1.30 meters thick is located under which a thick (deep) peat layer of 2 till 2.40 meters is located. This is all founded on a base sand layer with an undefined depth. The uncertainties in depths are used to insert the transition layers, used to overcome the mentioned errors.

Base sand

The only available test results for the base sand layer were five triaxle soil sample tests carried out in 2008 from which three test were assumed relevant for this research (the other two test were sand mixed with humus materials, soil sample were taken at a lower depth so the base sand was partially mixed with peat).

Base sand	Test 1	Test 2	Test 3
Cohesion [kN/m2]	0.0	0	-3.56
Friction angle [deg]	36.63	36.66	39.81
Ywet [kg/m3]	1973	2056	1960
E50[MPa]	23.7	59.96	68.46

Table 33; Base sand triaxle test results (Deltares, 2012)

The cohesion of the base sand layer is on average zero (neglecting negative cohesion) which accords with the submissions which also all assumed a value of zero. For the friction angle, three test produce almost same values with an average of 36.4 degree. One test produced a value which is not corresponding to these values (39.8). According to the submissions, a value of 36 is correct. The average saturated weight is 2000 kg/m3 which is 19.8kN/m3 (submissions all assumed 20kN/m3). The Young modulus can be determined by multiplying the E50 factor with a factor 3; $[E_{50} = 1/3E]$. The average value for E50 out of the tests is 50 so this gives a value of 150 MPa. The submission of the UVA also used a value of 150MPa.

Clay top/Soft clay

There are multiple tests carried out for the clay layers. But it is sometimes not completely clear which test is done for which layer. The best indicator therefore is looking to the depth of the soil sample. For the top clay layer a triaxle test was carried out in 2006.

Clay	Triaxle Test 1	Triaxle Test 2	Triaxle Test 3	Triaxle Test 4
Cohesion [kN/m2]	9.63	3.55	6.30	11.08
Friction angle [deg]	33.75	38.73	26.84	23.21
Ywet [kg/m3]	1590/1438	1400/1413	1543/1655	1600 /1783
E50; undrained [MPa]	7.4	4.96	7.62	9.8
Depth below SL[m]	0.40-0.75		0.30-0.70	

Table 34; Soft clay triaxle test results (Deltares, 2012)

Despite the fact that the triaxle tests are conducted on soil sample which were located in the same region of the test side the results are quite variable. It will turn out that all the derived results for the clay layers have a wide range of variation.

The average cohesion of this layer is 7.6 kPa which is much higher than the submissions, respectively 3.8, 4.6 and 6.3 kPa. For the internal angle of friction an average of 30.6 degree is found with an extremely high variation of values (23 till 38). The submissions presented values of 29.4 and 33.4 degrees. A value in this range can be assumed.

The **Poisson value** can be determined by using the K_0 tests applying the following formula:

$$v = \frac{K_0}{1 + K_0} \quad \textbf{(30)}$$

Most of the time the K_0 value determined at the end of the test (K_0-final) is presented in the reports. The stated source mentions that this is only valid if taken the Poisson value determined in elastic state. This was not the case in many situation so it was rather difficult to determine the Poison value. The Poisson value is therefore mainly based on the prediction competition results.

The most variable soil parameter of clay is the unit weight. The average weight is 1555 kg/m3 which is 15.2kN/m^3. A K0-CRS test for the same clay gave an average unit weight of the soil (rho-wet) of 16.4 kN/m3. The submissions also varied between 14kN/m3 to 16.5 kN/m3.

For the undrained conditions the following can be assumed

$$E_{undr}^{50} = 3G_{50}$$

Since

$$G_{50} = 1/3G \; and \; G = \frac{E}{2(1+\nu')} \; assuming \; \nu = 0.5 \; \rightarrow \; \boldsymbol{G = 1/3E}$$

This leads to the following:

$$E_{undr}^{50} = 1/3E$$

The average E50 undrained strength of the top clay layer is 7.45 MPa. This gives a Young Modulus of 2.5 MPa. Odometer tests of 2008 with the NEN Bjerrum method and the Koppejan method for the same layer produced the following results:

Clay	**Test 1**	**Test 2**	**Test 3**
Young Modulus [MPa]	16.5 kPa /0.003 (strain rate) = 5.5	20.2/0.0038= 5.3	18.6/0.004 = 4.6

Table 35; Young modulus determination soft clay (Deltares, 2012)

The average of these tests is 5 MPa. The UVA assumed an undrained strength of 11.6 MPa, which is recalculated value of 4MPa.

For the organic clay Odometer test and DSS test are carried out in 2012. The organic clay is the soil layer located at a depth between -2.5 and -3.1 meter.

Organic clay	**Young Modulus [MPa]**
DSS Test 1	20.2 kPa / 0.008 = 2.52
DSS Test 2	35 kPa/0.015 = 2.33
DSS Test 3	39 kPa/ 0.012 = 3.25
DSS Test 4	17.5 kPa / 0.009 = 1.94

Table 36; Young Modulus organic clay (Deltares, 2012)

The DSS produced an average value of 2.5 MPa for the organic clay layer. The Odometer test including the Koppejan method and the Isotachen method produced an average value of 1.8 MPa, using the assumption that $E \approx 2/3E_{odo}$. In brief, there is a wide variation in the values of the Young Modulus. Determination of this value will therefore also be a calibration with the produced results.

Clay cover

The clay cover tests were conducted in 2008. Since the clay cover layer is in comparison to the subsoil layers constructed, the results from this tests are less reliable and could only be interpreted as indication if the chosen values of the submissions are in the right order of magnitude.

There is quite some uncertainty in the unit weight of the clay cover. The classification tests out of 2008 gave unit weights varying between 15.2 and 16.1 kN/m^3. The DSS tests produced an average of 1800 kg/m^3 which is 17.6 kN/m^3. The submissions of the UVA and Siemens both used a value of 18kN/m^3. A value between 16kN/m^3 and 18kN/m3 seems therefore plausible.

For the unit dry weight Proctor tests were carried out. These gave an average dry weight of 13.8kN/m^3. Assuming a 50% standard saturation means a dry weight of 16 kN/m^3 seems therefore most plausible.

For the determination of the Young Modulus the results of a DSS test are used. This tests produced an average value for the Young Modulus of 28 MPa. The submission of UVA and Siemens both used an undrained strength of 75MPa which is almost equal to the results of the DSS test (E_u=1/3E).

Clay cover	**Young Modulus [MPa]**
DSS Test 1	22/0.0006 = 36.6
DSS Test 2	35 kPa/0.0015 = 23.3
DSS Test 3	39 kPa/ 0.0012 = 32.5
DSS Test 4	17.5 kPa / 0.0009 = 19.4

Table 37; Young modulus clay cover (Deltares, 2012)

Core sand

The only test representative for the sand used in the core of the dike is a triaxle test carried out in 2008 by Deltares. There is not any data available of test done in 2012 which makes these results more uncertain.

Core sand	**Triaxle Test 1**	**Triaxle Test 2**	**Triaxle Test 3**
Cohesion [kN/m2]	0.02	4.97	2.65
Friction angle [deg]	30.94	28.29	30.17
Ywet [kg/m3]	2003	2017	2035
Ydry [kg/m3]			1631
E50[MPa]	7.52 [MPa]	7.56[MPa]	8.92[MPa]

Table 38; Triaxle test results core sand (Deltares, 2012)

Based on three tests the average cohesion is 2.55 kPa. The submissions used values of respectively 0, 0.6 and 1.95 kPa. The higher cohesion values of the triaxle tests can be explained by the fact the soil sample were partially mixed with some humus materials. A value for the cohesion between 0 and 2 kPa seems reasonable for the cohesion of the sand core. The average friction angle is 29.8 degree. Submissions of the friction angle vary between 26.5 and 30.5 degree.

The average weight is 2020 kg/m3 which is 19.8 kN/m^3. This is comparable with the 20kN/m^3 used by the UVA and Arcadis. The dry weight is fully dry weight, in the model the soil will be saturated or partially saturated (40%). A dry weigth of 18 kN/m^3 seems a respectable value.

For the determination of the strength three loading stages were implied. The third loading stage is the normative stage of which the results are shown in the table. This gives an average E50 of 8 MPa so a Young Modulus value of 24 MPa. The report of the UVA presents a value of 30MPa. A value between 24MPA and 30MPa is therefore considered.

Peat

For the determination of the soil strength of peat multiple tests were conducted for the two different peat layers (see depth). The following data was received for depths which are not comparable with the depth of the peat layer. The triaxle test is also conducted in 2006 so the results are quite uncertain.

Peat	**Triaxle Test 1**	**Triaxle Test 2**
Cohesion [kN/m2]	9.59	7.64
Friction angle [deg]	21.21	19.93
Ywet [kg/m3]	1050	1006

E50; undrained[MPa]	3.12	1.6
Depth [m]	1.75-2.75	2-30-2.90

Table 39; Triaxle test peat deep (Deltares, 2012)

The average cohesion is 8.6 kPa. In comparison, the submissions produced values of 4.6, 5.8 and 9.7 kPa. The average friction angle of test is 20.6 degrees while submissions showed values of 25.3 and 26.4 degrees. Confirmation is found in the unit weight of peat, a weight of 1030 kg/m3 which is 10.1kN/m3 is found completely in line with the submissions. An average value for E50 is 2.36 MPa which gives a Young Modulus of 0.8MPa.

Triaxle test in undrained condition carried out in 2008 for the same depth produced the following results.

Peat	**Triaxle Test 1**	**Triaxle Test 2**	**Triaxle Test 3**	**Triaxle Test 4**	**Triaxle test 5**
C_U [kN/m2]	25.27	27.55	26.41	16.94	35.99
Friction angle [deg]	0	0	0	0	0
Ywet [kg/m3]	1096	1045	1141	1064	1095
E50; undrained[MPa]	2.05	2.1	2.25	1.32	3.39
Depth below SL [m]	0.55-0.73	1.25-1.40	0.95-1.05	0.55-0.75	0.95-1.10

Table 40; triaxle test peat (Deltares, 2012)

An undrained triaxle test provides an undrained shear strength (C_U). A rough estimation for the cohesion is $c=0.5C_u$. Appling this rule provides us with an average cohesion of 14 kPa, quite comparable with the cohesion of the test of 2006. The average unit weight is higher compared with the previous tests, 1085kg/m3 (10.6kN/m3). The average E50 value is 2.25 MPa which is a value of 0.75 MPa.

Information for the lower peat layer is provided by an odometer tests from 2008 and 2012.

Peat	**Test 1 2012**	**Test 2 2012**	**Test 3 2008**
Young Modulus [MPa]	20 kPa / 0.03 = 0.66	25kPa/0.038= 0.833	22kPa/0.02=1.1
Depth [m]	-4.91-4.96m	-4.91-4.96m	

Table 41; Young modulus determination peat (Deltares, 2012)

The average E_{odo} is 0.86 MPa which is equal to a Young Modulus of 1.3MPa. In the submissions almost the same value is presented (1.6 MPa UVA).

C. Interface COMSOL

In Figure 78 the complete interface of the CMS-model is presented. It shows all the possibilities within COMSOL, and how these components are defined within COMSOL. Based on this interface the schematized model build-up, see chapter 3 is made. The colors and arrows in this figure are used to visualize the relation.

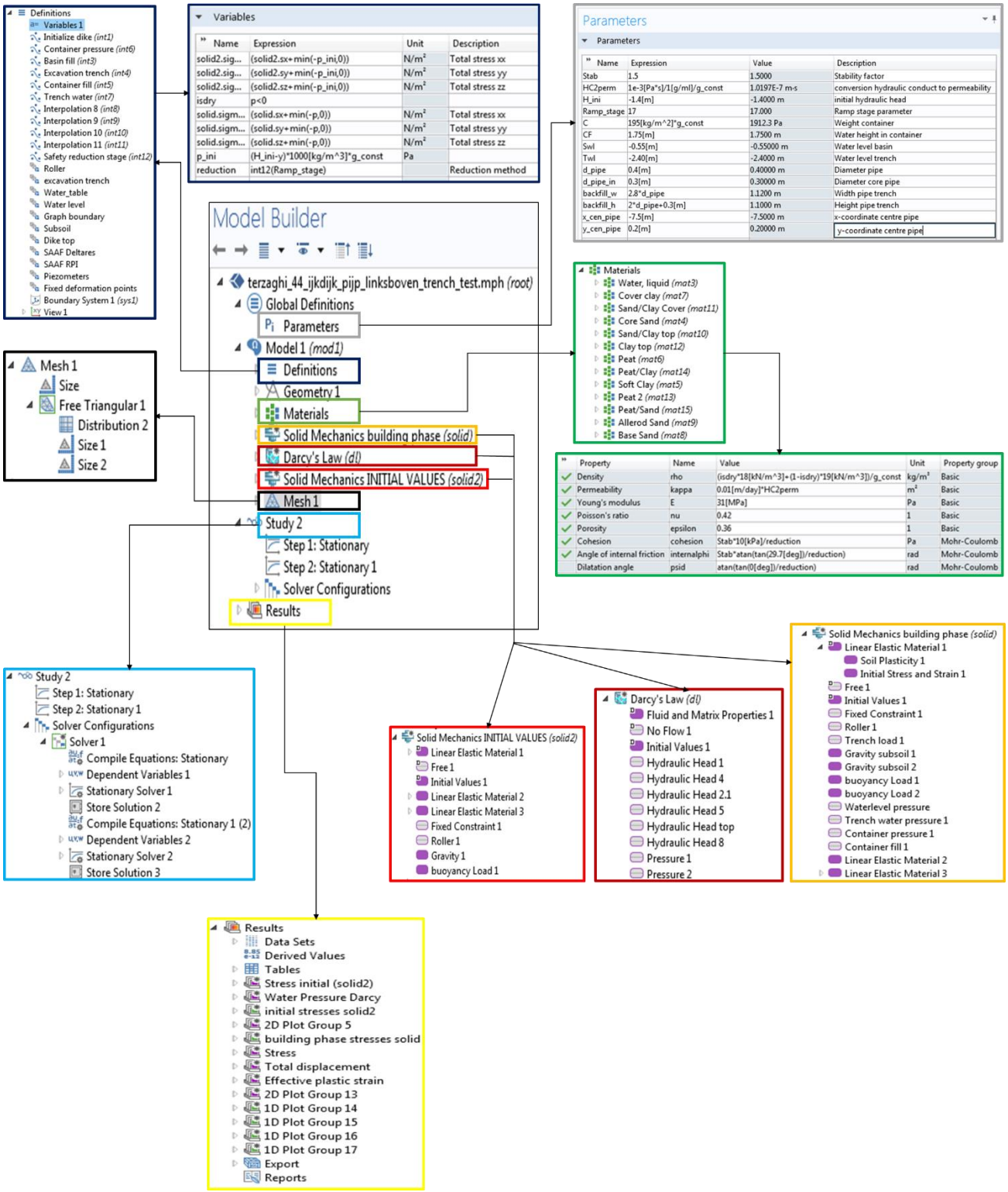

Figure 78; Interface (modules) used in CMS-model

D. Why use linear elastic perfectly plastic calculation model?

For the behavior of the soil various constitutive models have been developed: Linear or non-linear elastic models, Elastic-perfectly plastic models, Isotropic hardening single surface plasticity models, Isotropic hardening double surface plasticity models and Kinematic hardening multi-surface plasticity models. Examples are the Mohr- Coulomb, Drucker-Prager, hardening models: cam-clay models, HS model, soft soil model (SSC) and there are some other non-linear soil models (Chi Fai Ng, 1994). All these models are all simplifications of the real soil behavior and concentrated on some particular aspect.

The choice for the elastic-perfectly plastic model (i.e. Mohr-Coulomb, Drucker-Prager) is because it is a relative simple model and it seems to be sufficient for the many areas of geotechnical problems (Jiang & Xie, 2011). Mohr-Coulomb and Drucker-Prager models also work well for stiff cohesion less soils like sands which exhibit plastic shear deformations and elastic volume deformations (Melnikova, 2014). The choice to use the Drucker Prager soil model for simulating the deformations is argued by Melnikova and Paul Chi Fai because this model is quite simple and hence fast in computations while soft soil models like Cam-Clay model are computationally heavy because they have to calculate the 'Critical state Theory' of the soil (Melnikova, 2014)(Chi Fai Ng, 1994).

The soft soil models incorporates a hardening law, specifying the state variable evolvement with plastic straining, which together with the yield surface and flow rule define a critical state criterion. This critical state is very difficult to qualitatively assess and a lot of soil data from dikes don't provide necessary parameters for this module (Vermeer & Neher, 1999). This makes the elastic-perfectly plastic model much more applicable in use.

A disadvantage of elastic-perfectly plastic models is that they can over-predict soil strengths of soft soils. Models capable of modeling soft soils are soft soils models and a Cam-Clay model. Cam-clay and other soft soil models have been developed for soft clays and peats, which generally produce significant nonlinear elastic deformations, with volume deformations becoming plastic at some load level.

These plastic volume deformations modeled in the soft soil models and the Cam-Clay model can be taken into account in the Drucker Prager an Mohr Coulomb model by adding elliptic cap to a Mohr-Coulomb yield surface (Melnikova, 2014). With this tool the rate independent plastic equations of the Mohr-Coulomb models are slightly similar to the constitutive equations for Cam-clay.

E. Why use Drucker Prager instead of Mohr Coulomb

There are two elastic perfectly plastic models, Mohr-Coulomb and Drucker Prager, which are appropriate to use for this research. The Mohr Coulomb criterion is the most popular criterion in soil mechanics. Based on the Mohr's circle, Mohr Coulomb plasticity model can be written as;

$$F = \frac{1}{2}(\sigma_{max} - \sigma_{min}) + \frac{1}{2}(\sigma_{max} - \sigma_{min}) \cdot sin\phi - c \cdot cos\phi = 0$$

Where σ_{max} and σ_{min} are the biggest and smallest principal stresses. F, the yield function, is a difference between magnitudes of the normal effective compressive stress. A yield criterion serves to define the stress condition under which plastic deformation occurs.

The Mohr-Coulomb failure criterion has however some disadvantages which limits its wider application. The first one is that the major principal stress σ_1 is independent of the intermediate principal stress σ_2 for the M-C criterion, which leads to underestimate the yield strength of materials and disagrees with the test results reflecting the influence of σ_2 to strength of material in many cases (Jiang & Xie, 2011).

The second one is the trace of the yield surface on deviatoric plane is an irregular hexagon which impairs the convergence in flow theory due to the six sharp corners. Therefore the Mohr-Coulomb criterion causes numerical difficulties when treating the plastic flow at the corners of the yield surface (Inc, 2012; Jiang & Xie, 2011).

So in order to avoid the issues associated with the sharp corners the Drucker-Prager yield criterion has been developed by modifying the von Mises yield criterion to take into account the Coulomb friction (Inc, 2013a). The Drucker-Prager yield surface passes through the inner or outer apexes of the Mohr-Coulomb pyramid, depending on whether the symbol ± is positive or negative (Inc, 2013a).

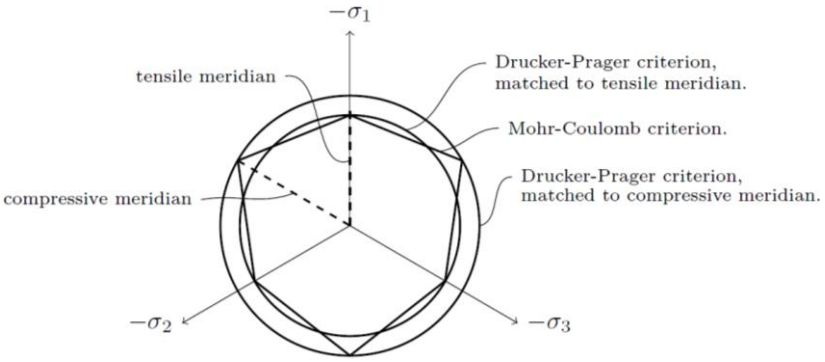

Figure 79; Yield surface Drucker Prager vs Mohr Coulomb (Inc, 2013a)

The Drucker Prager soil model therefore has the advantage to the Mohr Coulomb model that it is smooth and does not cause numerical solution problems due to singularities in the flow rule (Melnikova, 2014). It is therefore far more stable than the Mohr-Coulomb plasticity model. The advantage is clearly shown in Figure 80 were the load-displacement curves for both the Mohr-Coulomb and the Drucker-Prager criteria are plotted. The figure shows clearly that the Drucker Prager simulation is smoother.

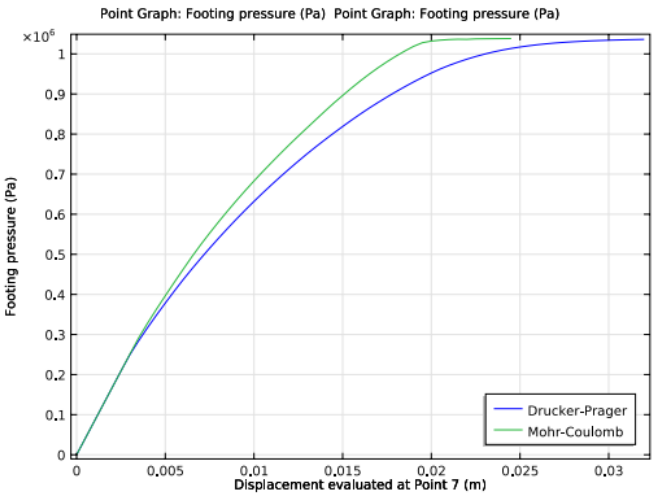

Figure 80; Footing pressure versus vertical displacement for Mohr Coulomb and Drucker Prager criteria (Inc, 2013a)

F. Critical slip circle criteria

Explanation of the effects of the pipe to macro-instability in this research is based on the Bishop principles. This states that the factor of safety is defined as the ratio between the restoring forces M_R (soil shear strength + externally applied restoring forces) to the disturbing forces M_D (soil self-weight + externally applied forces). The location of the origin of the slip surface is of influence since the resultant of shear and normal stress on slip surface is always located towards the O (origin).

Using this method also implies the critical slip circle has to be known. Problem is that the used FEM software of COMSOL cannot clearly define the critical slip surface after the stress and deformation analysis (Tan, 2006). COMSOL can only simulate the potential slip circle. Therefore we have to define the critical slip surface out of the potential slip circle to compare them for different situations of the pipe.

Multiple methods who describe how to determine the critical slip circle cannot be used because their will not be a line within the dike at which the effective plastic strains take consistently the local maximum with the FEM calculation (Tan, 2006). Therefore drawing of the critical slip surface must be based on certain contours of strains. Like most engineers we have to thereby rely on the search for the critical slip surface in the stress field (Tan, 2006).

This will also be done in this research in which the critical slip circle will be determined based on interpretation of the predicted CMS-model results. This is especially important in case 2 slip circles occur. For this report some criteria are used to determine the area/location of the critical slip circle.

Critical slip circle criteria

The criteria on which the main potential slip circle will be determined are the following:

- The shape of the total displacement. This will give a first indication of how the soil will slide, highest differences in displacement will mean high shear stress so plastic strains
- The slip circles which contains the highest values of effective plastic strains. Locations with effective plastic strain values higher than 0.05 will probably fail the earliest.
- When two slip circles have high effective plastic strains (>0.05), the slip circle with the highest strains (for example on one side of the pipe) will be preferable.
- A last step is to determine the slip circle based on an interaction with the safety factor results.

A practical example of how the critical slip criteria are used to define the main potential slip circle, in this case for the general Southdike (without pipe), is shown in Figure 81. In this case the shape of the total displacement, especially were the largest differences occur, is equal to the slip circle of the effective plastic strains. The exact location is in this case based on the locations were the highest effective plastic strains occur. These are the left corner of the trench, in the core of the dike and above the base sand layer. A line (no always circle) is drawn through these points to show the main potential slip circle.

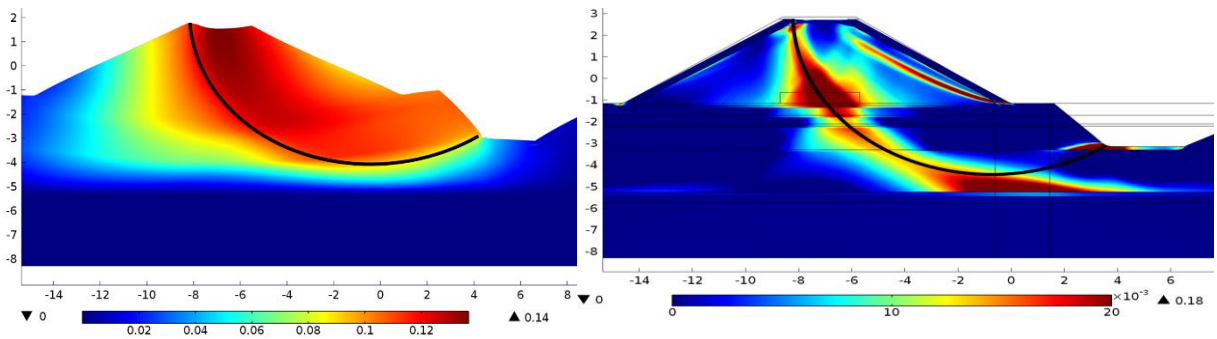

Figure 81; Determination critical slip circle

G. Simulations pipe locations

The simulation results of all the different locations are presented in the table below. All the figures show the effective plastic strains in the Southdike after placing the pipe. Effective plastic strains do not have a dimension, so only indicate the shape of the slip circle. For all situations the same scale is used to present the effective plastic strains. In some case this implies that the exact location of the potential slip circle is less well visible due to the broad variation of strains of the slip circle area, in these case the potential slip circle is determined changing the scale. All the observations and defined slip circles are based on the critical slip circle criteria (see Appendix F).

Left Top Safety factor: 1.1175 Observations: - 2 slip circles - Deep slip circle is main slip circle - Safety factor reduces - Slip circle relocate left around pipe - Pipe will induce cut - Due to cut less driving force needed to force failure (<SF)	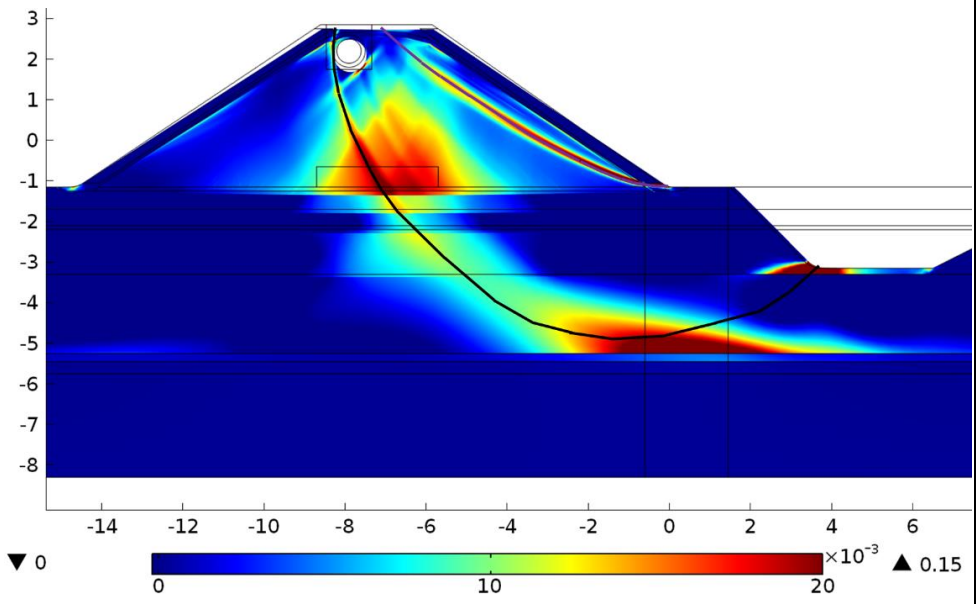
Right Top Safety factor: 1.1475 Observations: - No influence on main slip circle - Safety factor increases marginal due less weight pipe - Effect pipe at this location larger when dike is more stable	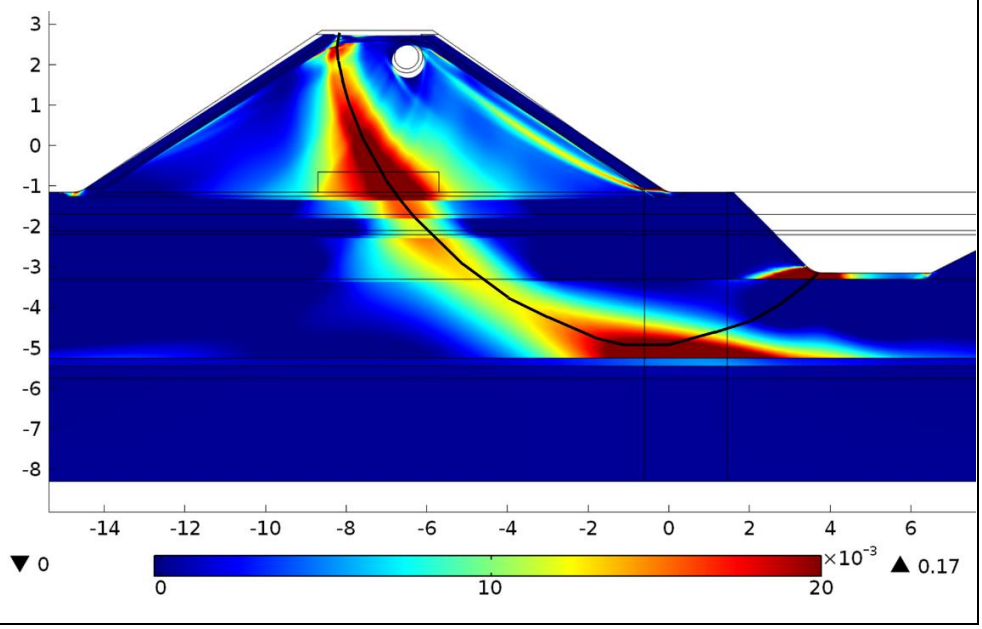

Middle Top <u>Safety factor:</u> 1.1825 <u>Observations:</u> - No influence on shape potential (deep) slip circle - Less driving force due to weight deficit pipe, positive influence on safety factor, so this increases	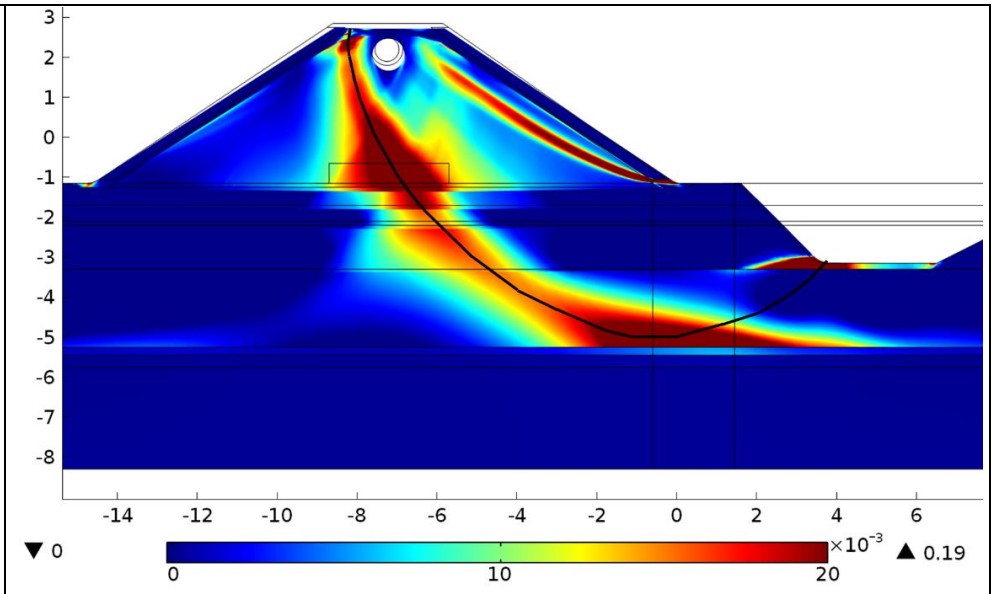
Right Middle <u>Safety factor:</u> 1.08 <u>Observations:</u> - Dike fails due to local slip on top → SF not representative - Strain parallel to pipe -> uplift	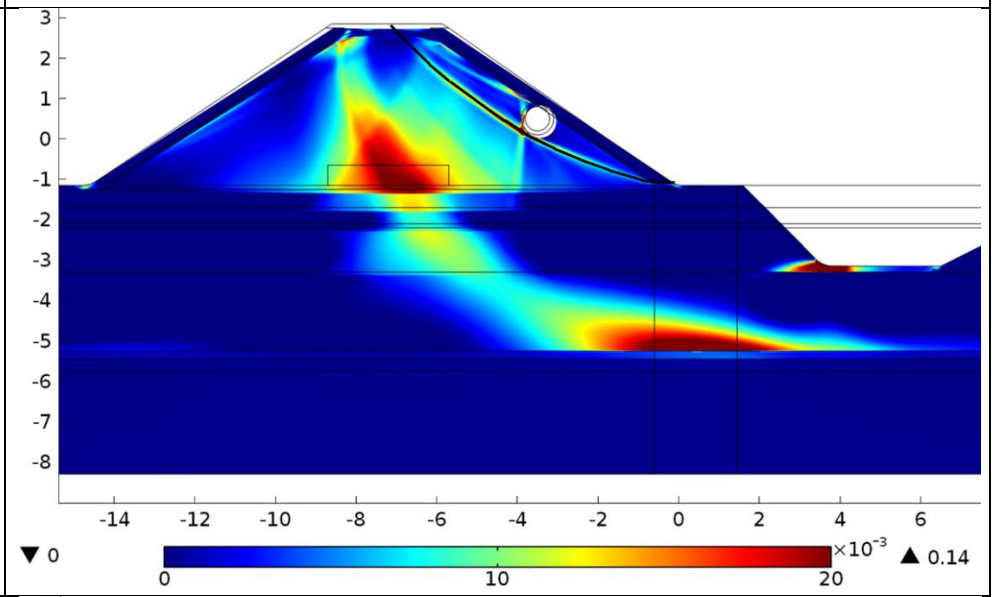
Left Middle <u>Safety factor:</u> 1.1425 <u>Observations:</u> - Pipe has no influence on shape potential (deep) slip circle	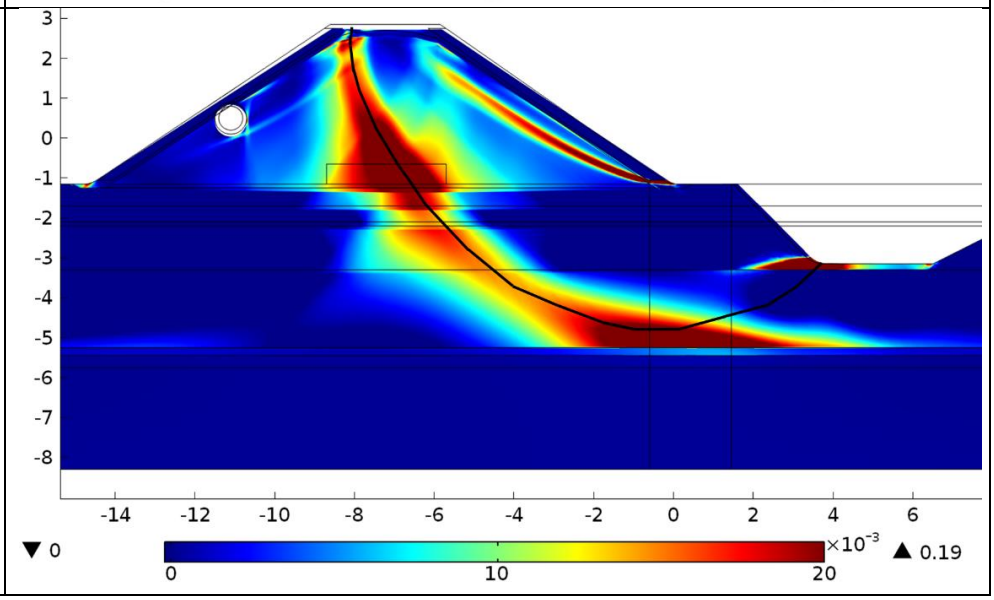

Right next to <u>Safety factor:</u> 1.1425 <u>Observations:</u> - No influence on shape potential (deep) slip circle and safety factor - Remarkable constant safety factor, close to surface less influence on momentum	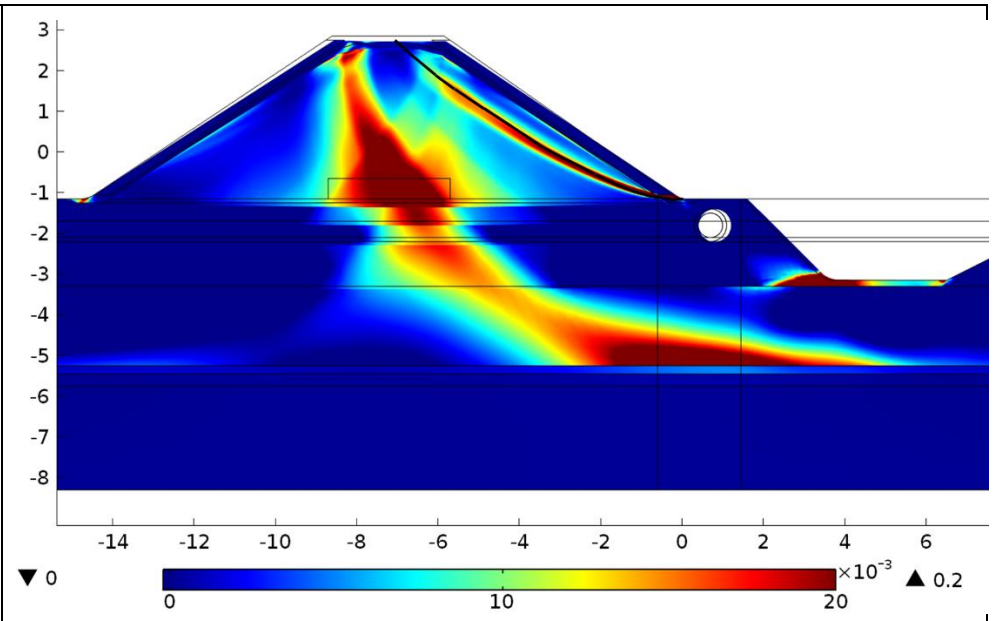
Left next to <u>Safety factor:</u> 1.1425 <u>Observations:</u> - Pipe has no influence on shape potential (deep) slip circle and safety factor	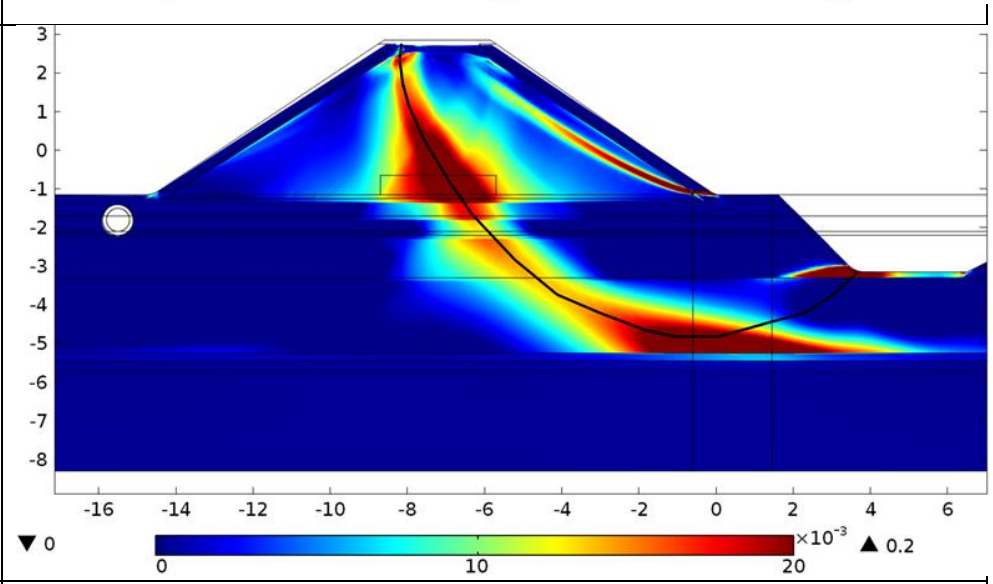
Core middle <u>Safety factor:</u> 1.1675 <u>Observations:</u> - 2 potential slip circles -Radius shape slightly increases → decrease SF -Pipe inside slip surface [>SF] -Slip circles in counter direction due to container + movement pipe	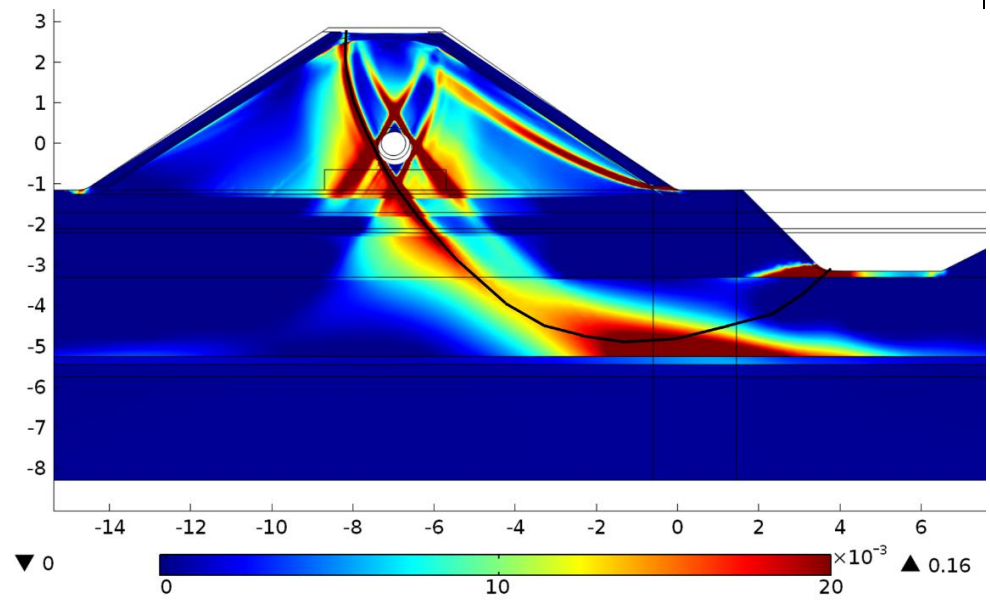

Core left <u>Safety factor:</u> 1.205 <u>Observations:</u> - Shape slip circle reduces [>SF] - 2nd slip circle - Higher plastic strain needed to force failure	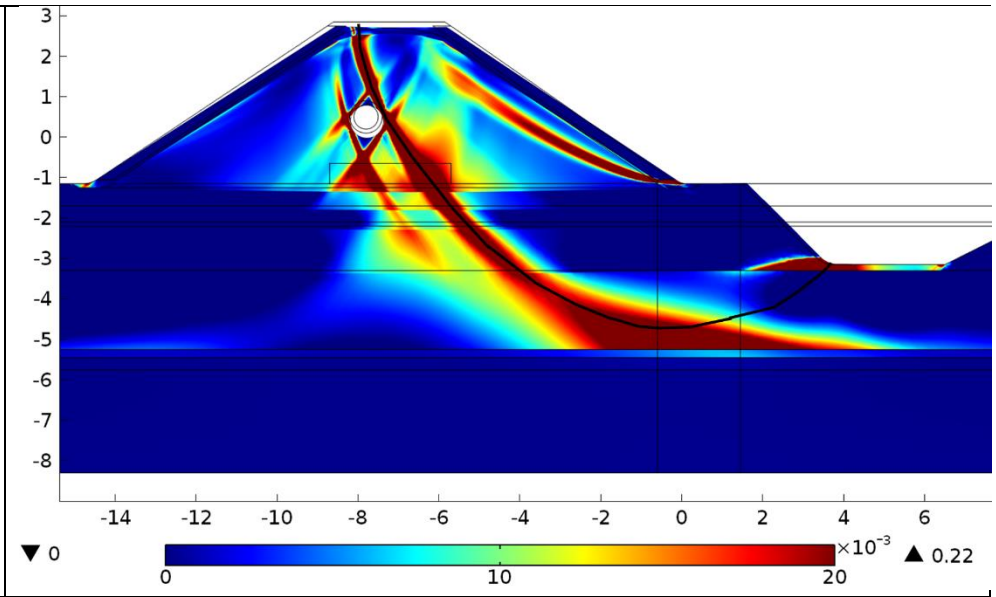
Core right <u>Safety factor:</u> 1.1825 <u>Observations:</u> - no influence on shape potential (deep) slip circle - Weight loss due to pipe [>SF] - Cross directional slip circles	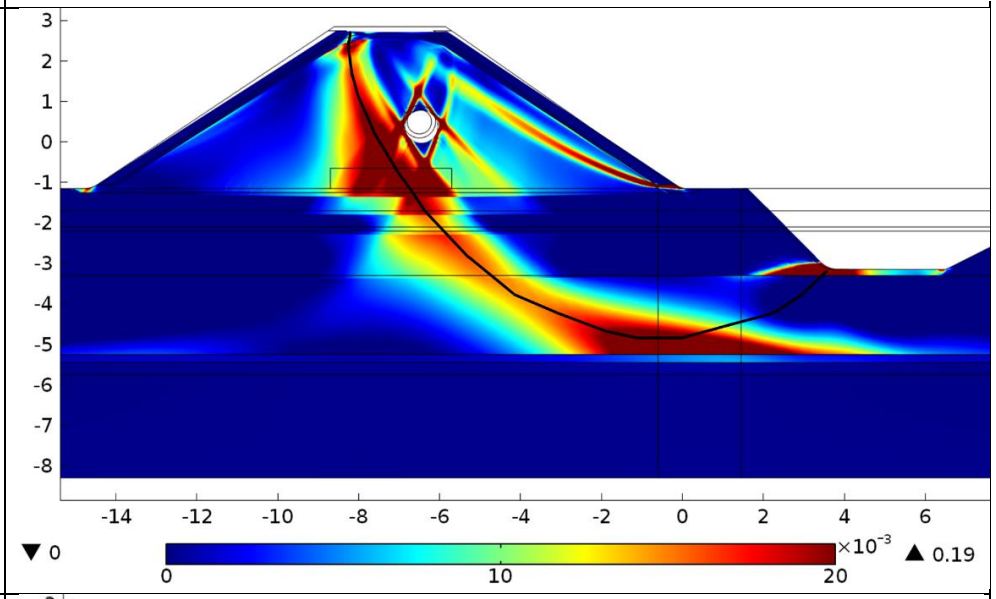
Low core left <u>Safety factor:</u> 1.1425 <u>Observations:</u> - no influence on shape potential (deep) slip circle and safety factor	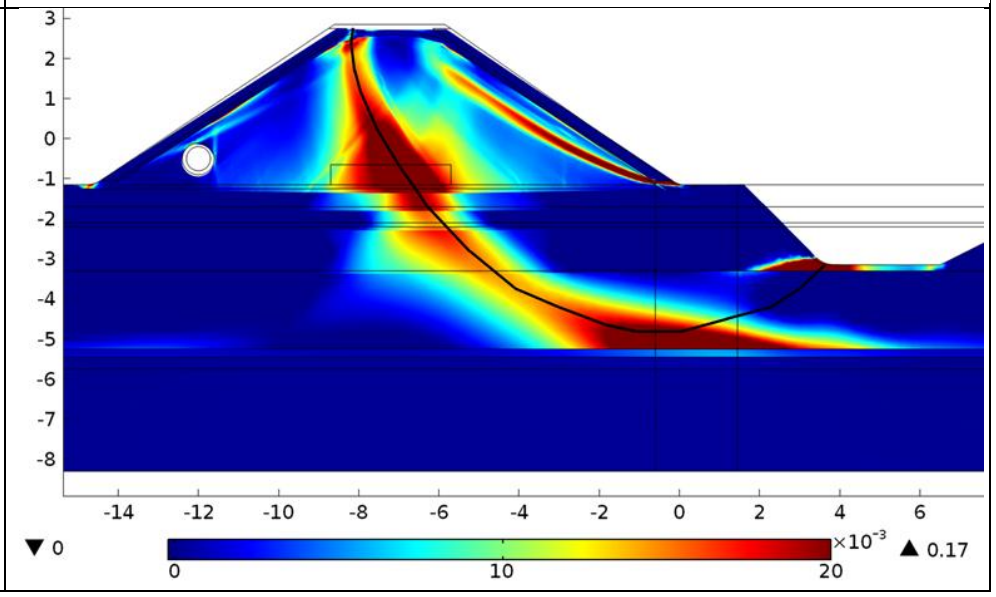

Low core right <u>Safety factor:</u> 1.165 <u>Observations:</u> - Small rotational slip circle enhanced due to pipe - Weight loss due to pipe [>SF]	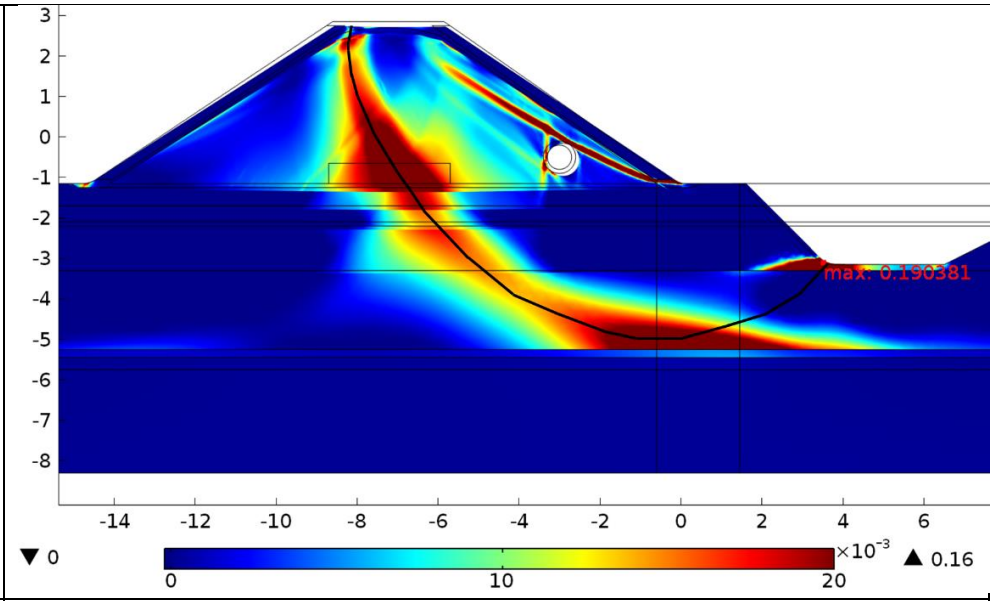
Low core middle <u>Safety factor:</u> 1.2225 <u>Observations:</u> - Double slip circle - Decrease radius slip circle [>SF] - Pipe is major resistance, will force slip circle to relocate, compression force [>SF]	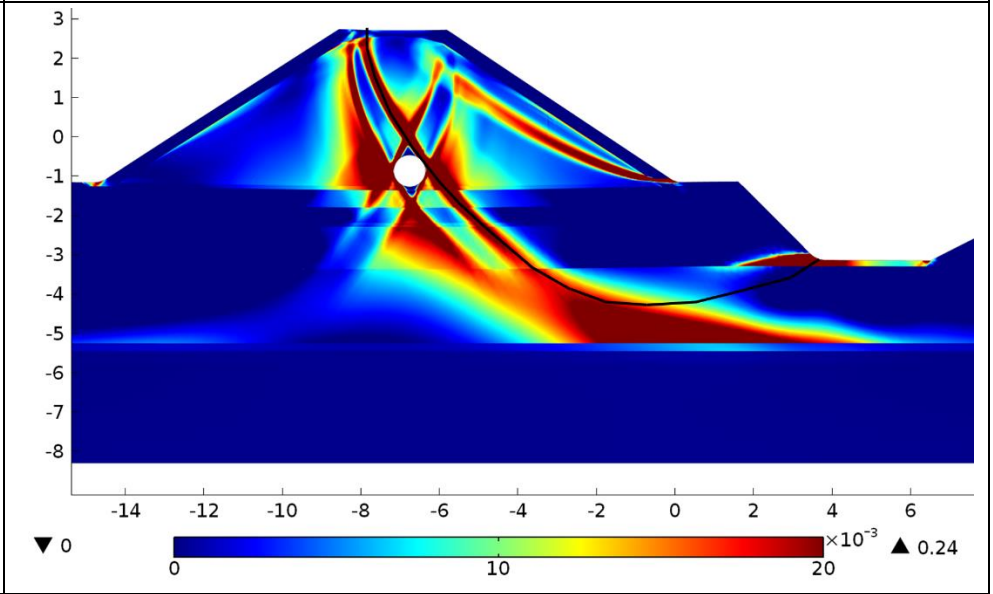
Deep Middle <u>Safety factor:</u> 1.205 <u>Observations:</u> - Double slip circle - Decrease radius slip circle [>SF] - Pipe is major resistance, will force slip circle to relocate, compression force [>SF] - increase displacements	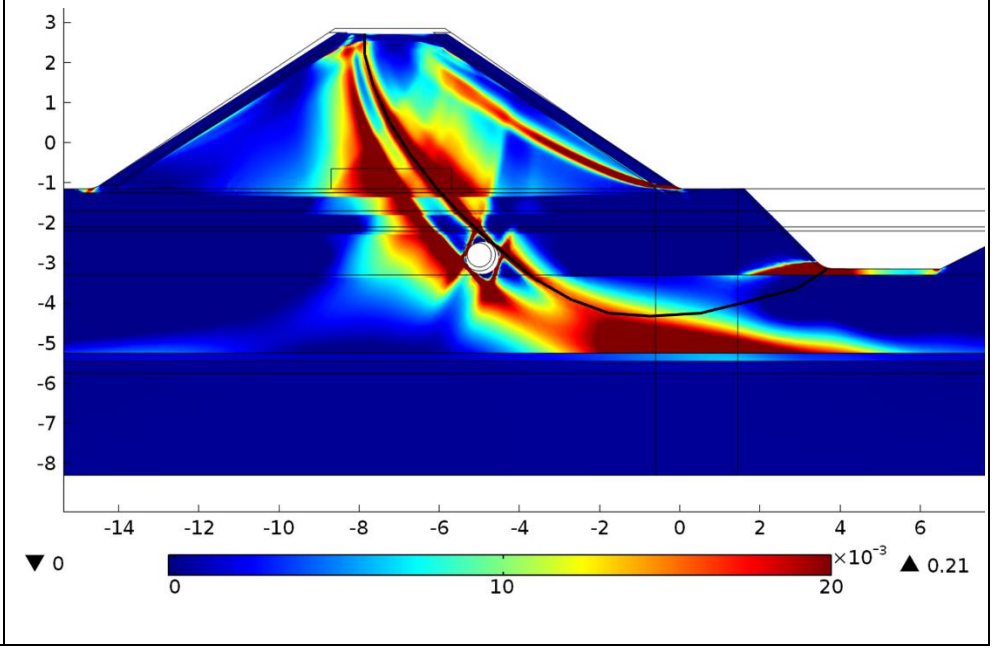

Deeper right <u>Safety factor:</u> 1.2275 <u>Observations:</u> - Decrease radius slip circle [>SF] - Pipe is a major resistance, induces high compression forces, forcing slip circle to decrease	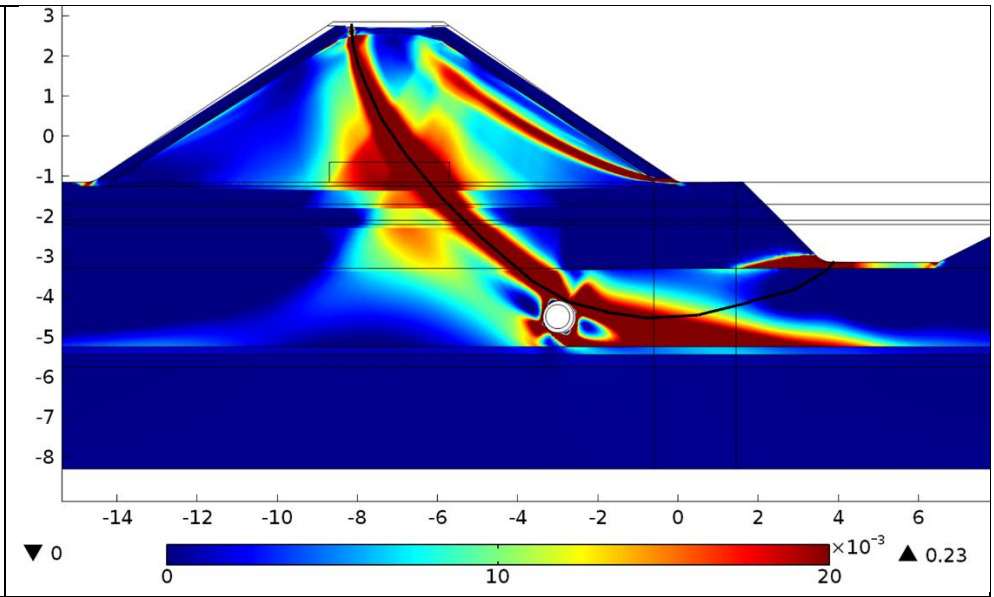
Deep under toe <u>Safety factor:</u> 1.08 <u>Observations:</u> - Extreme high plastic strains around pipe, bigger strains needed to induce failure of larger slip surface - Increase radius slip circle [<SF]	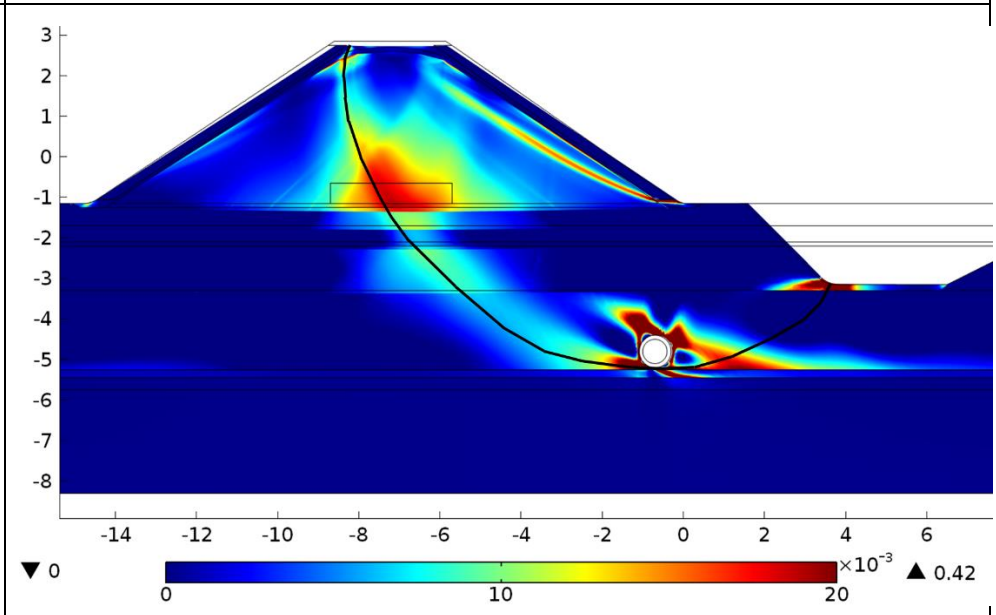

Table 42; Effective plastic strains of all locations investigated

H. Filled pipe

In all the tests done in this research the pipe is assumed to be empty. When the pipe is used for practical reason, it will however be filled with for example water, oil or gas. The density of these fluids/gasses transported by the pipe can have an influence on the safety of the buried pipe.

The effect of the filled pipe is therefore tested by addressing the geometry inside the pipe for three-quarters with the properties of oil (linear elastic material node). The density of oil is assumed to be 900kg/m^3 (Poisson value 0.33 and Young Modulus 0.01MPa).

The test is performed for multiple locations, results are presented in Table 43.

Locations	Safety factor		Influence
	Pipe without oil	Pipe filled with oil	
Low core middle (11)	1.2225	1.205	Negative influence (-1.5%)
Middle top (2)	1.1825	1.1825	No influence (0%)
Deep middle (14)	1.205	1.205	No influence (0%)
Core Middle (6)	1.1675	1.165	Negative influence (-0.2%)

Table 43; Effect filled pipe on safety factor

The results indicate that a filled pipe has a small negative influence on the safety situation of the dike when the pipe is located inside the slip circle. Due to an increase of weight (density of oil) the pipe creates a higher driving momentum for the slip surface leading to a more unsafe situation. This also explains that when the pipe is located outside the potential slip circle, locations 2 and 14, the oil has no effect on the safety factor. A probably second effect of a filled pipe is that is provides more resistance against buoyancy which can increase the safety of the dike. This is only not tested in this research.

For the location 'low core middle', which was mostly influenced by the oil located in the pipe, the slip circle did not change as consequence of the higher density, as shown in Figure 82.

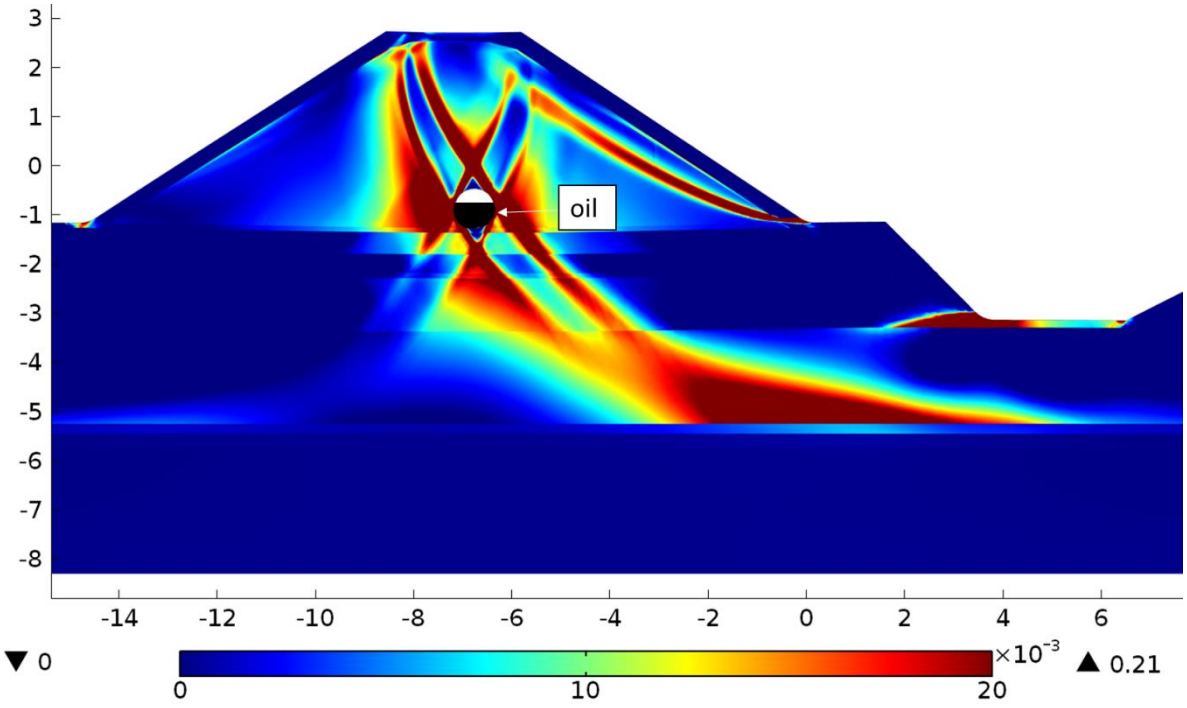

Figure 82; Slip circle at filled pipe

I. Direction of the pipe

The direction in which the pipe is located towards the dike should be of high importance based on the norms for buried pipes placed in embankments. Pipes can be situated in parallel direction of the dike, which is investigated in this research, or in in perpendicular direction towards the dike. This appendix shows that because of the 2D model environment, this study is limited in only investigating parallel directional placed pipes. It supports the recommendation that further research has to be carried out in a 3D environment to investigate the effect of perpendicular placed pipes. This is proved by a test shown in Figure 83, for which a pipe is placed in perpendicular direction towards the dike. Therefore a small layer with the characteristics of the pipe is assigned within the Southdike.

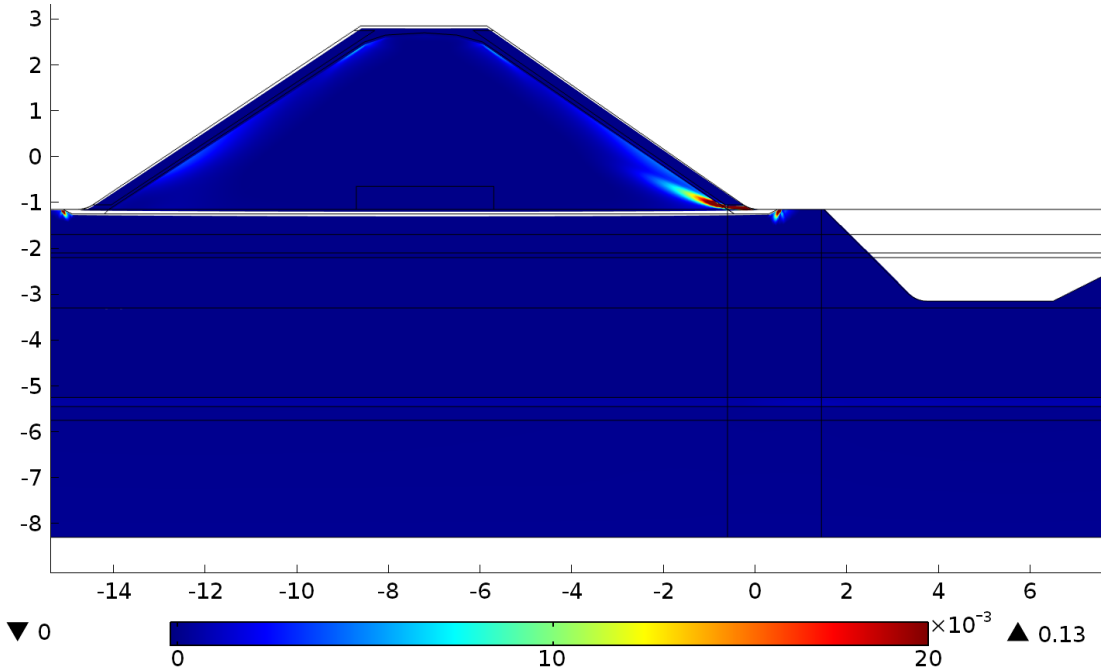

Figure 83; Effective plastic strains cross directional pipe

Figure 83 shows that with the deep slip circle will not occur. Instead a small slip circle will be occur to the toe of the dike. Due to the extremely stiff layer of the pipe the soil cannot slip into the trench. This is visualized by the displacement pattern of Figure 84, which is completely different compared to the patterns seen from earlier simulations. This plot also shows that the soil cannot sag into deeper soil layers due to the unrealistic stiff layer. In overview, all these effects show that assigning one layer with the characteristics of the pipe in a 2D environment will not represent a realistic situation.

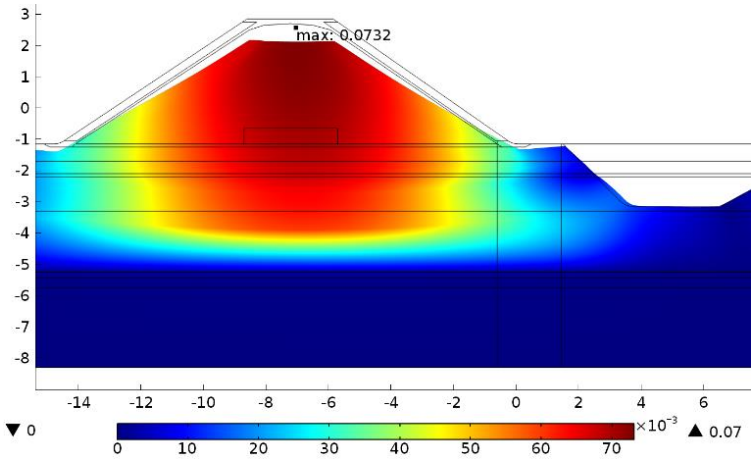

Figure 84; Displacements cross directional pipe

J. High water level instead of container

The Southdike has been forced to fail by macro-instability by means of a container and infiltration of water into the dike core. The container represents the mass and pressure increase of the soil due to a high water level. The shift of load from normally at the side of the dike to in this situation at the top of the dike can have some influence on the results. Therefore the situation is modeled in which the containers are neglected and a high water level is simulated at the left of the dike. The water level is simulated with a height of 3.90 meters (-1.15 -- 2.75meter). Goal of this test is to investigate if the conditions under which the dike is been subjected, influence the effect of the pipe to the development of macro-instability.

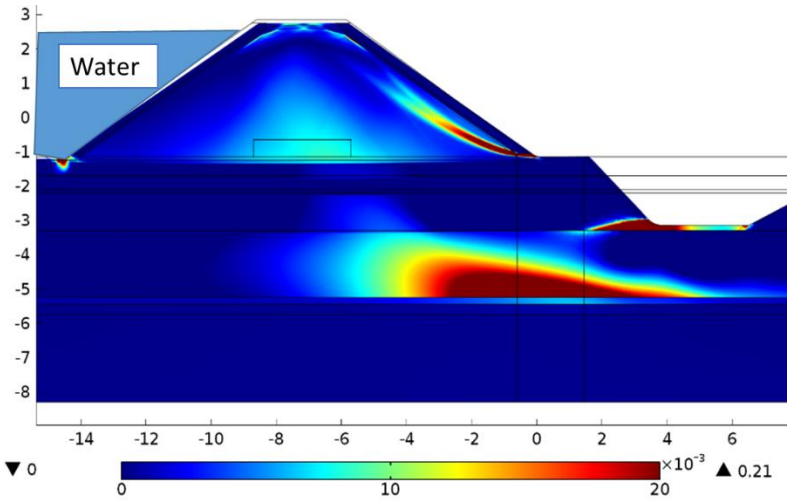

Figure 85; Effective plastic strains high water level (no container)

By changing the boundary conditions, the safety factor increased from 1.1425 to 1.29. Figure 85 shows that no deep rotational slip circle occurs in the dike, failure occurs due to a local small slip circle at the right side of the dike. The high water condition will also force the dike to displace more in horizontal direction into the trench, see Figure 86.

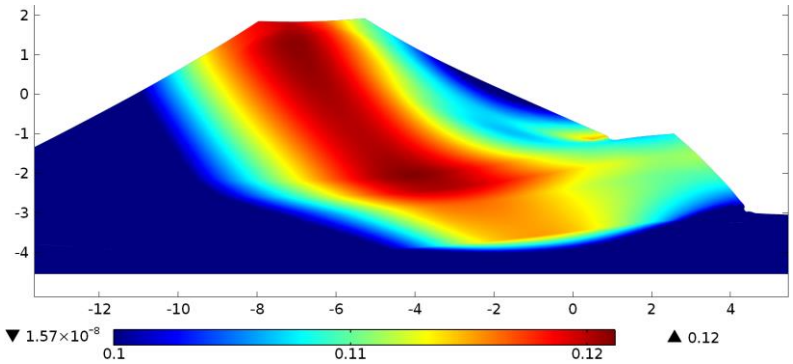

Figure 86; Displacements high water left side [scaled with factor 10]

Multiple tests show that due to the changed boundary conditions the effect of the pipe on the safety factor changes. In case the pipe is placed at location 11, see Figure 87, the safety factor increase with +3% while in the situation with containers the safety factor increased with 7%.

A second observation from these test is that even without container strains in cross direction still occur. This implies that these strains more probable occur due to the movement of the pipe, which creates resistance within the soil (tension +compression on both sides pipe).

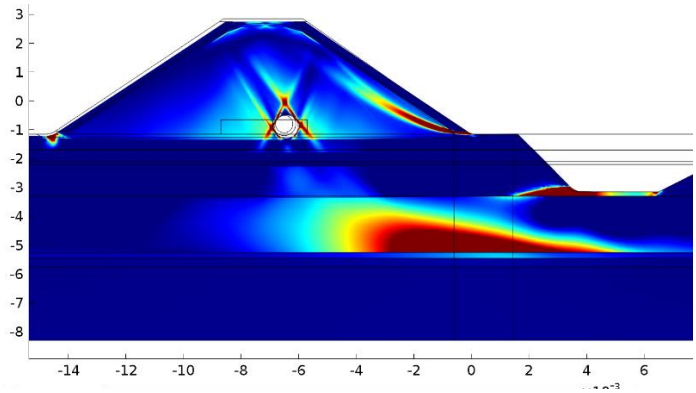

Figure 87; Effective plastic strains high water level (no container) + pipe